PROPOSITIONS

accompanying the thesis
**"Hydrothermal synthesis and characterization of 3R polytypes of
Mg-Al Layered Double Hydroxides"**
by Widya Nugraha Budhysutanto

1. Polytypism is different from polymorphism, since polytypes do not only have different crystal structures but they also have different molecular compositions.

2. The formation of donut-like crystals in the experiments with microwave heating is due to uniform heating rather than to the effect of microwave radiation.

3. The stacking sequence of the octahedral layers in polytype $3R_2$ is determined by the presence of the grafted tetrahedral aluminates, the hydrogen bonding of which governs the position of the subsequent octahedral layer.

4. Transformation of the polytypes is a solvent mediated process.

5. The reluctance of foreign students to learn Dutch is encouraged by the advertisement of Dutch educational institutions that English only is sufficient for people to live in Holland.

6. Against the appealing advertisement of discounts, one should keep in mind that unless the advertised goods are essentially needed, not buying them is still cheaper.

7. The challenge of a student coming to a foreign country is not only to improve the scientific knowledge, but also to learn to live independently and to integrate in the society. The integration process is not promoted by exposure to foreigners only.

8. A person who has no religion is not necessarily an atheist, since by definition, atheism means the rejection of belief in the existence of a god.

9. People should learn how to express their thoughts, but in the end the art of expressing them is a personal skill.

10. The Dutch did not colonize Indonesia for three centuries, but it took them that long to unite Indonesia, and Indonesia still occasionally struggles to keep its unity.

These propositions are considered opposable and defendable and as such have been approved by the supervisor, Prof. dr. ir. A.I. Stankiewicz.

STELLINGEN
behorende by het proefschrift
"Hydrothermal synthesis and characterization of 3R polytypes of Mg-Al Layered Double Hydroxides"
door Widya Nugraha Budhysutanto

1. Polytypisme verschilt van polymorfisme want polytypen hebben niet alleen een andere kristalstructuur, maar ook een andere moleculaire samenstelling.

2. De vorming van donut-achtige kristallen in experimenten met een magnetron als warmtebron wordt veroorzaakt door de gelijkmatig verwarming van het mengsel van reactanten en is niet gerelateerd aan de specifieke effecten van de microgolfstraling.

3. De stapelings volgorde van de octaëdrische lagen in polytype $3R_2$ wordt afgedwongen door de aanwezigheid van de verankerde tetraëdrische aluminaten. Hun waterstofbruggen bepalen de positie van de volgende octaëdrische laag.

4. Transformatie van polytypen geschiedt via processen in de oplossing.

5. De terughoudendheid van buitenlandse studenten om Nederlands te leren wordt gestimuleerd door de reclame van nederlandse onderwijsinstellingen dat de kennis van Engels voldoende is om in Nederland een bestaan op te bouwen.

6. In tegenstelling met wat aantrekkelijke advertenties met hoge kortingen beloven, moet men in gedachten houden dat tenzij de aangeboden produkten nuttig zijn, niet kopen altijd goedkoper is.

7. De uitdaging voor een student die naar het buitenland vertrekt is niet alleen om zijn wetenschappelijke kennis te verbreden, maar ook om zelfstandig te leren leven en te integreren in een andere samenleving. Dit integratieproces in het gastland wordt niet bevorderd door selectief contact met mede-buitenlanders.

8. Een persoon die niet behoort tot een geloofsgroepering, is niet noodzakelijkewijs een atheïst, omdat per definitie het atheïsme het bestaan van een god afwijst.

9. Een mens moet leren hoe zijn gedachten te verwoorden, maar uiteindelijk is de kunst van expressie een persoonlijke vaardigheid.

10. Nederlanders hebben Indonesië niet drie eeuwen lang gekolonialiseerd. Het duurde echter zo lang om van Indonesië één land te maken, en af en toe heeft Indonesië nog steeds moeite om deze eenheid te handhaven.

Deze stellingen worden opponeerbaar en verdedigbaar geacht en zijn als zodanig goedgekeurd door de promotor, Prof. dr. ir. A.I. Stankiewicz.

Hydrothermal synthesis and characterization of 3R polytypes of Mg-Al Layered Double Hydroxides

Widya Nugraha Budhysutanto

Hydrothermal synthesis and characterization of 3R polytypes of Mg-Al Layered Double Hydroxides

Proefschrift

ter verkrijging van de graad van doctor
aan de Technische Universiteit Delft,
op gezag van de Rector Magnificus Prof. ir. K.C.A.M. Luyben,
voorzitter van het College voor Promoties,
in het openbaar te verdedigen op maandag 20 december 2010 om 10:00 uur

door

Widya Nugraha BUDHYSUTANTO

scheikundig ingenieur
geboren te Semarang, Indonesië

Dit proefschrift is goedgekeurd door de promotor:
Prof. dr. ir. A.I. Stankiewicz

Copromotor:
Dr. ir. H.J.M. Kramer

Samenstelling promotiecommissie:

Rector Magnificus   Voorzitter
Prof. dr. ir. A.I. Stankiewicz   Technische Universiteit Delft, promotor
Dr. ir. H.J.M. Kramer   Technische Universiteit Delft, copromotor
Prof. dr. ir. P.J. Jansens   Technische Universiteit Delft
Prof. dr. P.W.A. Cains   Technische Universiteit Delft
Prof. dr. E. Vlieg   Radboud Universiteit Nijmegen
Prof. dr. K.J. Roberts   University of Leeds
Dr. D.T.L. van Agterveld   AkzoNobel
Prof. ir. J. Grievink   Technische Universiteit Delft, reservelid

Prof. dr. ir. G.M. van Rosmalen heeft in belangrijke mate aan de totstandkoming van het proefschrift bijgedragen.

Cover design by W.N. Budhysutanto (2010)
Cover picture: M.C. Escher's "Symmetry Drawing E103" © 2010 The M.C. Escher Company-Holland. All rights reserved. www.mcescher.com

To my beloved parents

Table of Contents

Chapter 1

Introduction

1.1. Layered Double Hydroxides

Layered Double Hydroxides (LDH) forms a unique group of clays that have an anionic exchange capability[1]. Contrary to the large number of cation exchanger materials, the number of known anion-exchange frameworks is rather limited. In recent decades, LDH have been widely examined for many different applications such as their use as catalysts[2-4], adsorbents[5-7], in flame retardant materials[8-10] and traditionally as medicine for ulcers[11]. The structure of LDH is based on that of brucite $Mg(OH)_2$, where magnesium ions are octahedrally coordinated with hydroxide ions positioned as double hydroxide sub-layers[12,13]. In Mg-Al LDH, some of the magnesium ions are replaced by aluminium ions, which results in a positively charged metal layer. Anions are therefore incorporated in the lattice between the so-called octahedral metal layers to maintain electroneutrality. These anions are arranged together with water molecules in interlayers between the octahedral metal layers. The general formula for LDHs, based on a combination of divalent and trivalent metal cations, can be written as:

$$[M^{II}_{1-x}M^{III}_x(OH)_2][A^q_{x/q} \cdot nH_2O]$$
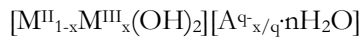
where M^{II} and M^{III} represent divalent and trivalent cations in the brucite-type octahedral layers, A is the interlayer anion with charge q, x is the fraction of the trivalent cation, and n is the number of water molecule incorporated in the crystal. Based on the general formula, LDH include a range of divalent versus trivalent ratios $R = M^{II}/M^{III} = \dfrac{(1-x)}{x}$, corresponding to the amount of anions needed for charge compensation.

The formation of pure LDHs is reported to vary in the range of $1.5 \leq R \leq 4.0$[12].

The divalent and trivalent metal cations in LDHs mainly belong to the third and fourth periods of the periodic classification of elements[14]:

- divalent cations: Mg, Mn, Fe, Co, Ni, Cu, Zn
- trivalent cations: Al, Mn, Fe, Co, Ni, Cr, Ga

In most cases, only weak bondings are formed between the interlayer anions and the octahedral metal layers. For that reason, a large variety of anion species can occupy the interlayer spacings[14]:

- halides: fluoride, chloride, bromide, …
- oxo-anions: hydroxide, carbonate, nitrate, sulfate, bromate, …
- oxo and polyoxo-metallates: chromate, dichromate, $(Mo_7O_{24})^{6-}$, $(V_{10}O_{28})^{6-}$, …
- anionic complexes: ferro and ferricyanide, $(PdCl_4)^{2-}$, …
- organic anions: carboxylates, phosphonates, alkyl sulphates, …

Shown in Figure 1 is an example of naturally occurring LDH called hydrotalcite. This LDH contains magnesium and aluminium in the octahedral metal layer and carbonates compensating the charge of the layer. Hydrotalcite is the mostly studied LDH, so sometimes LDH is also referred to as hydrotalcite-like compounds (HTlc).

Octahedral metal layer
$[M^{II}_{1-x}M^{III}_x(OH)_2]$
ex: $Mg_{0.66}Al_{0.33}(OH)_2$

Interlayer anions
$[A^q_{x/q}.nH_2O]$
ex: CO_3^{2-}
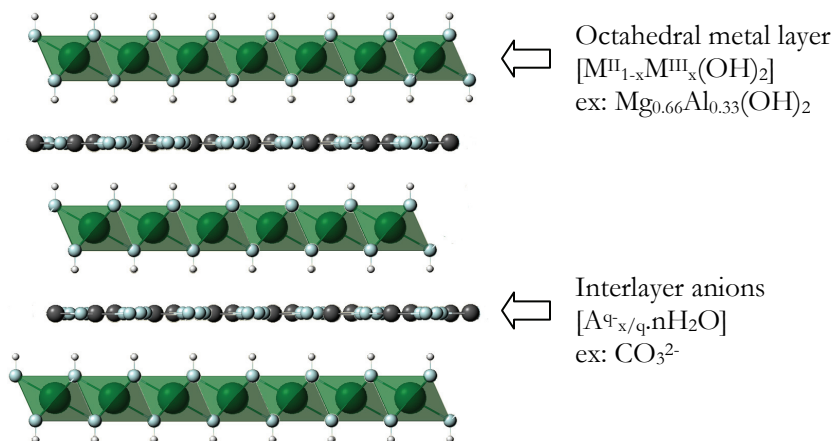
Figure 1. Structure of Layered Double Hydroxides (LDH)

Despite their numerous possible applications, the commercial applications of LDH are limited because of their complicated production process. Synthetic LDHs are produced batch wise, and the most common synthesis method is co-precipitation from pre-mixed metal salt solutions by addition of a basic solution to reach the crystallization pH of about 10 to 11[1,12]. In such precipitation process the local supersaturation at the mixing point is very high, resulting in high nucleation rates and thus in the formation of many very small crystals[15]. The basic shape of an LDH crystal is a hexagonal platelet. These large amounts of tiny crystals hardly grow out; instead they agglomerate in regions of less turbulence, resulting in a broad size distribution of agglomerated particles. In the agglomerated particles, the platelets are piled on top of each other. If the precipitation starts at a very high supersaturation, a number of the agglomerates are shaped as dessert roses.

The urea method is an alternative method to produce LDH, in which the alkalinity is provided by the hydrolysis of urea [16,17]. This method is seen as an ideal way for synthesis of LDH with carbonate in the interlayer because both of the anions liberated by the urea hydrolysis, hydroxides and carbonates, are the main components of the product[18]. By using urea as precipitating agent, the pH evolution and the nucleation rate can be better controlled, and a narrower particle size distribution of the primary hexagonal shaped crystals can be obtained [18-20]. Zhao[21] avoided a broad size distribution by completing the mixing and nucleation step in a very short time followed by a separate aging process. The agglomeration of the tiny particles was prevented by the use of a colloid mill. In all cases, however, heat treatment to improve the crystallinity of the product and extensive washing to remove the salt by-product are necessary. These processes are time consuming, expensive and produce a lot of waste.
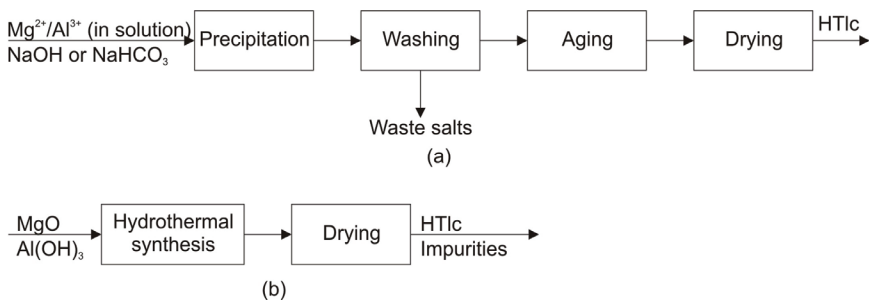
Figure 2. Block diagram of co-precipitation process (a) and hydrothermal synthesis process (b)

An alternative cleaner process for LDH synthesis is by hydrothermal treatment of the metal oxides in water [22,23]. The method involves dissolution of the metal oxides, subsequent precipitation of the LDH at the suitable pH, and heat treatment to improve product crystallinity in one pot.

No additional anion species or basic solutions are added as reactants, which contributes to the simplicity and sustainability of the method. As a consequence, this method is limited to the production of LDH with only hydroxides and for metal cations that are soluble in water. Of the listed possible cations for the formation of LDH, magnesium oxide is the only suitable candidate for the method. Upon contact with water, magnesium oxide slightly dissolves in water increasing the pH to approximately 11, a suitable pH for the precipitation of LDH. Aluminium, the trivalent metal cation in hydrotalcite is amphoteric; it does not dissolve in water, but in acidic and alkaline solutions. Newman[24] investigated the hydrothermal treatment of slurries of magnesium oxide (MgO) and aluminium trihydroxide (ATH) in water for direct conversion into Mg-Al LDH. The synthesis resulted in the formation of two different polytypes of Mg-Al LDH, namely $3R_1$ and $3R_2$ at 90 °C and 170°C, respectively.

1.1.1. Polytypes of LDHs

In layered materials, polytypes are structures that result from the sequence of the oxygen packing in subsequent layers. These sequences also determine the number of layers per unit cell. As the polytype is only defined by the layer stacking sequence of the octahedral metal layers, the chemical composition of the compounds varies based on the composition of the divalent and trivalent metal ratio, as well as on the composition of the interlayer anion. For the explanation of LDH polytypes, the close packing of the hydroxyl groups with respect to the metal cations in the octahedral layers is first considered. In the atomic arrangement of the layers, the oxygen atoms surrounding the metal cation can occupy an A, B, or C position (Figure 3a). Analogously, the cation can occupy an interstitial a, b, or c position. Using this notation, an octahedral metal layer can be denoted

for example as an AbC layer. The oxygens of the following octahedral metal layer can again occupy an A, B, or C position, thus forming different types of interlayer arrangements. A trigonal prismatic (P-type) interlayer arrangement is formed when the next top oxygen sub-layer occupies the same position as the bottom oxygen sub-layer of the previous octahedral metal layer, such as in Ab**C** = **C**aB (Figure 3b-1). An octahedral (O-type) interlayer is formed in arrangements such as AbC – **B**cA **(**Figure 3b-2) or **A**bC – **A**bC (Figure 3b-3), where the next top oxygen sub-layer occupies the same position as the cation or the top oxygen sub-layer of the previous octahedral metal layer.
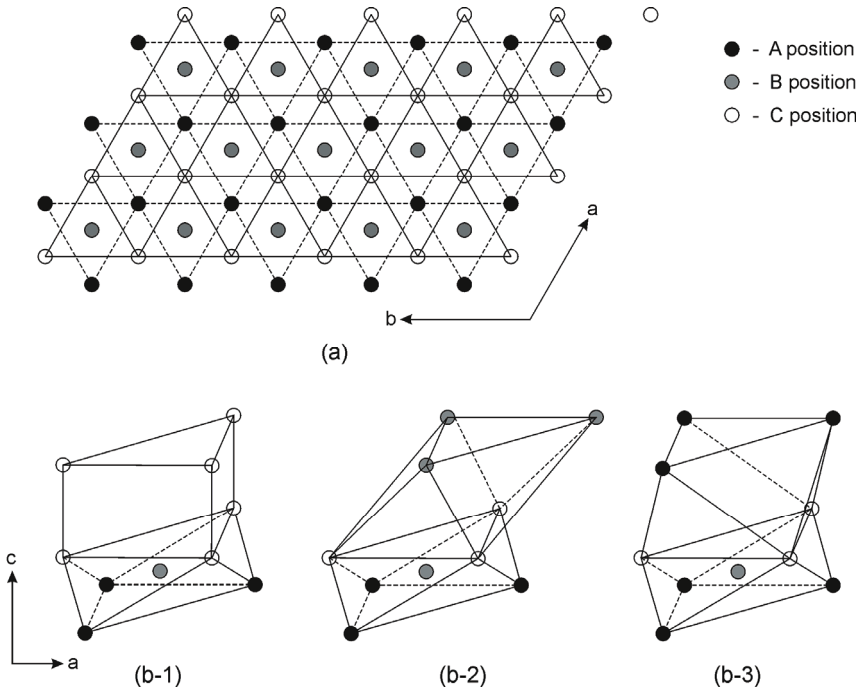
Figure 3. Atom positions for octahedral metal coordination in the layer (a) and the interlayer sites: trigonal prismatic (b-1), octahedral interlayer (b-2, b-3). Adapted from Bookin and Drits [25]

Based on the oxygen sequence in the octahedral metal layer, various polytypes of LDH can be deduced. The simplest, single layer polytype with hexagonal symmetry is 1H polytype, denoted as AC – AC, where the unit cell repeats itself after each layer. Notice that the cation position is omitted to simplify the notation. Bookin and Drits[25] explored the variety of polytypes, and concluded that there are three possible two layers polytypes, all having hexagonal symmetry, and nine possible three layers polytype with either hexagonal or rhombohedral symmetry. The naturally occurring Mg-Al LDH exists as two different polytypes[26]: two layer $2H_1$ polytype with hexagonal symmetry known as manasseite and three layer $3R_1$ polytype with rhombohedral symmetry known as hydrotalcite. The interlayers of both polytypes, having only trigonal prismatic arrangements, are occupied by carbonates. These two polytypes are commonly intergrown in nature, with manasseite generally forming the core and hydrotalcite the outer part of the grain[23].

Hydrotalcite is known to have a three layer unit cell with a rhombohedral symmetry. Of the three layer polytypes, only two polytypes have rhombohedral symmetry (space group $R\bar{3}m$): polytype $3R_1$ stacked as …=AC=CB=BA=AC=… with only P-type interlayer positions, and polytype $3R_2$ stacked as …– AC–BA–CB–AC–… with only O-type interlayer positions. Hydrothermal synthesis is the only reported method that results in the formation of both polytype $3R_1$ and $3R_2$ Mg-Al LDH[24]. All other methods produce only polytype $3R_1$ or 1H. In hydrothermal synthesis, polytype $3R_2$ is up to now considered to be the high temperature modification of polytype $3R_1$[24]. The interconversion of these polytypes was only reported to be possible through calcination of the material and rehydration at the corresponding temperature[24]. So far however, the

structure and the characteristics of polytype $3R_2$ Mg-Al LDH, which can only be synthesized by the hydrothermal method are still unknown.

1.1.2. Characterization of 3R Mg-Al LDH polytypes

X-Ray Powder Diffraction (XRPD) is the main technique for characterization of the interlayer spacing, layer stacking and Mg/Al ratio of the octahedral metal layers in LDHs. The diffractogram consists of basal and non basal reflections. The basal reflections (00l) represent the thickness of an l number of layers, each consisting of one octahedral metal layer and one interlayer. For the 3R polytype, the c-parameter of the crystal equals three times the d-spacing of the (003) reflection. Another important reflection is the (110), which represents the distance between two metal cations in the octahedral layer. The a-parameter of the crystal equals two times the d-spacing of the (110) reflection[13]. Since aluminium is smaller than magnesium, the isomorphic replacement of magnesium ions by aluminium ions in the octahedral metal layer causes a distortion. The Mg/Al ratio in the layer is therefore reflected by the d(110)-spacing[27,28].

The intensities of the non basal reflections are used to distinguish between the various polytypes. Bookin and Drits[25] calculated those intensities for various polytypes based on the stacking of the octahedral metal layer, while not taking into account the X-ray scattering of anions and interlayer water, the changes in the cation composition of the octahedral metal layer and the distortions in the hydroxide framework. Based on the calculation, polytype $3R_1$ is indicated by the strong intensities of the (01(l+1)) over the (10l) reflections with $l = 3n + 1$ (n = integer) and vice versa for polytype $3R_2$. Owing to the platelet shape of the primary LDH crystal, the specimens for

XRPD measurement usually have a preferred orientation. This preferred orientation results in the stronger measured intensity of the basal reflections.

Fourier transformed infrared (FT-IR) is the main technique to identify the anion present in the interlayer of the LDH. An intercalated anion would interact with the interlayer water molecules and/or hydroxides from the octahedral metal layer of LDHs. Thus changes can be expected in the FT-IR bands compared to those of the free anion. For example the intercalated carbonates mostly show infrared banks around roughly 1360-1400, 875 and 670 cm^{-1} compared to the bands around 1415, 880 and 680 cm^{-1} for the free carbonate [Rives, 2001]. Although in hydrothermal synthesis the attraction of carbonate ions from the air by the strongly basic solution is avoided, there still are some carbonate ions present which come from the raw materials. According to the measured FT-IR spectra by Newman, the synthesized $3R_2$ contains less carbonates compared to the $3R_1$ polytype. The polytype $3R_2$ was therefore postulated to contain more hydroxide interlayer anions.

1.2. Objectives and Scope of the research

Hydrothermal treatment of MgO and ATH is an alternative method for a sustainable and simple production of Mg-Al LDH. This method can furthermore yield a unique polytype $3R_2$ which structure and properties are not yet understood. The main objectives of this thesis are the following:

1. exploration and optimization of the hydrothermal method for the synthesis of 3R polytypes of Mg-Al LDHs,
2. characterization of 3R polytypes of Mg-Al LDHs, especially of polytype $3R_2$.

In the first part of the thesis, the production of Mg-Al LDH by hydrothermal treatment of MgO and ATH was explored. It is the only method to produce both polytypes $3R_1$ and $3R_2$, so optimization of the method was needed for each polytype. Because the synthesis proceeds by dissolution of the solid reactants and precipitation of the product, the effect of reactant pre-treatment towards the conversion rate, product yield and polytype selectivity was investigated. Another optimization parameter investigated was the heating rate towards the designated temperature and its effect upon the crystal shape. Furthermore, in order to optimize the conditions for the synthesis of each polytype, the transition temperature between the two 3R polytypes of Mg-Al LDH was established.

The second part of the thesis is focused on polytype $3R_2$ Mg-Al LDH known as the high temperature modification formed during hydrothermal synthesis. The chemical composition is however, unknown and was subject for investigation in this thesis. As this polytype arises from a different interlayer stacking arrangement (octahedral) compared to $3R_1$ (trigonal prismatic), the interlayer of polytype $3R_2$ was studied in detail. The unravelling of the structure of polytype $3R_2$ was also carried out. Finally the stability of polytype $3R_2$ towards various anions as known to be accommodated in the $3R_1$ interlayer was investigated as well as the possibility to synthesize $3R_2$ hydrothermally in the presence of such ions.

1.3. Outline of the thesis

In chapter 2, the conversion rate, product yield and polytype selectivity by hydrothermal synthesis were optimized by varying the particle size of the MgO and ATH reactants. Various pre-treatment methods such as blender, ultrasound and wet grinding were applied to influence the reactant particle

sizes. The blending and pre-treatment with ultrasound were carried out for the mixture of both reactants in water. While for wet grinding, the pre-treatment was also studied for each reactant separately. The synthesis was carried out at 80 °C and 170 °C in an autoclave to obtain polytype $3R_1$ and $3R_2$ respectively.

In chapter 3, the conversion rate to reach similar product crystallinity was compared for conventional heating in an autoclave and for microwave heating in a multi-mode microwave cavity. The microwave heating was then studied further for variation of initial Mg/Al ratio of 1, 2 and 3, and for variation of microwave power of 400, 800 and 1600 watts. The shape of the crystals was characterized with SEM, AFM and STEM-EDX. Also the mechanism of crystal growth was explored.

Chapter 4 deals with the transformation between polytype $3R_1$ and $3R_2$. The transformation temperature, the transformation kinetics at different temperatures, and the relative solubility of the two polytypes were studied. This determines the chemical conditions and synthesis temperature required for the formation of pure $3R_1$ or $3R_2$. The transformation study was carried out by seeding with the other polytype followed by hydrothermal treatment at 50, 80, 110, 140, and 170 °C.

The next chapters are focused on polytype $3R_2$ Mg-Al LDH. The synthesis of polytype $3R_2$ Mg-Al LDH has only been reported as feasible by hydrothermal synthesis, and its composition and interlayer arrangement were thoroughly explored in chapter 5. Polytype $3R_2$ was synthesized by a direct hydrothermal synthesis and by a two-step hydrothermal synthesis method. The chemical composition of polytype $3R_2$ was investigated by the

direct synthesis method from a reaction mixture with an initial Mg/Al ratio of 1.0 to 2.0, and determined on the basis of by product formation. The interlayer arrangement of polytype $3R_2$ was explained from the product of the two-step synthesis method by XRPD, FT-IR, and 27-Al solid NMR.

In chapter 6, a detailed analysis of the crystal structure of polytype $3R_2$ was carried out based on the XRPD diffractogram measured by CuKα and by synchrotron radiation. The synchrotron measurement was carried out in a spinning capillary to eliminate the preferred orientation effect of the sample. In order to solve the structure of polytype $3R_2$, structural models, based on possible interlayer arrangements as revealed by FT-IR and 27-Al solid-state NMR was build. The simulated diffractogram from the model was then subjected to a Rietveld refinement against the measured XRPD diffractogram.

In chapter 7 various anions that could possibly mediate the formation of polytype $3R_2$ were studied. Polytype $3R_1$ was synthesized and subsequently subjected to various anion salt solutions at 170 °C. Further, the stability of synthesized polytype $3R_2$ towards exchange by various anions was examined at 170 °C. The anion salts studied include, carbonates, sulphates, bromide, dihydrogen phosphate, oxalate, oleate and stearate.

Reference List

[1]   P.S.Brateman, Z.P.Xu and F.Yarberry, Layered Double Hydroxides
       (LDHs), in: S.M.Auerbach, K.A.Carrado, P.K.Dutta (Eds.) ,
       Handbook of Layered Materials, Marcel Dekker, Inc., New York,
       2004, pp. 373-474.

[2]   P.D.Damien , M.G.Eric , B.Guido, Exploring, Tuning, and
       Exploiting the Basicity of Hydrotalcites for Applications in
       Heterogeneous Catalysis, Chemistry - A European Journal 15 (2009)
       3920-3935.

[3]   Y.Ono, Solid base catalysts for the synthesis of fine chemicals,
       Journal of Catalysis 216 (2005) 406-415.

[4]   D.Tichit, B.Coq, Catalysis by Hydrotalcites and Related Materials,
       CATTECH 7 (2003) 206-217.

[5]   K.Kuzawa et. al., Phosphate removal and recovery with a synthetic
       hydrotalcite as an adsorbent, Chemosphere 62 (2006) 45-52.

[6]   Z.Yong, A.E.Rodrigues, Hydrotalcite-like compounds as adsorbents
       for carbon dioxide, Energy Conversion and Management 43 (2002)
       1865-1876.

[7]   Y.You, H.Zhao, G.F.Vance, Surfactant-enhanced adsorption of
       organic compounds by layered double hydroxides, Colloids and
       Surfaces A: Physicochemical and Engineering Aspects 205 (2002)
       161-172.

[8]   Y.-J.Lin et. al., Modulating effect of Mg-Al-CO3 layered double
       hydroxides on the thermal stability of PVC resin, Polymer
       Degradation and Stability 88 (2005) 286-293.

[9]   P.Loffeld,P.Loffeld, Universiteit Utrecht(2004).

[10]   L.van der Ven et. al., On the action of hydrotalcite-like clay materials
       as stabilizers in polyvinylchloride, Applied Clay Science 17 (2000) 25-
       34.

[11] C.Del Hoyo, Layered double hydroxides and human health: An overview, Applied Clay Science 36 (2007) 103-121.

[12] F.Cavani, F.Trifiro, A.Vaccari, Hydrotalcite-type anionic clays: Preparation, properties and applications, Catalysis Today 11 (1991) 173-301.

[13] D.Evans and R.Slade, Structural Aspects of Layered Double Hydroxides, in: 2006, pp. 1-87.

[14] A.de Roy, C.Forano and J.-P.Besse, Layered Double Hydroxides: Synthesis and Post-Synthesis Modification, in: V.Rives (Ed.) , Layered Double Hydroxides: Present and Future, Nova Science Publisher, Inc., New York, 2001, pp. 1-38.

[15] J.He et. al., Preparation of layered double hydroxides, Layered Double Hydroxides 119 (2006) 89-119.

[16] M.M.Rao et. al., Hydrothermal synthesis of Mg-Al hydrotalcites by urea hydrolysis, Materials Research Bulletin 40 (2005) 347-359.

[17] U.Costantino et. al., New Synthetic Routes to Hydrotalcite-Like Compounds - Characterisation and Properties of the Obtained Materials, European Journal of Inorganic Chemistry 1998 (1998) 1439-1446.

[18] M.Ogawa, H.Kaiho, Homogeneous Precipitation of Uniform Hydrotalcite Particles, Langmuir 18 (2002) 4240-4242.

[19] M.Adachi-Pagano, C.Forano, J.P.Besse, Synthesis of Al-rich hydrotalcite-like compounds by using the urea hydrolysis reaction-control of size and morphology, J. Mater. Chem. 13 (2003) 1988-1993.

[20] J.-M.Oh, S.-H.Hwang, J.-H.Choy, The effect of synthetic conditions on tailoring the size of hydrotalcite particles, Solid State Ionics 151 (2002) 285-291.

[21] Y.Zhao et. al., Preparation of Layered Double-Hydroxide Nanomaterials with a Uniform Crystallite Size Using a New Method Involving Separate Nucleation and Aging Steps, Chemistry of Materials 14 (2002) 4286-4291.

[22]   G.Mascolo, Synthesis of anionic clays by hydrothermal crystallization
       of amorphous precursors, Applied Clay Science 10 (1995) 21-30.

[23]   I.Pausch et. al., Syntheses of disordered and Al-rich hydrotalcite-like
       compounds, Clays Clay Miner. 34 (1986) 507-510.

[24]   S.P.Newman et. al., Synthesis of the 3R(2) polytype of a hydrotalcite-
       like mineral, J. Mater. Chem. 12 (2002) 153-155.

[25]   A.S.Bookin, V.A.Drits, Polytype diversity of the hydrotalcite-like
       minerals; I, Possible polytypes and their diffraction features, Clays
       Clay Miner. 41 (1993) 551-557.

[26]   A.S.Bookin, V.I.Cherkashin, V.A.Drits, Polytype diversity of the
       hydrotalcite-like minerals; II, Determination of the polytypes of
       experimentally studied varieties, Clays Clay Miner. 41 (1993) 558-564.

[27]   M.Bellotto et. al., A Reexamination of Hydrotalcite Crystal Chemistry,
       The Journal of Physical Chemistry 100 (1996) 8527-8534.

[28]   C.de la Calle et. al., A crystal-chemical study of natural and synthetic
       anionic clays, Clays Clay Miner. 51 (2003) 121-132.

Chapter 2

Pre-treatment of reactants for the hydrothermal synthesis of Mg-Al Layered Double Hydroxides

ABSTRACT

Mg-Al Layered Double Hydroxides are layered materials with anionic exchange and adsorption properties. Alternatively, this material is synthesized by hydrothermal treatment of magnesium oxide (MgO) and aluminium trihydroxide (ATH). Since this synthesis deals with solid raw materials, and the reaction proceeds through a solution mediated dissolution-precipitation process, it is a challenge to enhance the reactivity of the raw materials. This chapter aims to compare the effect of three different pre-treatments: blending, ultrasound treatment, wet grinding and no pre-treatment on the conversion rate. In experiments at 80 °C, only $3R_1$ polytype Mg-Al LDHs was formed, while a mixture of $3R_1$ and $3R_2$ polytypes was found in the experiments at 170 °C. All the pre-treatment techniques cause a decrease in particle size of the raw materials whereby wet grinding induced the strongest effect. Experimentally the fastest conversions at both synthesis temperatures were achieved by wet grinding. A reaction mechanism is proposed which explains the observed conversions as a function of the particles size of the reactants, the exposure time of the MgO to water and the reaction temperature. Two important parameters to be taken into account in the synthesis are thus exposure to water prior to the reaction and the particle size of the raw materials.

2.1. Introduction

Hydrotalcite is an example of naturally occurring Layered Double Hydroxides (LDH), having anion exchange and adsorption properties. The crystal structure of LDH consists of positively charged layers built of specific combinations of metal hydroxides, with anions and water molecules in between [1]. The crystal structure of hydrotalcite is related to that of brucite, $Mg(OH)_2$, with some of the Mg^{2+} cations in the layer structure replaced by Al^{3+}. In order to maintain electroneutrality carbonate anions are intercalated between the layers. The formula of a naturally occurring hydrotalcite is $Mg_6Al_2(OH)_{16}(CO_3).4H_2O$.

Widespread use of the material is still limited due to its complex production process. Mg-Al LDHs are currently produced by precipitation from magnesium and aluminium salts solution in a batch reactor at an increased pH. This process suffers from a product with a low crystallinity, extreme long aging times to improve the product quality and extensive washing to remove the salt by-product. Hydrothermal synthesis is an alternative process to make Mg-Al LDHs. In this simple process, slurries of magnesium oxide (MgO) and aluminium trihydroxide (ATH) in water are hydrothermally treated. Compared to the conventional precipitation process the hydrothermal process consists of less processing steps and produces no waste. Because there are no carbonate ions in the solution, the chemical formula of the Mg-Al LDH is $Mg_4Al_2(OH)_{14}.4H_2O$. Furthermore, two different polytypes of Mg-Al LDHs namely $3R_1$ and $3R_2$ can be formed at different synthesis temperatures. These polytypes differs in its layer stacking sequences, which resulted in two types of interlayer position. Polytype $3R_2$ with an octahedral interlayer has a smaller interlayer distance compared to

the $3R_1$ counterpart with a trigonal prismatic interlayer [2]. The naturally occurring hydrotalcite with carbonate ions in the interlayer belongs to polytype $3R_1$. Other anions, such as nitrate, chloride, bromide, fluoride, have been reported also to occupy the interlayer in polytype $3R_1$[1]. The only reported occurrence of polytype $3R_2$ LDHs contains sulphate anion in its interlayer [3]. In the hydrothermal synthesis, polytype $3R_1$ is produced at temperatures below 90°C while the other polytype, $3R_2$, is produced at higher temperatures [4]. Staminirova suggested that the synthesis mechanism proceeds via a solution mediated dissolution-precipitation process. However, this conversion normally proceeds slowly [5].

In this study different pre-treatment techniques of the raw materials were applied, and their effect on the conversion rate, the polytype and the purity of the Mg-Al LDHs was investigated. The pre-treatment techniques include blending, ultrasound treatment, and wet grinding in a ball mill. The pre-treatment techniques reduce the particle size of the raw materials. All techniques may also induce stress in the pre-treated particles, which increases the chemical potential of the materials and therefore their solubility. The applied blender is a very simple equipment for home use, where the strongest collisions occur between the particles and the rotating knife. A commercial ultrasonic probe was used. Since there are a number of inherent cracks in any material, the application of ultrasonic energy to the raw materials is expected to have the capacity to induce crack propagation from within the particles towards their surface [6]. The raw material pre-treatment by wet grinding is performed in a commercial ball mill, in which the materials experience mechanical stress enforced by the collisions between the balls, the wall and the materials themselves.

2.2. Experimental Methods

Mg-Al LDHs were synthesized via a hydrothermal method. Starting materials consisted of Magnesium Oxide (MgO) from Martin Marietta (Zolitho 40), Aluminium Trihydroxide (ATH) from Alumill (F505) and distilled water. The ATH used is in the form of gibbsite. After the pre-treatment, the synthesis was carried out in a 1 litre high-pressure double walled Buchi autoclave. The autoclave was heated using an oil bath. In order to ensure a good mixing, the autoclave was also equipped with a Buchi magnetic drive stirrer, which was run at 1000 rpm during all experiments. The temperature inside the autoclave was measured with a Pt-100 thermometer. A manometer indicated the autoclave pressure while a rupture disc and a relief valve were installed as safety devices.

The feed of the synthesis was a 15%wt solid in water mixture, which was subjected to a pre-treatment method prior to the hydrothermal synthesis. The solid in water mixture consisted of a 2:1 ratio of MgO and ATH on a molar base. The blending was performed in a BL 101 GL blender from Miyako, the ultrasound treatment in a sonicator UIP250 from Hielscher GmbH., and the wet grinding in a Dispermat SL-M 100 from VMA-Getzmann GmbH. During pre-treatment samples were taken every 15 minutes. The pre-treated samples were analyzed for their particle size distribution by wet sampling in Microtrac S3500 laser diffraction unit and for their composition by X-Ray powder diffraction (XRPD). In most cases the raw materials were pre-treated together and only in one experiment they were treated separately. The pre-treated slurry was subsequently subjected to the hydrothermal synthesis at either 80 or 170 °C, in order to produce $3R_1$ or $3R_2$ polytype respectively. After 1 hour reaction, the autoclave was cooled down to 80 °C before the slurry product was taken out. The slurry

samples were then dried overnight in an oven at 50 °C and subsequently analyzed by Scanning Electron Microscopy JEOL 5400 and XRPD with CuKα radiation at a wavelength of 1.5406 Å. The experimental conditions are given in Table 1.

Table 1. Experimental conditions of pre-treatment and synthesis

Experiment	Pre-treatment time (mins)	Reaction temperature (°C)	Reaction time (mins)
No Pre-treatment	-	80	60
		170	
Blender	60	80	60
		170	
Ultrasound	60	80	60
		170	
Mixed wet ground	30	80	60
	90	170	
Separately wet ground	MgO = 30 ATH = 30	170	60

An additional experiment was also performed to investigate whether the synthesis already starts during prolonged grinding at room temperature. This slurry was subjected to 4 hours of grinding and samples were taken every 30 minutes. In some of the experiments, the MgO was also ground separately in ethanol.

2.3. Results and Discussion

Of all the pre-treatment techniques wet grinding gave the largest reduction in particle size, while ultrasound was the least effective size reduction method. The mean average particle sizes before the synthesis are presented in table 2. The degree of conversion after 1 hour synthesis was established by the conversion of the ATH by XRPD. In all experiments $3R_1$ polytype

Mg-Al LDHs was formed, and only at 170 °C where the conversion was almost complete for ATH (96-98%) some $3R_2$ polytype Mg-Al LDHs was also formed. Partial formation of $3R_1$ in the 170 °C experiments apparently already occurred during the heating up period. With respect to Mg-Al LDHs purity, two different impurities are detected in the end product, namely MgO and crystalline $Mg(OH)_2$ or brucite. MgO impurities indicate un-reacted MgO raw material, while brucite is a by-product of the synthesis. Only in the wet grinding experiments no trace of MgO was left at the end of the experiment. The low content of MgO in these experiments corresponds with the low brucite content. This indicates that wet grinding is an effective pre-treatment technique.

Table 2. Experimental Results

T (°C)	Experiment	D-50 Before Synthesis (µm)	Gibbsite (Al(OH)$_3$) Conversion	Periclase (MgO) Content*	Brucite (Mg(OH)$_2$) Content*	3R$_2$/3R$_1$ ratio
80	No Pre-treatment	8.5	81 ± 2%	++	++	no 3R2
	Blender	6.7	77 ± 2%	+	++	
	Ultrasound	7.6	74 ± 2%	+	+++	
	Mixed wet ground	6.7	88 ± 2%	-	+	
170	No Pre-treatment	8.5	96 ± 2%	++	++	1.1 ± 0.1
	Blender	6.7	93 ± 2%	++	+++	1.9 ± 0.2
	Ultrasound	7.5	92 ± 2%	++	++++	1.8 ± 0.2
	Mixed wet ground	3.6	98 ± 2%	-	+	1.1 ± 0.1
	Separately wet ground	MgO = 2.4 / ATH = 2.6	98 ± 2%	-	++	2.1 ± 0.2

* the qualitative amount is indicated by the number of '+' signs.

The conversions as presented in Table 2 were derived from XRPD patterns such as shown in Figure 1. The XRPD pattern in this figure relates to the synthesis products after 1 hour at 170 °C. On the X axis, the reference

patterns of the LDH-3R$_1$, LDH-3R$_2$, ATH, brucite, and MgO are indicated by vertical bars. Preferred orientation of the Mg-Al LDHs platelets during sample preparation is likely to occur. Therefore the intensities of the (003) and (006) Mg-Al LDHs reflections at about 12 and 24 degrees 2-theta are much stronger than would be the case for random orientation. The XRPD patterns have many overlapping reflections especially for brucite, which makes quantitative interpretation of the patterns difficult. In order to interpret the results of the experiment, several distinct reflections for each component were chosen. For gibbsite the 18.4 degree 2-theta reflection was selected, while for periclase (MgO) and brucite the 42.9 and 37.9 degree 2-theta positions were chosen respectively. The ATH conversion was calculated by comparing the integrated gibbsite reflection area at the range of 17.0-19.0 2-theta degree from the pattern with that of the ATH raw material. The periclase and brucite contents are only represented qualitatively. For ratio of polytype 3R$_2$/3R$_1$, the reflections at 34 and 35 degree 2-theta degree were chosen for the 101 and 012 reflections respectively.
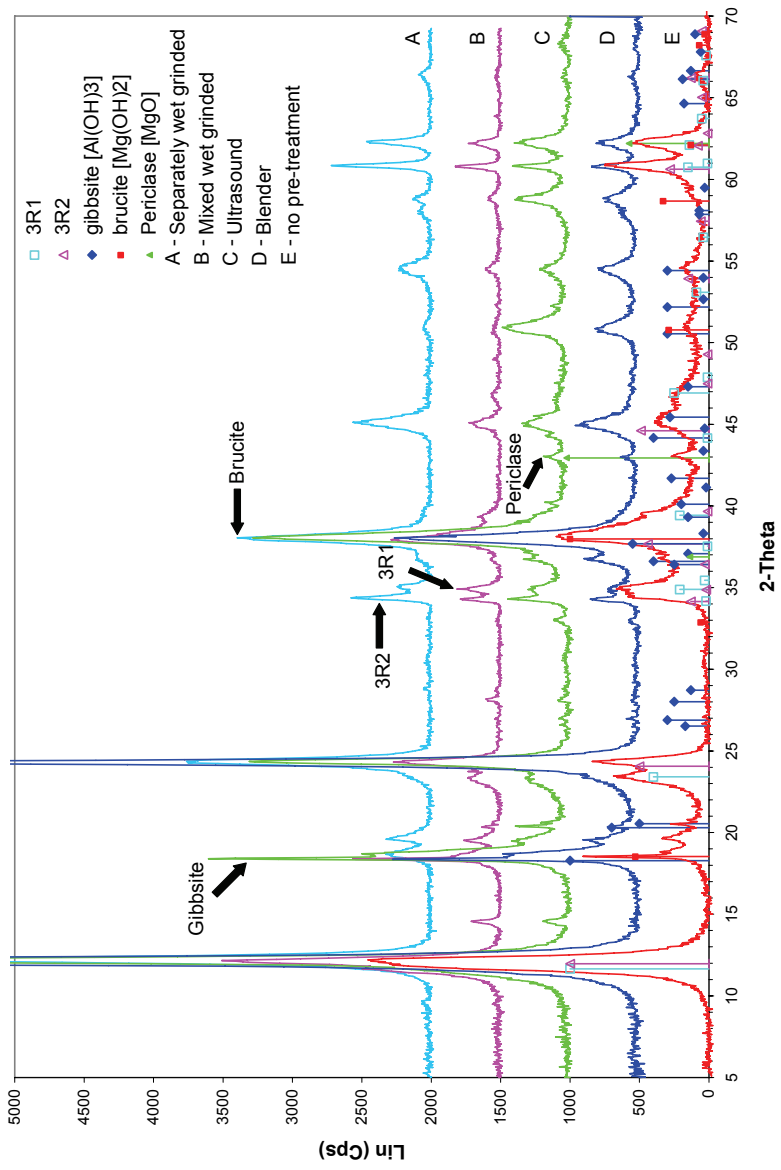
Figure 1. XRD pattern of synthesis at 170 °C with different pre-treatments

Comparison of the ATH conversion at 80 °C indicates that the best result was obtained for mixed wet grinding (88%) corresponding with the smallest particle size achieved after pre-treatment. Mixing of the raw materials during wet grinding also has a positive effect on the conversion. Pre-treating the raw materials by blending (77%) and ultrasound treatment (74%) does not improve the gibbsite conversion compared to the un-treated raw materials (81%) even though the particle sizes decrease due to the pre-treatment. A similar trend is observed in the ATH conversion at 170 °C for the pre-treatment by blending (93%) and ultrasound (92%). Here the conversion was even lower than that of the un-treated samples (96%). Apparently blending and ultrasound treatment are not effective pre-treatment techniques for this synthesis. On the other hand, the ATH conversion at 170 °C increases to 98% when the raw materials are wet ground. The $3R_2$ and $3R_1$ ratio for both experiments with wet ground raw materials show a significant difference. When MgO and ATH were ground together, the $3R_2/3R_1$ ratio is smaller. This suggests that in the mixed milling experiment some $3R_1$ polytype Mg-Al LDH is already formed during the grinding process. The XRD patterns of the samples taken during 4 hours mixed wet grinding, showing Mg-Al LDH peaks, support this suggestion.

In order to explain the observed results a mechanism as illustrated in Figure 2 is proposed. When brought into contact with water MgO forms a layer of amorphous $Mg(OH)_2$ on its surface. Upon prolonged contact with water, this amorphous $Mg(OH)_2$ layer will transform into crystalline $Mg(OH)_2$ or brucite. Amorphous $Mg(OH)_2$ has a higher solubility and is therefore more reactive than the crystalline form. However, when the amorphous $Mg(OH)_2$ has transformed to its crystalline form, this crystalline layer prevents the

MgO core from further dissolution. Thus, blinding of the MgO core occurs. This blinding phenomenon will inhibit further conversion of the reactants. Grinding of the MgO decreases the particle size and thus increases the specific surface area of the crystals so more amorphous $Mg(OH)_2$ can be formed, and less blinding occurs. The formation of amorphous $Mg(OH)_2$ is accompanied by an increase in pH of the solution to pH>11. At this basic condition, ATH dissolves in the solution as $Al(OH)_4^-$. Grinding of the ATH causes size reduction and possibly internal stress that contribute to its dissolution rate. When MgO is separately wet ground in water, formation of crystalline brucite can occur. Thus more brucite is observed than in the mixed wet grinding experiment.
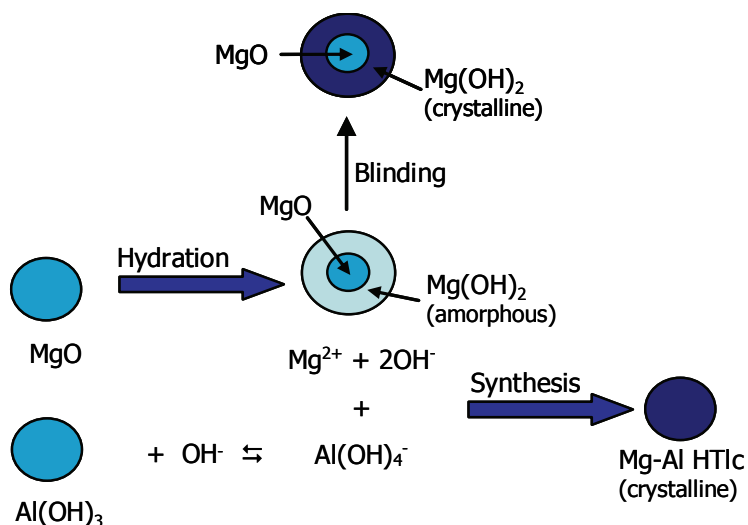

Figure 2. Proposed Synthesis Mechanism for Hydrothermal Synthesis

The slow conversion of amorphous into crystalline $Mg(OH)_2$ explains why the no pre-treatment experiment at 80 °C show better results than those of blending and ultrasound treatment. In the last two cases the MgO is longer exposed to water before the temperature is increased. At 170 °C, a high $3R_2$

polytype content can be achieved by preventing the formation of $3R_1$ polytype during pre-treatment and heating up time. Both requirements can be achieved by separate MgO and ATH pre-treatment and by feeding the ATH at the highest temperature possible (90 °C). The higher brucite formation in the case of the separately wet ground experiments may be prevented when the MgO is ground in an organic solvent.

In order to verify this proposition, MgO was ground in ethanol and ATH in water separately. The MgO slurry was heated up to and kept at 90 °C in order to evaporate the remaining ethanol before the ATH slurry was fed. The synthesis time was increased to 2 hours in order to ensure a complete ATH conversion. Only $3R_2$ polytype and less crystalline brucite compared to separate wet grinding in water are detected in the synthesis product. This indicates that by wet grinding in ethanol, a small MgO particle size along with less brucite formation can be achieved. In case of separate milling, the ATH pre-treatment also plays in important role in the formation of brucite. An additional experimental series with MgO pre-treated in ethanol and various ATH pre-treatments show that the smaller the ATH particle size is, the lower the amount of brucite found in the synthesis product.

2.4. Conclusions

The hydrothermal synthesis of hydrotalcite using the solid reactants MgO and ATH has been investigated. Especially the process conditions which affect the formation of two different polytypes and the influence of different methods of pre-treatment of the raw materials to improve the conversion rate have been analyzed.

Two polytypes of Mg-Al LDHs were produced in this research; the $3R_1$ polytype at 80 °C and $3R_2$ polytype at 170 °C. However, in the experiments at 170 °C, formation of $3R_1$ polytype also occurred during the pre-treatment and heating up period resulting in a mixture of both polytypes in the end product. A reaction mechanism is proposed in which an amorphous $Mg(OH)_2$ layer is formed at the surface of the MgO particles. This amorphous layer slowly converts into crystalline $Mg(OH)_2$ or brucite with lower solubility. If the particle size of the MgO is not small enough, the MgO can be blinded by a thin layer of brucite. This process in particular hampers the conversion of amorphous $Mg(OH)_2$ and ATH into LDHs at a prolonged exposure to the water before the temperature is increased and reaction takes place.

All pre-treatments methods have resulted in a smaller particle size of both MgO and ATH. The decrease in the MgO particle size gives rise to a higher surface area, decreasing the blinding of the MgO particles. Grinding is therefore effective to boost the conversion because it reduces the particle size significantly. In the synthesis of $3R_2$ polytype at 170 °C the formation of $3R_1$ polytype can be prevented by separate wet grinding of MgO and ATH. Additionally, grinding of MgO in an organic solvent can be an option to prevent the formation of brucite during pre-treatment.

2.5. Nomenclature

LDHs = Layered Double Hydroxides
ATH= Aluminium Trihydroxide = Gibbsite= $Al(OH)_3$
Periclase = MgO
Brucite= $Mg(OH)_2$

Reference List

[1] F.Cavani, F.Trifiro, A.Vaccari, Hydrotalcite-type anionic clays: Preparation, properties and applications, Catalysis Today 11 (1991) 173-301.

[2] A.S.Bookin, V.A.Drits, Polytype diversity of the hydrotalcite-like minerals; I, Possible polytypes and their diffraction features, Clays Clay Miner. 41 (1993) 551-557.

[3] D.L.Bish, Anion-Exchange in Takovite - Applications to Other Hydroxide Minerals, Bulletin de Mineralogie 103 (1980) 170-175.

[4] S.P.Newman et. al., Synthesis of the 3R(2) polytype of a hydrotalcite-like mineral, J. Mater. Chem. (2002) 153-155.

[5] T.Staminirova, G.Kirov, Cation composition during recrystallization of layered double hydroxides from mixed (Mg, Al) oxides, Applied Clay Science 22 (2003) 295-301.

[6] L.F.Gaete-Garreton, Y.P.Vargas-Hermandez, C.Velasquez-Lambert, Application of ultrasound in comminution, Ultrasonics 38 (2000) 345-352.

Chapter 3

Microwave as an Alternative Energy Source for Hydrothermal Synthesis of Mg-Al LDHs - Formation of a Novel Crystal Morphology

ABSTRACT

Hydrothermal synthesis of Mg-Al layered double hydroxide (LDH) from its oxides is an attractive alternative to the precipitation LDH from its salts. To optimize the efficiency of this synthesis and the product properties, the use of microwave as an alternative energy source is studied. The results show that compared to conventional heating, synthesis with microwave can lead to a four times faster conversion to obtain a comparable crystallinity. Microwave heating also resulted in smaller particle sizes and in a novel crystal shape. The novel shape is a hexagonal platelet with a hole in the middle. These donut-like crystals are formed at lower Mg/Al ratios and at a relatively high microwave power of 1600 W. This morphology provides enlargement of the specific surface area of the {hkl} faces, needed for adsorption application. A growth mechanism for the donut-like crystals is proposed based on AFM and STEM-EDX studies.

3.1. Introduction

Layered Double Hydroxides (LDH) forms a group of anionic clays with a general formula $[M^{II}_{(1-x)}M^{III}_{(x)}(OH)_2][A^{n-1}] \cdot mH_2O$ [1]. An example of naturally occurring LDH is hydrotalcite (Mg-Al LDH) with a brucite like, lamellar structure. The repeating structure consists of three layers of octahedrally coordinated magnesium and aluminium ions, with water and carbonate anions for charge compensation in the interlayer [2]. This interlayer can accommodate a large variety of organic and inorganic species such as pesticides, anionic surfactants, dyes, sulphates, chromates, carbonates, etc [3]. For that reason, it has been widely investigated as an adsorbent, an anionic exchanger, and as a basic catalyst [1].

Naturally occurring Mg-Al LDH is scarce, which has triggered the investigation of several synthesis methods. The most common way to produce Mg-Al LDH is by co-precipitation from magnesium and aluminium salts solutions at pH values ranging from 9-12 [4]. In such a precipitation method, however, nucleation, growth and agglomeration of the crystals occur simultaneously resulting in a broad particle size distribution. By using a base retardant such as urea as precipitating agent, the pH evolution and the nucleation rate can be better controlled and a narrow size distribution can be obtained [5]. Zhao [6] avoided a broad size distribution by completing the mixing and nucleation step in a very short time followed by a separate aging process. Agglomeration of the tiny particles was prevented by the use of a colloid mill. In all cases, however, heat treatment to improve the crystallinity of the product and extensive washing to remove the salt by-products are necessary. Microwave radiation has been applied after the precipitation process in LDH synthesis as an

alternative aging step, resulting in several advantages such as higher crystallinity and better ordering of the water molecules in the interlayer [7].

Hydrothermal synthesis is an alternative process to make Mg-Al LDH. In this less complicated process, slurries of magnesium oxide (MgO) and aluminium trihydroxide (ATH) in water are converted directly into hydrotalcite by a hydrothermal treatment. Compared to the conventional precipitation process the hydrothermal process consists of less process steps, and produces no waste. Furthermore, two different polytypes of Mg-Al LDH, namely $3R_1$ and $3R_2$ can be formed at different synthesis temperatures. The transition temperature of these polytypes is around 110 °C with $3R_1$ being the stable polytype at lower temperatures [8]. The crystal structure of polytype $3R_1$-carbonate has been solved from natural single crystal XRD [2]. The space group of the $3R_1$ polytype crystal is trigonal $R\bar{3}m$ with its lattice parameters given in the hexagonal setting (a = b, α= β= 90°, and γ= 120°). The XRPD pattern of $3R_1$-hydroxide is similar to that of the carbonate one.

In this research, microwaves are used as an alternative energy source in the hydrothermal synthesis of Mg-Al LDH from its oxides. Application of microwave radiation is expected to have a strong effect not only on the aging step but also on the synthesis step due to the fast and homogeneous heating. The Mg/Al ratios were varied from 1 to 3 and the microwave power from 400 to 1600 W. For comparison also a conventional hydrothermal synthesis was performed. The polytype, crystal shape, crystallinity and impurity content of the product were analyzed. In addition, the growth mechanism of such donut-like crystals was studied by Atomic Force Microscopy (AFM) and by Scanning Transmission Electron

Microscopy – Energy Dispersive X-Ray Spectroscopy (STEM-EDX). Compared to Scanning Electron Microscopy (SEM), the use of AFM for layered material permits a more detailed morphological observation, in particular measurement of the step heights [9]. STEM-EDX enables the identification of the chemical entities of the crystal.

3.2. Experimental Methods

3.2.1. Hydrothermal Synthesis Procedure

The synthesis of Mg-Al LDH was carried out by hydrothermal treatment of a 6 % solid wt mixture of magnesium oxide (MgO) from Martin Marietta (Zolitho 40), and aluminium trihydroxide (ATH) from Alumill (F505) in distilled water. The initial MgO and ATH have an average particle size (D-50) of 6 micron and 10 micron respectively. Prior to the synthesis, the particle sizes of the reactants were reduced by wet-grinding in two types of mills. The average PSD of the slurry was measured by laser diffraction with a Microtrac S3500. The synthesis was carried out by conventional heating in a 1 litre high-pressure double walled Buchi autoclave or by a Microwave Assisted Reaction System (MARS) provided by CEM.

In order to ensure good mixing, the autoclave was also equipped with a Buchi magnetic drive stirrer rotating at 1000 rpm during all experiments. The temperature inside the autoclave was measured with a Pt-100 thermometer. A manometer indicated the autoclave pressure while a rupture disc and a relief valve were installed as safety devices. The synthesis with MARS was carried out in a set of high pressure vessels XP-1500 Plus. Each vessel had a 100 ml volume, and in total 6 vessels mounted on a turntable was inserted in the microwave cavity. The temperature was

controlled with a fibre optic sensor (RTP-300 Plus) in the reference vessel and monitored in the other vessels with an infrared sensor. Commercial software dynamically controls the temperature profile adjusting the actual microwave power. The pressure was monitored with an ESP-1500 Plus pressure sensor with a pre-set maximum pressure for safety. Each vessel was also equipped with a magnetic stirrer.

In the first set of experiments MgO and ATH were wet-ground together in a Fritsch planetary micro mill Pulverisette 7 premium line. A 40% wt slurry with a Mg/Al ratio of 2.5 was ground at 400 RPM for 20 minutes, and diluted to 6% wt with preheated water. The 600 ml slurry was then charged into an autoclave at 90 °C for conventional hydrothermal heating. A set of 50 ml slurries was also prepared for synthesis with MARS. The microwave power was set at a maximum of 1600 W, reaching 90 °C in 100 s. Samples were taken after 15, 30, 60, 120, 180, and 240 minutes synthesis time. The samples were named M for microwave and C for conventional heating followed by the synthesis time, e.g. M-30, C-60.

In the second set of experiments 15% wt reactant slurries were wet-ground separately in a Dynomill KDL-Pilot. The MgO slurry was wet-ground for 15 minutes and the ATH slurry for 30 minutes. Afterwards, both slurries were diluted to 6% wt and mixtures with a Mg/Al ratio of 1:1, 2:1 and 3:1 were prepared. Each series of experiments consisted of 3 different Mg/Al ratios performed in duplicate. Each vial was filled with 50 ml slurry, sealed and mounted inside the MARS. The microwave power was set at a maximum of 1600 W with 12 minutes heating time to reach the pre-set temperature of 140 °C. The synthesis time of 140 °C was kept constant for

10 minutes. The samples were labelled M1600-1, M1600-2, and M1600-3 according to their Mg/Al ratio.

In the third set of experiments the effect of microwave power was studied at a Mg/Al ratio of 2:1. The microwave power was kept constant at 400, 800 and 1600 W until the synthesis temperature was reached. The corresponding heating times needed to reach 140 °C were 16, 7.5 and 3 minutes respectively. The synthesis time was set at 30 minutes. The samples were labelled as MP1600-2, MP800-2, and MP400-2 after the microwave power. Some of the separately wet-ground reactant slurries were kept overnight prior to the synthesis.

3.2.2. Characterization of the samples

After each synthesis, the system was cooled down until 70 °C before the slurry samples were collected. Part of the slurry sample was diluted with distilled water for SEM, STEM-EDX and AFM studies. For the preparation of the electron microscopy samples, 3 drops of the slurry were diluted with 15 ml distilled water. Of that dilution, 0.5 ml was added to another 15 ml of distilled water. One ml of the sample was then vacuum-filtered over a ceramic membrane filter Anodisc 25, which is used as sample support for SEM measurement. SEM images were taken with a Zeiss Gemini 1550. The STEM-EDX measurements were done for the diluted sample with a JEOL 2010F transmission electron microscope using an accelerating voltage of 200 kV and equipped with Thermo Noran EDX. A Carbon coated Cu grid was pulled through a diluted slurry sample and dried for 10 minutes before introducing the sample into the system vacuum. AFM images were made in tapping mode using a Digital Instrument Nanoscope Dimension D310

from the initial slurry sample diluted 4000x. Several drops of the diluted slurry were put upon a mica film and dried at 50 °C.

The rest of the slurry samples were then dried overnight in a 50 °C oven for X-Ray Powder Diffraction (XRPD) and Fourier Transform-Infrared (FT-IR) measurements. The XRPD measurements were done using a Bruker-AXS D5005 diffractometer with a Huber incident-beam Cu Kα monochromator and a Braun position sensitive detector. The 2θ-range was 5–70° with a step size of 0.0387° and a counting time per step of 1 s. The FT-IR measurements were done with a Nexus Thermo Nicolet 5700 spectrometer. Powder samples were pressed in small discs using a KBr matrix. The IR bands were recorded at a spectral range of 650-4000 cm $^{-1}$.

3.3. Results and Discussion

3.3.1. Comparison of conventional and microwave heating

The mixed grinding of the reactants in the first set of experiments resulted in a bimodal PSD with peaks at 0.53 and 2.5 micron. The smaller peak represents the MgO particles since its hardness on Mohs scale is less compared to that of ATH. XRPD measurements showed that both for microwave and conventional heating Mg-Al LDH was produced. Only polytype $3R_1$ was formed since the synthesis temperature of 90 °C was below the $3R_1/3R_2$ transition temperature of 110 °C [8]. Platelets were formed perpendicular to the c-axis. The unit cell parameter c is calculated to be 22.84 Å and the (003) reflection is the strongest. The unit cell parameter a, calculated mainly from the (110) reflection equals 3.05 Å. No crystalline $Mg(OH)_2$ (or brucite) impurities were detected in FT-IR spectra.
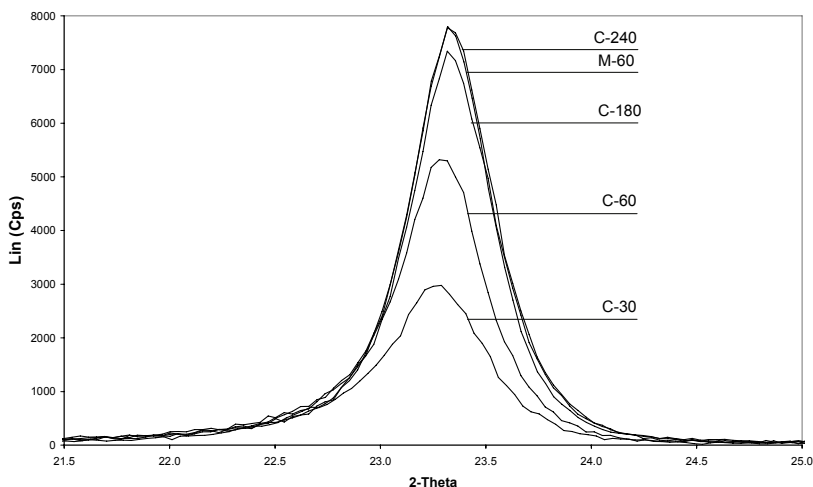
Figure 1. (006) reflection of the microwave (M-x) and autoclave (C-x) samples, x represents the heating time in minutes

The (006) reflection given in Figure 1 gives an indication of the quality of the product based on the extent to which crystallization of $3R_1$ has occurred. A longer synthesis time clearly enhances the crystallinity of the conventionally heated (C-x) samples. The same trend is observed for the microwave samples (data not shown). A comparable crystallinity was obtained after 240 and 60 minutes for the conventionally heated and the microwave heated experiments respectively. Microwave coupling seems to result in a better and more oriented ordering of water molecules in the interlayer, leading to the accommodation of additional water molecules [10]. Figure 1 demonstrates that microwave heating reduces the synthesis time. Furthermore, the average PSD of the microwave sample is smaller than that of the autoclave samples. Microwave introduces rapid and homogeneous heating, enhancing the overall nucleation rate, and thus smaller particle sizes are produced. Benito [10] consistently showed that when aged in a microwave field, LDH prepared by precipitation has a better crystallinity.

3.3.2. Influence of Mg/Al ratio in microwave synthesis

In the second set of experiments the magnesium and aluminium slurries were milled in water separately to prevent the formation of $3R_1$ during grinding. Separate grinding of the reactants in Dynomill resulted in D-50 values of 0.5 and 2.5 μm for MgO and ATH respectively. According to XRPD and FT-IR spectra, the hydrothermal synthesis resulted in the formation of Mg-Al LDH polytype $3R_1$ along with some crystalline $Mg(OH)_2$ (or brucite) by-product or unreacted ATH (gibbsite), depending on the experimental conditions. During the separate wet grinding process, some of the magnesium oxide converts into brucite, that is no longer reactive as a MgO source and remains as a by-product after the hydrothermal synthesis.

Despite the synthesis temperature of 140 ºC, the LDHs formed are those of polytype $3R_1$. Due to the rapid heating by microwaves, nucleation of polytype $3R_1$ apparently already happens during the heating up time within the metastable zone of polytype $3R_1$ that could even stretch beyond the solubility line of polytype $3R_2$. In a carbonate free solution, formation of polytype $3R_2$ beyond 110 ºC takes place (see chapter 4). If enough carbonate ions are present, this formation is inhibited by the inclusion of carbonate ions in the interlayer [11]. Although the amount of CO_2 in the synthesis mixture is low, $3R_1$ nuclei apparently have the chance to grow out and consume the supersaturation before $3R_2$ nuclei are formed or before any transformation of the developed $3R_1$ crystals into $3R_2$ crystals takes place. At 140 ºC the transformation rate is anyway very slow (see chapter 4).

The XRPD pattern (Figure 2) showed that all three samples contain Mg-Al LDH, while only sample M1600-1 with Mg/Al ratio 1 contains a large

amount of residual ATH. This result is understandable because in the lattice, two aluminium ions cannot be located next to each other due to charge repulsion, thus the lowest possible Mg/Al ratio in the octahedral layer is two [12]. The large excess of aluminium remained in the slurry as unreacted ATH. The Mg/Al LDH are of polytype $3R_1$, as shown by the stronger $(01(l+1))$ over $(10l)$ ($l = 3n + 1$, n = integer) reflections [13] (see chapter 1). The unit cell parameters a and c of the LDH, calculated from the 006 and 110 reflection respectively are 3.05 Å and 22.75 Å. The other two samples also have similar unit cell parameters.
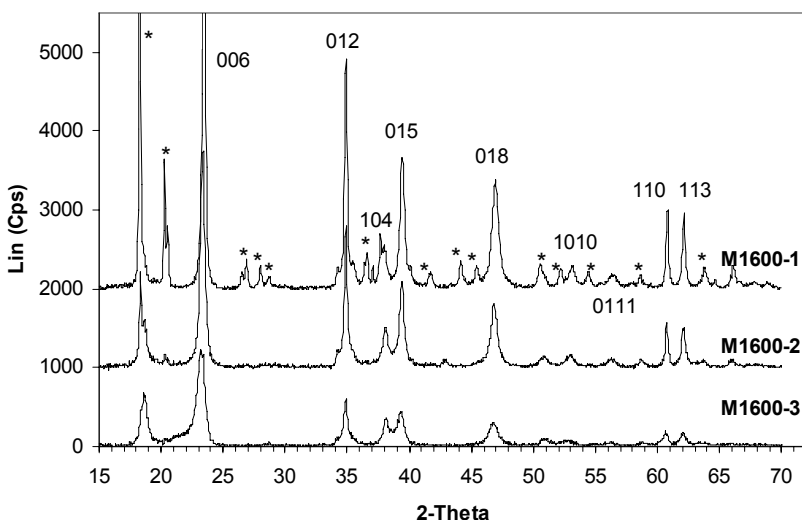
Figure 2. XRPD patterns of Mg-Al LDH synthesised at various initial Mg/Al molar ratios. The reflections denoted by * are of the residual ATH.

Figure 3 shows the FT-IR spectra of the samples at various initial Mg/Al molar ratios. The bands at around 3000-3700 cm^{-1} are the hydroxyl stretching mode of Mg–OH, Al–OH, H_2O and CO_3^{2-}–H_2O [14]. The band at 3698 cm^{-1} indicates the formation of brucite by-product [15], which increases

along with a higher Mg/Al ratio. The presence of unreacted ATH in sample M1600-1 is indicated by the bands at 3621, 3525, and 1022 cm^{-1} [16]. The band at 1640 cm^{-1} which corresponds to the bending mode of water (v_2) and the carbonate anti symmetric stretching mode band (v_3) at 1369 cm^{-1} indicate that the interlayer of the LDH is occupied by water and carbonate anions, where the latter anions form the charge compensation for the Al ions. The bands at 786 and 682 cm^{-1} represent the deformation mode of Al-OH [17] and the stretching mode of Al (octahedral) – O [18], respectively.
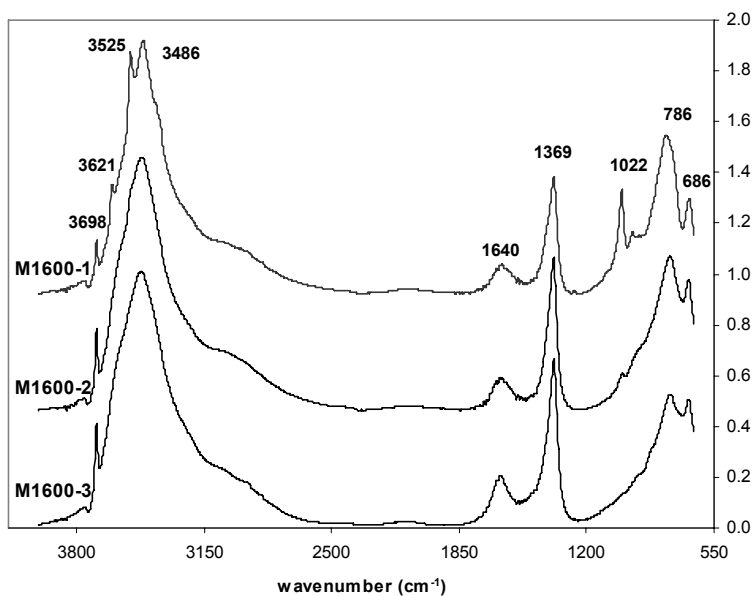
Figure 3. FT-IR spectra of Mg-Al LDH synthesised at various initial Mg/Al molar ratios.

Observation of the crystal shape with SEM revealed a unique crystal shape with a hole at the centre of the platelet (Figure 4). A crystal with this shape will further be referred to as a donut-like crystal. Mostly donut-shaped crystals were found at the lowest initial Mg/Al ratio. As the ratio increased

the crystals grow to closed platelets. At an initial Mg/Al ratio of 1, some sickle-shaped crystals were found along with the donut-shaped. At initial Mg/Al ratio of 2, thicker donut-shaped crystals were formed with some closed hexagonal platelets (Figure 4b). At an initial Mg/Al ratio of 3, where the ratio is closest to that of natural hydrotalcite, mostly closed hexagonal platelets were found (Figure 4c). The top and bottom faces of the platelets are (001) and $(00\bar{1})$.
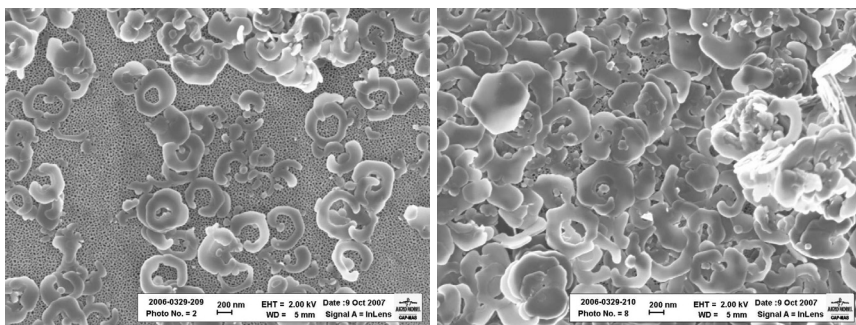
(a) Mg/Al = 1   (M1600-1)   (b) Mg/Al = 2 (M1600-2)
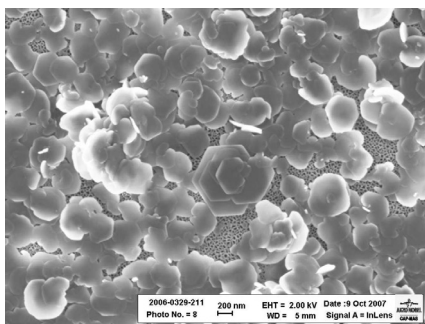
(c) Mg/Al = 3 (M1600-3)

Figure 4. SEM pictures of Mg-Al LDH formed at different initial Mg/Al molar ratios in microwave

An AFM image of a donut-shaped crystal from the sample with an initial Mg/Al ratio of 1 is given in Figure 5. The small rounded particles on top of the crystal are artefacts from drying of the sample. The donut-shaped crystal

has a diameter of approximately 1 µm and a total thickness of approximately 35 nm as measured by AFM. As shown in the image, the central opening in the middle part of the crystal (Figure 5a) has a closed surrounding form leading to a donut shape. On the crystal area surrounding the contact hole, growth patterns are still visible. The steps seem to grow from two directions, closing to a donut shape. The height of these steps is about 1.5 nm or approximately two octahedral LDH layers Figure 5b shows two LDH platelets growing from a single MgO sphere, indicating a double nucleation.

(a)   (b)
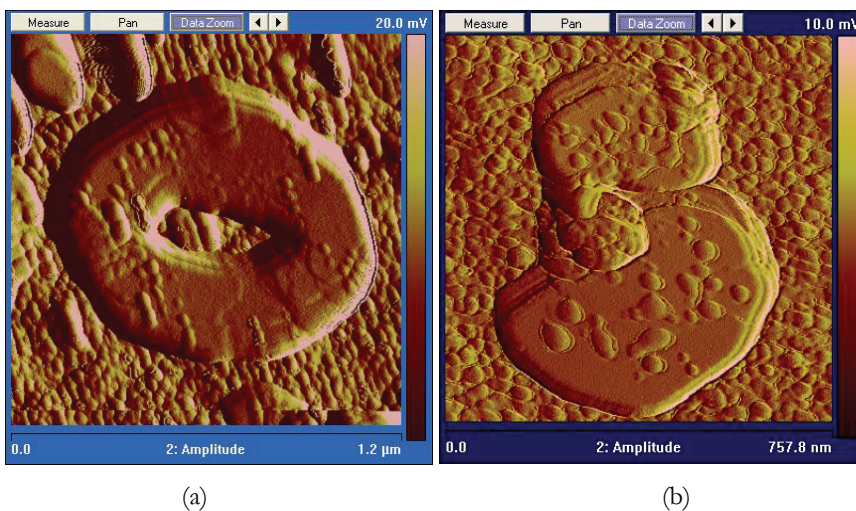
Figure 5. AFM images of sample M1600-1 with a Mg/Al ratio 1: donut-like crystal (a), initial sickle shaped crystal (b)

Figure 6 shows STEM-EDX element maps of a sickle-shaped LDH crystal from the sample with Mg/Al ratio 2. The STEM image shown at the top left side indicates that the diameter of the sickle is approximately 1 µm. A $Mg(OH)_2$ core, which is almost detached from the crystal, is visible at the centre of the crystal. According to the element maps, the core consists of only magnesium and oxygen entities (left bottom and top right). No

aluminium entity is found in the core (bottom right). Furthermore, the element maps also identify small particles of magnesium and oxygen entities (circled in black), corresponding to the brucite impurities found in the sample. The darker area at the bottom of the sickle, which consists of all the three elements, is another LDH sickle shaped crystal lying on top of the previous one. According to the EDX, the Mg/Al ratio of the donut crystal is approximately 2.0.
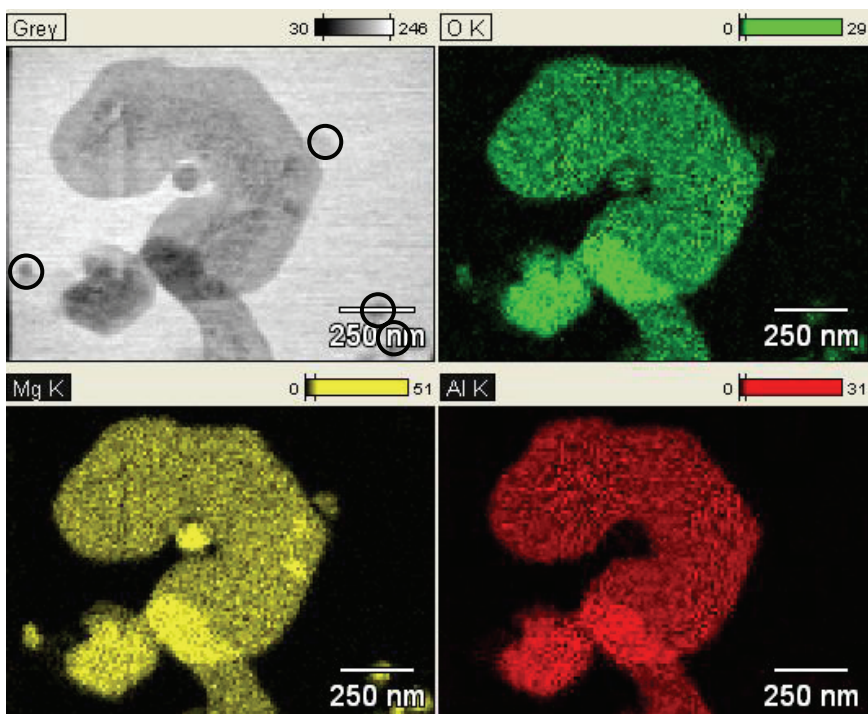
Figure 6. STEM-EDX element maps of a sickle shaped LDH crystal from sample M1600-2 with Mg/Al ratio 2, showing the distribution of oxygen, magnesium and aluminium.

At the highest Mg/Al ratio of 3, the SEM picture (Figure 4c) shows that all crystals formed closed platelets. A closer look at the crystals using AFM and STEM however shows that the centre of the crystal is thicker than the outer

ring (Figure 7). The STEM image also shows a possible gap between the crystal and its core. The element maps by STEM-EDX in Figure 8 show that the core has a higher Mg/Al ratio than the periphery. The EDX measurement of the single crystal shown in this figure resulted in an overall Mg/Al ratio of 2.6, with the core and the side of the crystal having Mg/Al ratios of 7.1 and 2.3 respectively. These results indicate that the synthesis of the LDH crystal has not yet been completed. They support, however the proposed mechanism of crystal growth in the microwave hydrothermal synthesis as given in section 3.3.4.

(a)   (b)
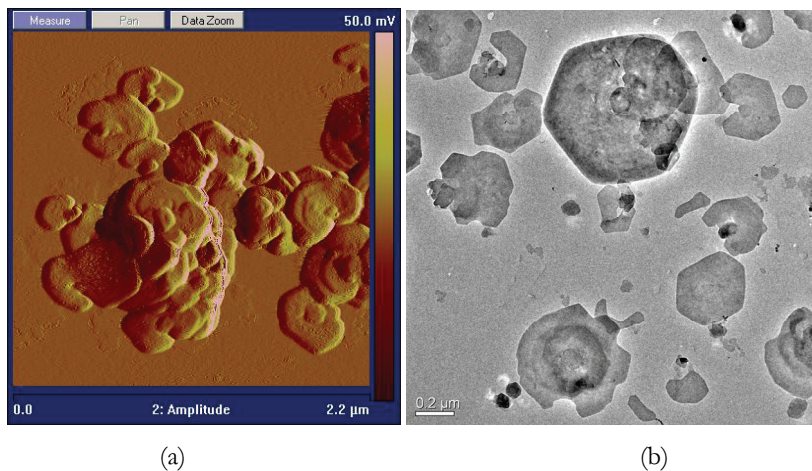
Figure 7. AFM images (a) and TEM images (b) of sample M1600-3 with an Mg/Al ratio 3.
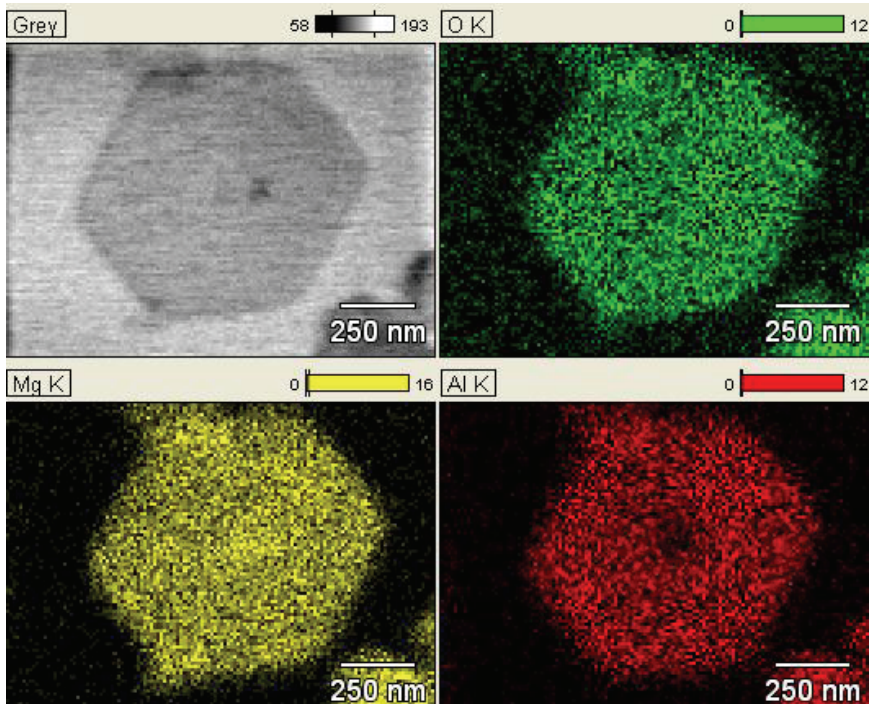
Figure 8. STEM-EDX element maps of sample M1600-3 with Mg/Al ratio 3.

3.3.3. Influence of microwave power in microwave synthesis

As microwave heating reduces the synthesis time of Mg-Al LDH, the influence of microwave power was investigated. In the third set of experiments, syntheses at 400, 800 and 1600 W with a Mg/Al ratio of 2 were carried out at 140 ºC. According to XRPD, the products contain $3R_1$ polytype Mg-Al LDH, along with un-reacted ATH and a small amount of brucite impurity. The separately wet-ground reactants in this series were kept overnight prior to the synthesis. Aging of the wet-ground MgO causes it to consolidate as the crystalline phase, which explains the high brucite content as shown by the FT-IR and XRPD. Accordingly, more unreacted ATH or gibbsite are found in product. The SEM pictures in Figure 9a also

suggest small particles of brucite or at least Mg rich particles among the larger Mg-Al LDH crystals. On SEM pictures with less magnification (pictures not shown) the unreacted ATH can also be spotted.
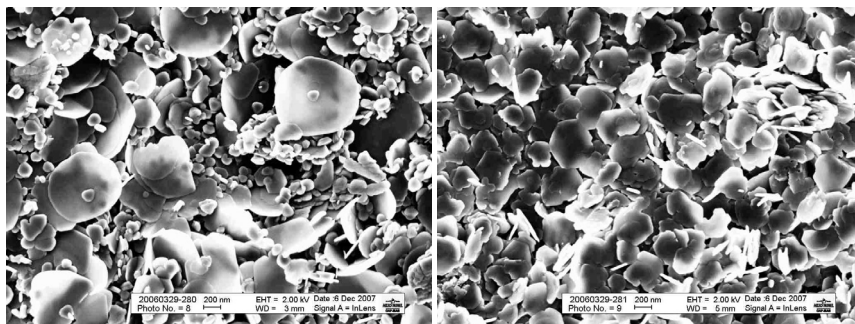
(a) 400 W (MP400)   (b) 800 W (MP800)
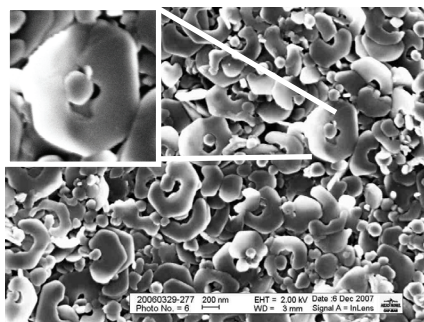
(c) 1600 W (MP1600)

Figure 9. SEM pictures of Mg-Al LDH formed at different microwave power

As shown in Figure 9, higher microwave power promotes the formation of smaller particle sizes and only at the highest microwave power of 1600 W, donut shaped crystals are found in the SEM pictures. A higher microwave power results in a steeper heating curve and thus in a higher supersaturation. This uniformly higher supersaturation favours nucleation to take place on a larger number of MgO particles resulting in a smaller particle size. On the other hand, at lower microwave power, the nucleation apparently takes place on a smaller number of MgO particles, enabling the growth of

platelets. The observation that smaller particles are formed at higher microwave power is consistent with the results of Rivera [19] for co-precipitated Mg-Al LDH after microwave aging. A similar trend of the particle size is also visible in the AFM measurement. However, in the AFM images (shown in Figure 10), sickle and donut-shaped crystals were found at every microwave power. Thus it can be concluded that the growth mechanism does not differ for the different conditions.
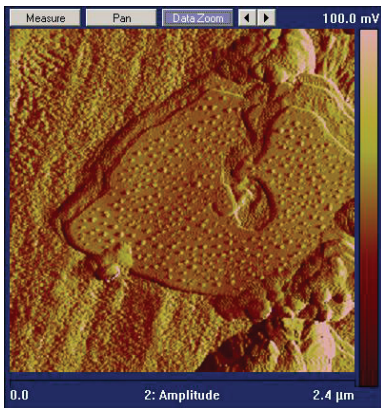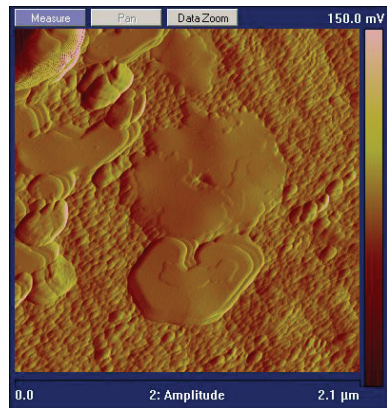
(a) 400 W (MP400-2)   (b) 800 W (MP800-2)
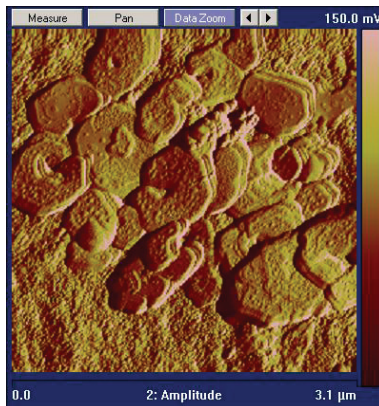
(c) 1600 W (MP1600-2)

Figure 10. AFM images of Mg-Al LDH formed at different microwave power

3.3.4. Proposed growth mechanism of the donut-like crystals

Based on the observation of the crystallites, a growth mechanism for the donut-shaped crystal is proposed. Upon the partial dissolution of the MgO, the pH of the solution increases to the synthesis pH of ~11. At this pH, the solubility of MgO is much lower than that of ATH, so it is assumed that nucleation of Mg-Al LDH starts upon the amorphous surface of spherical MgO particles, where the supersaturation is the highest [20]. This assumption is supported by the higher Mg/Al ratio of the crystal core as shown by the STEM-EDX element maps (Figure 8). The outgrowing platelet-shaped nucleus on the MgO sphere provides re-entrant corners on both sides of the platelet (see Figure 11a, points a). These re-entrant corners are preferential sites for the addition of new growth units [21]. Accordingly, the LDH crystal will grow laterally from both sides of the nucleus encircling the dissolving MgO particle (Figure 11b). The dissolving MgO contributes to the supersaturation, and once depleted the donut-like structure remains.

(a)   (b)
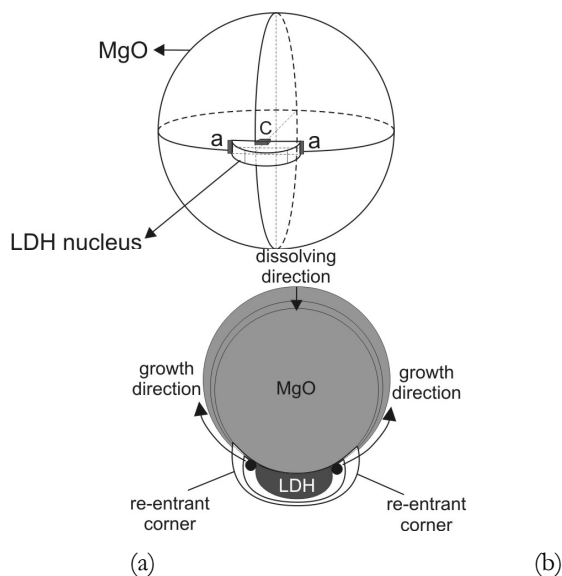
Figure 11. Schematic 3D LDH nucleation upon an MgO sphere (a) and the proposed growth mechanism for the formation of donut-shaped LDH crystal (b)

Okamoto [22] has also reported the formation of a similar donut-like Mg-Al LDH crystal formed by a urea precipitation method. Contrary to our case, the centre of the crystal contains aluminium hydroxide precursor. As the synthesis started at a pH<7, aluminium hydroxide precursor is initially precipitated, upon which the LDH crystal nucleated as the pH increased due to the dissociation of the urea at around 90 ºC. Liu [23] also reported the synthesis of a ring-like morphology of Mg-Al LDH from co-precipitation with sodium dodecylsulfate together with Na_2-EDTA.

As explained in the fore mentioned mechanism, the LDH expands in its fastest growing directions, which are perpendicular to the c-axis. However, growth in the c-direction is also observed (Figure 5a). The growth in the c-direction would be initiated by preferential deposition of growth units on top of the previous LDH layer at the re-entrant corner with the MgO sphere (Figure 11a, point c). So after 2D nucleation, the next layer will grow laterally over the layer underneath as observed in Figure 5a. The smallest growth step as measured by AFM has approximately the thickness of two octahedral layers with an interlayer in between. Higher growth steps were also found.

At the lower Mg/Al ratio, there is apparently not enough magnesium available to complete the growth into a platelet, so donut and sickle shapes are found along with residual aluminium hydroxide. The sickle shape might be formed when more than one nucleation event takes place on a single MgO sphere as shown in Figure 5b. In such a case, the MgO dissolves completely before it becomes surrounded by the laterally growing LDH crystal, and a sickle is formed. Most platelets are growing above the kinetic

roughening supersaturation for their *(100)* faces and are rounded, while a few become faceted at the later stages when the supersaturation is lower. As proposed in the growth mechanism, the formation of donut shaped crystals is related to the uniform and rapid heating rate, thus the influence of the microwave is mainly a thermal effect.

3.4. Conclusions

Application of microwaves in the hydrothermal synthesis has a strong influence both on the conversion rate as well as on the product properties of the Mg-Al LDH crystals. The use of microwave as a heat source in the hydrothermal synthesis of Mg-Al LDH resulted in a reduction of synthesis time. Comparison of both heating methods showed that the synthesis time needed to achieve a comparable crystallinity with microwave heating is four times lower than with conventional heating. In addition, the average particle size distribution (D-50) of the microwave-LDH is smaller. A higher microwave power induces a higher nucleation rate due to a higher supersaturation leading to a smaller particle size. Variation in Mg/Al ratio influences the product shape and impurity content. As pure Mg-Al LDH can only be produced at a Mg/Al ratio between 2 and 4, a lower Mg/Al ratio gives residual ATH. Furthermore, the use of microwave in hydrothermal synthesis of Mg-Al LDH resulted in novel donut-like crystals, i.e. in platelets with a hole in the middle.

The morphology of the hydrothermally synthesized LDH crystals under microwave heating is largely influenced by the magnesium/aluminium molar ratio of the reactants. Unique donut-like crystals were formed at Mg/Al ratios of two and lower. The intensity of the microwave power, however, has a less significant effect, since the donut-like crystals were

found in all cases, and more on the highest power according to SEM. Apparently, the rapid and uniform heating provided by microwave created a high supersaturation for nucleation of LDH which leads to the unique crystal morphology. A growth mechanism of the donut-like crystal was proposed based on the SEM, AFM and STEM-EDX observations of the crystallites obtained at various Mg/Al ratios. First, the LDH crystal nucleates on an amorphous surface of a MgO sphere because this reactant has a lower solubility at the synthesis pH ~11 compared to ATH. This nucleus provides re-entrant corners at two opposite sides, which are preferential sites for the addition of new growth units. As a result of the enhanced growth rate in these directions, perpendicular to the c-axis of the LDH, the planar crystal expands and encircles the MgO sphere. During the growth of the LDH crystal, the MgO sphere dissolves at the opposite side. The dissolving MgO provides the supersaturation needed for growth and once depleted, the donut-like structure remains.

Reference List

[1]   F.Cavani, F.Trifiro, A.Vaccari, Hydrotalcite-type anionic clays: Preparation, properties and applications, Catalysis Today 11 (1991) 173-301.

[2]   R.Allmann, Double Layer Structures with Layer Ions (Me(II)(1-X)Me(III)(X)(OH)2)(X+) of Brucite Type, Chimia 24 (1970) 99-108.

[3]   M.A.Ulibarri and M.del Carmen Hermosin, Layered Double Hydroxides in Water Decontamintaion, in: V.Rives (Ed.) , Layered Double Hydroxides: Present and Future, Nova Science Publisher, Inc., New York, 2006, pp. 285-321.

[4]   J.He et. al., Preparation of layered double hydroxides, Layered Double Hydroxides 119 (2006) 89-119.

[5]   M.Adachi-Pagano, C.Forano, J.P.Besse, Synthesis of Al-rich hydrotalcite-like compounds by using the urea hydrolysis reaction-control of size and morphology, J. Mater. Chem. 13 (2003) 1988-1993.

[6]   Y.Zhao et. al., Preparation of Layered Double-Hydroxide Nanomaterials with a Uniform Crystallite Size Using a New Method Involving Separate Nucleation and Aging Steps, Chemistry of Materials 14 (2002) 4286-4291.

[7]   S.Kannan, R.V.Jasra, Microwave assisted rapid crystallization of Mg-M(III) hydrotalcite where M(III) = Al, Fe or Cr, J. Mater. Chem. 10 (2000) 2311-2314.

[8]   W.N.Budhysutanto et. al., Stability and transformation kinetics of $3R_1$ and $3R_2$ polytypes of Mg-Al layered double hydroxides, Appl. Clay Sci. 48 (2010) 208-213.

[9]   Y.Kuwahara, S.Uehara, Y.Aoki, Atomic Force Microscopy Study Of Hydrothermal Illite In Izumiyama Pottery Stone From Arita, Saga Prefecture, Japan, Clays Clay Miner. 49 (2001) 300-309.

[10]   P.Benito et. al., Influence of microwave radiation on the textural properties of layered double hydroxides, Microporous Mesoporous Mater. 94 (2006) 148-158.

[11]   I.Pausch et. al., Syntheses of disordered and Al-rich hydrotalcite-like compounds, Clays Clay Miner. 34 (1986) 507-510.

[12]   P.J.Sideris et. al., Mg/Al ordering in layered double hydroxides revealed by multinuclear NMR spectroscopy, Science 321 (2008) 113-117.

[13]   D.Evans and R.Slade, Structural Aspects of Layered Double Hydroxides, in: 2006, pp. 1-87.

[14]   J.T.Kloprogge, L.Hickey, R.L.Frost, The effect of varying synthesis conditions on zinc chromium hydrotalcite: a spectroscopic study, Materials Chemistry and Physics 89 (2005) 99-109.

[15]   R.L.Frost, J.T.Kloprogge, Infrared emission spectroscopic study of brucite, Spectrochimica Acta Part A: Molecular and Biomolecular Spectroscopy 55 (1999) 2195-2205.

[16]   R.L.Frost et. al., Vibrational Spectroscopy and Dehydroxylation of Aluminum (Oxo)hydroxides: Gibbsite, Appl. Spectrosc. 53 (1999) 423-434.

[17]   J.T.Kloprogge, R.L.Frost, The effect of synthesis temperature on the FT-Raman and FT-IR spectra of saponites, Vibrational Spectroscopy 23 (2000) 119-127.

[18]   I.H.Joe et. al., FTIR as a Tool to Study High-Temperature Phase Formation in Sol-Gel Aluminium Titanate, Journal of Solid State Chemistry 131 (1997) 181-184.

[19]   J.A.Rivera, G.Fetter, P.Bosch, Microwave power effect on hydrotalcite synthesis, Microporous Mesoporous Mater. 89 (2006) 306-314.

[20]   Z.P.Xu, G.Q.Lu, Hydrothermal synthesis of layered double hydroxides (LDHs) from mixed MgO and Al2O3: LDH formation mechanism, Chemistry of Materials 17 (2005) 1055-1062.

[21]   W.J.P.van Enckevort, Contact nucleation of steps: theory and Monte Carlo simulation, J. Cryst. Growth 259 (2003) 190-207.

[22]   K.Okamoto, N.Iyi, T.Sasaki, Factors affecting the crystal size of the MgAl-LDH (layered double hydroxide) prepared by using ammonia-releasing reagents, Appl. Clay Sci. 37 (2007) 23-31.

[23]   C.X.Liu, W.G.Hou, Synthesis of Layered Double Hydroxides with Novel Morphologies, J. Dispersion Sci. Technol. 30 (2009) 173-176.

Chapter 4

Stability and Transformation Kinetics of 3R$_1$ and 3R$_2$ Polytypes of Mg-Al Layered Double Hydroxides

ABSTRACT

Two different polytypes of Mg-Al layered double hydroxide (LDH) with rhombohedral symmetry can be synthesized either by rehydration of calcined LDH or by hydrothermal synthesis. The structural differences of these polytypes, $3R_1$ and $3R_2$, could induce distinct characteristic performances, making it essential to study their thermal stability regimes and transformation kinetics. The results show that transformations of both polytypes are feasible. The transition temperature is at 110 °C with polytype $3R_1$ being stable at lower temperatures and polytype $3R_2$ at higher temperatures. The transformation kinetic of polytype $3R_1$ into $3R_2$ is inhibited by the presence of carbonate ions in the interlayer. In their absence, polytype $3R_1$ transforms faster into $3R_2$ than vice versa. Furthermore, the transformation of polytype $3R_1$ into $3R_2$ is accompanied by the formation of brucite, indicating the lower Mg-Al ratio in polytype $3R_2$. The transformation is solvent mediated and no solid state transformation was observed.

4.1. Introduction

Hydrotalcite refers to a group of layered double hydroxides (LDH) with anions in the interlayer domains. The basic structure of the layer consists of a $Mg(OH)_2$ lattice, in which some of the Mg^{2+} ions are replaced by Al^{3+}, which results in a positively charged layer. Hydrotalcite consists of stacked hydroxide layers which can be represented by A, B, or C according to their stacking position while the metal cations occupying the octahedral holes can be represented by a, b, or c analogously. A single layer can thus be represented by e.g. AbC, or simplified by AC. These AC layers can be stacked in various ways, resulting into a large number of possible polytypes as described by Bookin and Drits [1]. When the next hydroxyl layer is stacked as in AC=CB, a P-type interlayer with a trigonal prismatic arrangement (denoted by =) is formed. An O-type interlayer with an octahedral arrangement (denoted by -) results when the next hydroxyl layer is shifted from the position of the previous one, as in AC-BA or AC-AC. On the basis of the layer repetition, there are two possible 3 layer polytypes with a rhombohedral symmetry [1]:

- Polytype $3R_1$: …=AC=CB=BA=AC=… (with P-type interlayers)
- Polytype $3R_2$: …-AC-BA-CB-AC-…   (with O-type interlayers)

The most widely used analysis technique for the identification of LDH is powder XRD. The reflections in the XRD pattern can be grouped into[2]:

1. A series of strong basal ($00l$) reflections at low angles which allows the determination of the layer thickness (c-parameter).
2. The positions of the ($01l$) and/or ($10l$) reflections at intermediate angles which reflect the stacking pattern of the layers.

3. The position of the (110) reflection at high angle (near $2\theta=60°$ for Cu Kα radiation) for the determination of the lattice a-parameter, which corresponds to the distance between two metal cations in the layer.

Synthetically produced pure Mg-Al LDH can cover a range of Mg/Al ratios from 2 to 4 [2-4]. The values of the a- and c-parameter are correlated with the Al content of the LDH. The radius of Al^{3+} is smaller than that of Mg^{2+} which causes a decrease of the a-parameter with an increase of Al content. The c-parameter also diminishes with the Al content due to the stronger electrostatic attraction of the layer towards the anions [4-7].

Natural hydrotalcite, which always contains carbonate anions in the interlayer and most synthetic carbonate containing hydrotalcite are of the $3R_1$ polytype. Newman [8] reported the synthesis of the $3R_2$ polytype at a temperature of 180 ºC with less carbonate content in the interlayer than that of the $3R_1$ polytype. Presumably, the principal anion in the $3R_2$ polytype is then hydroxide, made during the hydrothermal synthesis from the water. At 70 ºC, the polytype formed with the hydrothermal synthesis is of the $3R_1$ polytype. Natural occurrence of the $3R_2$ polytype is only found for LDH minerals containing sulphate ions [9,10].

Polytype $3R_1$ and $3R_2$ can be distinguished from each other by presence of the (01*l*) and (10*l*) reflections respectively. Based on the XRD pattern, Newman [8] showed that compared to polytype $3R_1$, polytype $3R_2$ has a smaller layer thickness and a larger cations distance in the layer. Newman furthermore, also showed that the $3R_2$ polytype synthesized at 180 °C is relatively stable in water, even after 72 hours redispersion at 70°C. Based on

his findings with synthesized $3R_1$ and $3R_2$, Newman composed the transformation scheme of Figure 1.
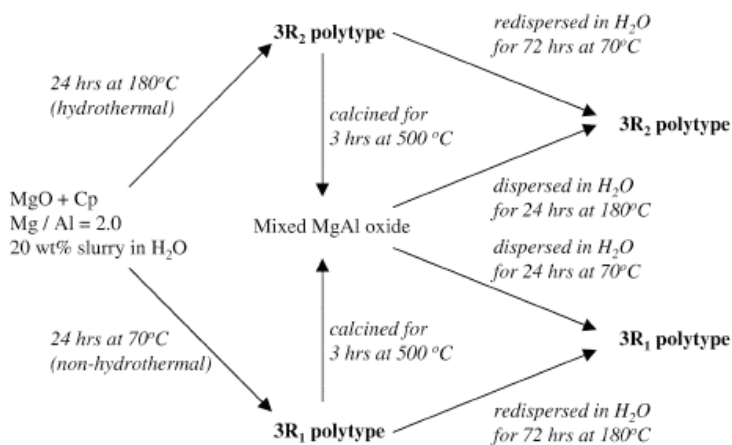
Figure 1. Formation and interconversion of hydrotalcite-like $3R_1$ and $3R_2$ LDH polytypes [8]

The differences in crystal structure of these polytypes provide the basis for their distinct performance characteristics in various applications. Newman suggested that interconversion of polytype $3R_1$ and $3R_2$ is only possible via calcination and rehydration at the corresponding temperature. This mechanism would imply that the polytype once formed is stable, but no information was provided about the stability of the polytypes. In this study the transformation of Mg-Al LDH from $3R_1$ polytype to $3R_2$ and vice versa was investigated. The temperature regimes, transformation kinetics, and the relative solubility of the two polytype were studied. It is also relevant to know whether such a transformation can occur in the solid state or only via a solvent mediated transformation in the slurry.

4.2. Experimental

4.2.1. Formation of Mg-Al LDH 3R₁ and 3R₂ polytypes

By calcination-rehydration

The pure polytypes were produced by a method described by Newman [8], which involves calcination of a commercial hydrotalcite-3R$_1$ powder product (Alcamizer from Kisuma chemicals) at 500 °C for 3 hours followed by 24 hours rehydration in distilled water at 80 °C and 170 °C to produce 3R$_1$ and 3R$_2$ polytype respectively.

By hydrothermal synthesis

Polytypes of Mg-Al LDH were synthesized according to another method described by Newman [8] from magnesium oxide (MgO from Martin Marietta as Zolitho 40), aluminium trihydroxide (ATH as Alumill F505) and distilled water. Prior to the synthesis, the reactants were wet-ground in a Dynomill. A slurry containing 10 wt% of solid with Mg/Al ratios of 2 was used as the starting materials. The synthesis was carried out for 4 hours at 90 °C and 170 °C.

4.2.2. Transformation of 3R polytypes

Transformation of calcination-rehydration polytypes

Polytypes of Mg-Al LDH produced by the calcinations-rehydration were subsequently subjected to a transformation step. The 3R$_1$ polytype was hydrothermally treated at 170 °C, while the 3R$_2$ polytype was kept at 80 °C for 24 hours. Additional experiments with the 3R$_1$ polytype were also done where the polytype was first subjected to ultrasound treatment for 15 minutes, dried, powdered and then rehydrated prior to the transformation step. Samples were taken after 24 hours.

Seeded slurry transformation

Polytype 3R$_1$ for the seeded transformation was synthesized by calcinations-rehydration, while polytype 3R$_2$ was made by the hydrothermal synthesis. This transformation study was carried out with 10% seeds of the other polytype at the pre-set temperature. Transformation of polytype 3R$_1$ into 3R$_2$ was carried out at 110, 140, and 170 °C. Transformation of polytype 3R$_2$ into 3R$_1$ was carried out at 50, 80, 100, 110, 120 °C. The scheme of the study is shown in the Figure 2. Samples were taken after 6 days of transformation for analysis.
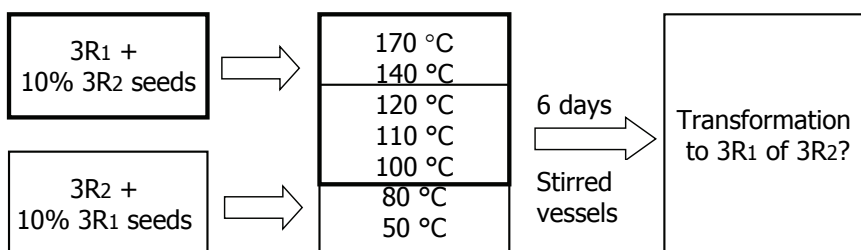
Figure 2. Scheme of the seeded slurry transformation

Transformation of hydrothermal synthesized polytype 3R$_1$

The 3R$_1$ polytype was synthesized via the hydrothermal method at 90 °C for 4 hours, immediately followed by its transformation into 3R$_2$ at 170 °C. The experiment conditions are given in Table 1. After cooling down, part of the slurry samples were dried overnight in an oven at 50 °C and subsequently analyzed by XRPD and FT-IR. The remaining slurry samples were analyzed by SEM.

Table 1. Transformation of hydrothermally synthesized polytype 3R$_1$

Experiment number	Mg-Al ratio for polytype 3R$_1$	Treatment prior to the transformation	Transformation time (hr)
H-1	2.3	no treatment	19
H-2	1.2	no treatment	21
H-3	2.3	addition of ATH to Mg-Al ratio = 1.2	4

4.2.3. Analytical techniques

X-Ray Powder Diffraction

Measurement of the powder samples were done with a Bruker-AXS D5005 diffractometer with an Huber incident-beam Cu Kα monochromator and a Braun position sensitive detector (PSD). The 2θ-range was 5–70° with a step size of 0.0387° and a counting time per step of 1 s.

FT-IR

The FT-IR measurements were done with a Nexus Thermo Nicolet 5700 spectrometer. Powder samples were pressed in small discs using KBr matrix for the measurement. The IR bands were recorded at a spectral range of 650-4000 cm $^{-1}$.

SEM

The SEM pictures were made with a JEOL JSM 6500F microscope. For the preparation of the sample, 3 drops of the slurry were diluted with 100 ml distilled water. One millilitre of the sample was then vacuum-filtered over a ceramic membrane filter Anodisc 25. The SEM pictures were taken of the filter.

4.3. Results & Discussion

4.3.1. Formation of Mg-Al LDH 3R₁ and 3R₂ polytype

The formation of $3R_1$ polytype from calcined HTC is feasible by rehydration at 80 °C for 24 hours. However, in contrast to the results of Newman [8] as seen in Figure 1, rehydration at 170 °C did not result in the $3R_2$ polytype; the $3R_1$ polytype was formed. The temperature difference between 180 °C chosen by Newman [8] and 170 °C in this work is too small

to explain the different result, so this difference might come from the different starting materials. Alcamizer, the reactant in our calcination step, is a carbonate containing Mg-Al LDH. The decomposition of the carbonate ions has been reported to occur at 405-580 °C [11] and even up to 650 °C [12], so after calcination at 500 °C still some carbonate ions are present in the calcined product. The presence of carbonate ions in the solution apparently prohibits the formation of polytype 3R$_2$ [13].

Hydrothermal synthesis of Mg-Al LDH from magnesium oxide and aluminium hydroxide produced polytype 3R$_1$ and 3R$_2$ at 90 and 170 °C, respectively. Identification of the polytypes was done with XRPD and FT-IR. The XRPD patterns differentiate polytype 3R$_1$ and 3R$_2$ from their (01l) and (10l) reflections, respectively. The basal reflections (00l) showed that the formed polytype 3R$_2$ has a smaller interlayer distance compared to polytype 3R$_1$. After four hours synthesis at 90 °C however, the XRPD pattern still reveals the presence of ATH in the slurry. Prolonging the synthesis time to 24 hours does not fully eliminate the ATH. The formation of polytype 3R$_2$ at 170 °C was completed in four hours with some brucite found as a by-product. The brucite content in the polytype 3R$_2$ was also confirmed by the FT-IR measurement showing a sharp band at 3680 cm^{-1} [14]. The FT-IR spectra also showed that polytype 3R$_2$ has a significantly lower carbonate content than the 3R$_1$.

4.3.2. Transformation of Mg-Al LDH 3R$_1$ and 3R$_2$ polytype

The transformation was carried out with the slurry from the polytype formation. The 3R$_1$ polytype obtained by calcination and rehydration at 80 °C was brought under hydrothermal conditions at 170 °C for 24 hours. No transformation into 3R$_2$ polytype was observed. An attempt to accelerate

the kinetics was made by applying ultrasonic treatment. The cavitation bubbles are expected to induce attrition/breakage of the crystal and thus increases the chemical potential of the solid phase and also its solubility. Additional experiments with ultrasound treatment however, also did not show any transformation after 24 hours. Only when the pure $3R_1$ slurry was dried and hand-ground prior to the rehydration at 170 °C, a slight transformation into $3R_2$ occurred. The phenomenon of a retarded or fully inhibited transformation can be explained by the presence of carbonate ions in interlayer of the calcined-rehydrated polytype $3R_1$. A carbonate ion, having a trigonal planar arrangement, fits very well into the trigonal prismatic interlayer sites of polytype $3R_1$. Their oxygen atoms can form hydrogen bonding with the hydroxyl groups in the metal layer of polytype $3R_1$ which stabilizes the $3R_1$ lattice [10].

The application of ultrasound treatment or dry-grinding on the $3R_1$ polytype transformation rate, did not work. Apparently the solubility of the polytypes is so low that some increase in solubility does not suffice. So in order to circumvent the nucleation barrier, seeds of the other polytype were added.

The transformation was performed with 10 wt% solid seeds of the other polytype. In addition, some transformations were prolonged to 63 days to compensate for the slow transformation rate, but the degree of transformation was also checked after 6 days. The results are shown in Table 2.

Table 2. Polytypic fraction of seeded transformation experiment calculated from the proportion of *(006)* reflection intensities

Transformation polytype $3R_1$ to $3R_2$			Transformation polytype $3R_2$ to $3R_1$		
T(°C)	time (day)	%wt $3R_2$	T(°C)	time (day)	%wt $3R_2$
110	0	10.0	50	0	90.0
	4	10.0		6	74.9
	6	8.8		14	68.7
	14	9.5		21	69.0
120	0	90.4		35	58.2
	6	95.2		63	45.9
	14	96.6	80	0	90.0
	21	100.0		7	49.3
140	0	10.0		14	44.4
	4	15.6	100	0	90.0
	6	15.6		6	61.3
170	0	10.3		14	61.3
	6	69.0	110	0	90.0
				6	56.1
				12	56.4
				19	64.4

Despite the presence of carbonate ions in the slurry, transformation of one LDH polytype into the other took place in almost all seeded experiments, although in all cases the transformations were not completed in 6 or even in 63 days.

The degree of conversion of polytype $3R_1$ into $3R_2$ (Table 2) at 140 and 170 °C shows that the transformation rate increases with temperature. At 110 °C no transformation was observed. The $3R_2$ content in the sample decreased slightly, indicating transformation of the $3R_2$ seeds added to the slurry. The transformation of polytype $3R_1$ into $3R_2$ was more pronounced at 170 °C, as indicated by the *(006)* reflection in Figure 3 along with the non basal reflections shown in the inset. Brucite, however, is also formed along with

the $3R_2$ polytype at 170 °C (Figure 3). Moreover, the magnesium which precipitated as brucite indicates that polytype $3R_2$ has a lower Mg/Al ratio compared to polytype $3R_1$.
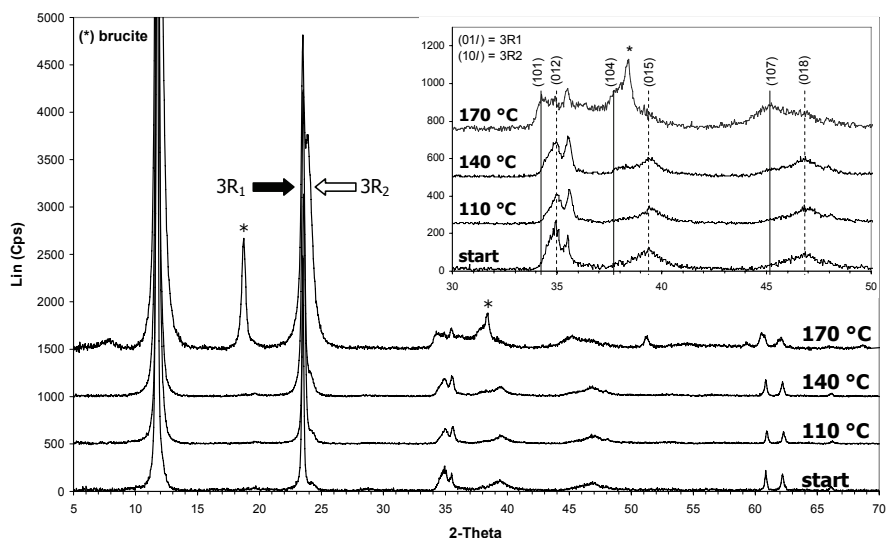
Figure 3. XRPD spectra of the seeded transformation experiment of polytype $3R_1$ to $3R_2$

The transformation of polytype $3R_2$ into $3R_1$ took place at 50, 80 and 110 °C, with the fastest rate at 80 °C. At 20 °C the driving force for the transformation of $3R_1$ to $3R_2$ is higher, however the kinetics are much slower, while at 80 °C the smaller driving force is compensated by the faster kinetics (Figure 4). Keeping the $3R_2$ slurry at room temperature does not lead to a transformation even after 6 months. Because of the low solubility of both polytypes, it was not feasible to measure the (stable and metastable) solubility lines presented in Figure 4. So, the vertical axis only serves to help explain the transformation procedure.
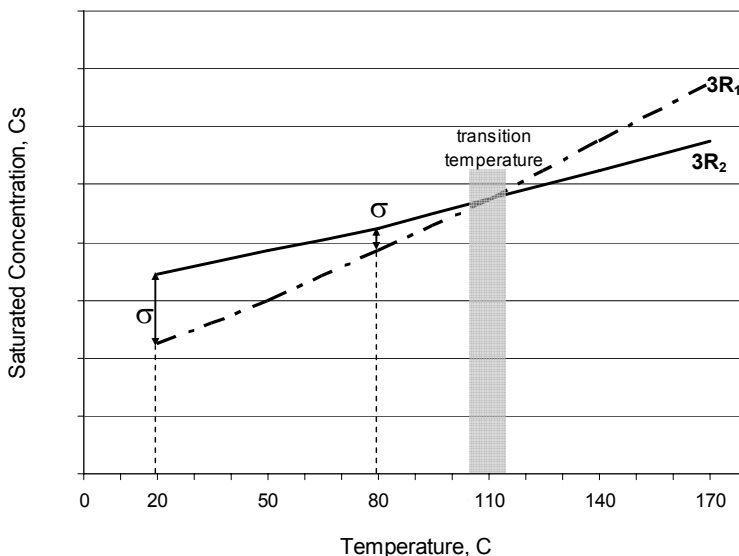
Figure 4. Solubility diagram of $3R_1$ and $3R_2$ polytype

The transformation of polytype $3R_2$ to polytype $3R_1$ at 110 ºC showed however some discrepancies: after 12 days of transformation, some of the originally formed $3R_1$ transformed back into $3R_2$. For that reason, additional experiments were done at 100 and 120 ºC. At 100 ºC the $3R_2$ transformed into $3R_1$ while at 120 ºC the 10 % wt of $3R_1$, which were originally meant as seeds, transformed into $3R_2$, and after 21 days the slurry contained only pure $3R_2$. This confirms that the transition temperature of $3R_1$ into $3R_2$ lays around 110 ºC.

With the addition of seeds, polytype $3R_2$ readily transforms into polytype $3R_1$ at a faster rate than vice versa. In the latter case, the residual carbonate ions from the calcination rehydration synthesis of polytype $3R_1$ were assumed to inhibit the formation of the $3R_2$ polytype. In order to confirm

this hypothesis, a transformation of $3R_1$ polytype produced by hydrothermal synthesis, into $3R_2$ polytype was performed. The results are summarized in Figure 5:

MgO-ATH   **170 °C**

Mg/Al = 2.3 (H-1)		$3R_1$ (Mg/Al = 2.3)	17 hr	$3R_2$ + Brucite
Mg/Al = 1.2 (H-2)	90 °C 4 hr	$3R_1$ (Mg/Al 2.3) + ATH	4 hr	$3R_2$ Boehmite Slight brucite
Mg/Al = 2.3 (H-3)		$3R_1$ (Mg/Al = 2.3)	+ATH → Mg/Al=1.2 4 hr	$3R_2$ + slight brucite
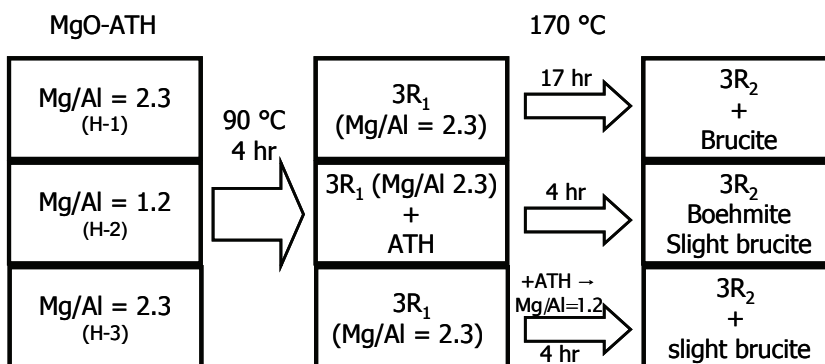
Figure 5. Transformation results of hydrothermal synthesized polytype $3R_1$

Polytype $3R_1$ with an Mg/Al ratio of 2.3 was synthesized at 90 °C for 4 hours (experiment H-1). With no carbonate added to the system, the compensating anions are hydroxides. Subsequently, the slurry was hydrothermally treated at 170 °C. After 4 hours of treatment, transformation into $3R_2$ was observed from its (10*l*) reflection. The (00*l*) reflections of polytype $3R_2$ were clearly seen after 19 hours of hydrothermal treatment when the transformation was also completed. Again, the formation of polytype $3R_2$ was accompanied by brucite formation, indicating that polytype $3R_2$ has a higher aluminium content. This transformation rate is significantly faster compared to the seeded transformation of polytype $3R_1$ from calcination rehydration at the same temperature which was not completed after 6 days. Without the presence of carbonate ions in the interlayer, the transformation of polytype $3R_1$ into $3R_2$ is faster than vice versa (Figure 6).
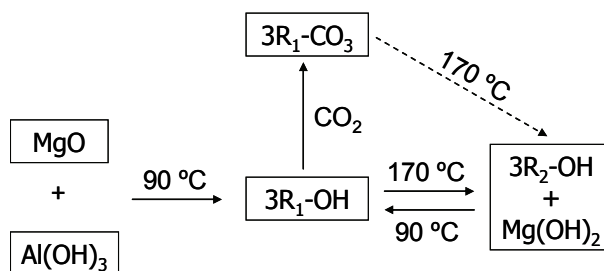
Figure 6. Transformation scheme of 3R polytypes Mg-Al LDH

The lower aluminium content in polytype 3R$_2$ was further confirmed by hydrothermally synthesizing polytype 3R$_1$ at 90 °C with a lower Mg/Al ratio of 1.2 (experiment H-2). Due to the excess ATH provided at the start, there was still a lot of ATH along with polytype 3R$_1$ after 4 hours synthesis. The slurry was then directly heated up to 170 °C. Sampling of the product after 2 hours treatment indicated transformation into polytype 3R$_2$ by showing the (00l) and (10l) reflections along with the formation of traces of boehmite and brucite. After 21 hours treatment, the transformation to polytype 3R$_2$ was completed with still some traces of impurities present. Another experiment (experiment H-3) was carried out by hydrothermally synthesizing polytype 3R$_1$ with an Mg-Al ratio of 2.3 for 4 hours at 90 °C. Prior to the treatment at 170 °C, ATH was added to the slurry until an Mg-Al ratio of 1.2. After 4 hours at 170 °C, the XRPD measurement of the slurry (Figure 7) showed full conversion into 3R$_2$ without any impurities. The polytype 3R$_2$ formed has a unit cell parameter a and c equals to 3.05 Å and 21.99 Å, respectively. Figure 7 shows the non basal reflections of the formed polytype 3R$_2$ with the *(10l)* reflections more pronounced compared to the *(01l)* reflections. The lines represent the calculated reflections based on the unit cell parameter of the sample. The intensities of those reflections were taken from that of polytype 3R$_2$ listed by Bookin and Drits [1].
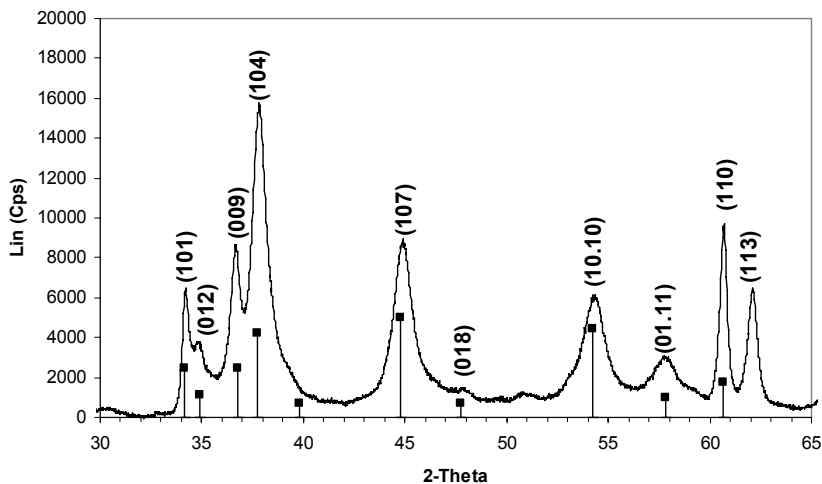
Figure 7. XRPD spectra of the polytype $3R_2$ produced in experiment H-3

This transformation study showed that the transformation of polytype $3R_1$ into $3R_2$ polytype or vice versa apparently is solvent mediated, because otherwise seeding would not have any effect.

In situ high temperature XRPD of polytype $3R_1$ in a nitrogen flow showed a decrease of the layer thickness at 150 °C, and disappearance of the (006) reflection at 200 °C. Some researchers [15,16] attributed these findings to the dehydration of the crystal along with migration of the aluminium cations from the layer to tetrahedral sites in the interlayer at 200 °C. While other [17] attributed them to the formation of turbostratically disordered 1H polytype. Upon decreasing of the temperature, the crystal structure remained the same under a nitrogen flow. However, after 4 hours exposure to air, rehydration of the sample occurred due to the humidity of the air, and the XRPD pattern showed that the crystal structure returns to its original

polytype $3R_1$. This dehydrated polytype $3R_1$ is clearly not the same as polytype $3R_2$ since the latter remains stable in water.

(a)   (b)
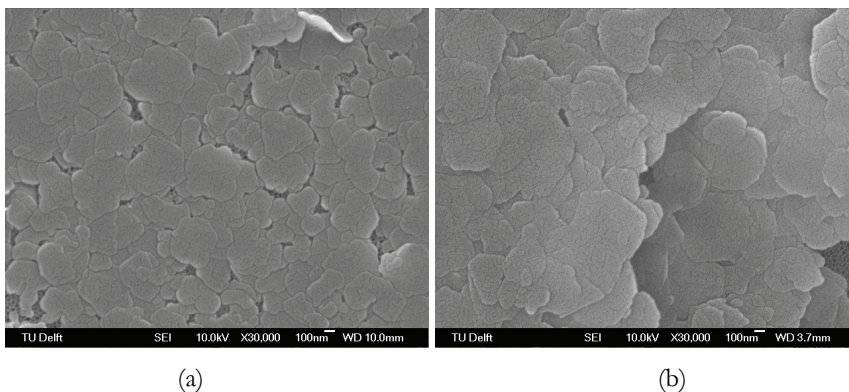
Figure 8. SEM pictures of experiment 091208: (a) polytype 3R1 synthesized at 90 °C with Mg/Al = 2.3; (b) polytype 3R2 synthesized at 170 °C with Mg/Al = 1.2

The SEM pictures (Figure 8) taken of the originally synthesized $3R_1$ and of the $3R_2$ after transformation, indicate different crystallite sizes, confirming again that the transformation is solvent mediated.

4.4. Conclusions

Transformation of the 3R polytypes Mg-Al hydroxide is feasible in a slurry. The transition temperature of the polytypes lies at about 110 °C with polytype $3R_1$ being the stable polytype at lower temperatures and polytype $3R_2$ at higher temperatures. The transformation kinetics in general is slow and can be accelerated by seeding. In absence of carbonate ions in the interlayer, the transformation kinetics of polytype $3R_1$ to $3R_2$ is faster than vice versa. Furthermore, the transformation of polytype $3R_1$ into $3R_2$ is accompanied by the formation of brucite, leading to a higher aluminium content in the $3R_2$ polytype. The transformation is solvent mediated, no solid state transformation is observed. Addition of ATH to $3R_1$ polytype

can also accelerate its transformation into polytype $3R_2$, confirming that $3R_2$ has a higher aluminium content and that the transformation is solvent mediated.

Reference List

[1]   A.S.Bookin, V.A.Drits, Polytype diversity of the hydrotalcite-like minerals; I, Possible polytypes and their diffraction features, Clays and Clay Minerals 41 (1993) 551-557.

[2]   D.Evans and R.Slade, Structural Aspects of Layered Double Hydroxides, in: 2006, pp. 1-87.

[3]   F.Cavani, F.Trifiro, A.Vaccari, Hydrotalcite-type anionic clays: Preparation, properties and applications, Catalysis Today 11 (1991) 173-301.

[4]   S.P.Newman and W.Jones, Layered double hydroxides as templates for the formation of supramolecular structures, in: W.Jones, C.N.R.Rao (Eds.) , Supramolecular Organization and Materials Design, Cambridge University Press, Cambridge, 2002, pp. 295-331.

[5]   M.Bellotto et. al., A Reexamination of Hydrotalcite Crystal Chemistry, The Journal of Physical Chemistry 100 (1996) 8527-8534.

[6]   C.de la Calle et. al., A crystal-chemical study of natural and synthetic anionic clays, Clays Clay Miner. 51 (2003) 121-132.

[7]   V.A.Drits and A.S.Bookin, Crystal Structure and X-ray Identification of Layered Double Hydroxides, in: V.Rives (Ed.) , Layered Double Hydroxides: Present and Future, Nova Science Publishers, Inc., Huntington, 2001, pp. 39-92.

[8]   S.P.Newman et. al., Synthesis of the 3R(2) polytype of a hydrotalcite-like mineral, J. Mater. Chem. 12 (2002) 153-155.

[9]   D.L.Bish, Anion-Exchange in Takovite - Applications to Other Hydroxide Minerals, Bulletin de Mineralogie 103 (1980) 170-175.

[10]   A.S.Bookin, V.I.Cherkashin, V.A.Drits, Polytype diversity of the hydrotalcite-like minerals; II, Determination of the polytypes of experimentally studied varieties, Clays and Clay Minerals 41 (1993) 558-564.

[11]   W.Yang et. al., A study by in situ techniques of the thermal evolution of the structure of a Mg-Al-CO_3 layered double hydroxide, Chemical Engineering Science 57 (2002) 2945-2953.

[12]   V.R.L.Constantino, T.J.Pinnavaia, Structure-reactivity relationships for basic catalysts derived from a $Mg^{2+}/Al^{3+}/CO_3^{2-}$ layered double hydroxide, Catalysis Letters 23 (1994) 361-367.

[13]   I.Pausch et. al., Syntheses of disordered and Al-rich hydrotalcite-like compounds, Clays Clay Miner. 34 (1986) 507-510.

[14]   J.A.Wang et. al., Characterizations of the thermal decomposition of brucite prepared by sol-gel technique for synthesis of nanocrystalline MgO, Materials Letters 35 (1998) 317-323.

[15]   J.A.van Bokhoven et. al., Unique structural properties of the Mg-Al hydrotalcite solid base catalyst: An in situ study using Mg and Al K-edge XAFS during calcination and rehydration, Chemistry-A European Journal 7 (2001) 1258-1265.

[16]   M.Bellotto et. al., Hydrotalcite Decomposition Mechanism: A Clue to the Structure and Reactivity of Spinel-like Mixed Oxides, The Journal of Physical Chemistry 100 (1996) 8535-8542.

[17]   G.S.Thomas et. al., Thermally Induced Polytype Transformations among the Layered Double Hydroxides (LDHs) of Mg and Zn with Al, The Journal of Physical Chemistry B 110 (2006) 12365-12371.

Chapter 5

Chemical Composition and Interlayer Arrangement of Polytype 3R$_2$ Mg-Al Layered Double Hydroxides

ABSTRACT

The polytype $3R_2$ of Mg-Al layered double hydroxide (LDH) can be synthesized either directly by hydrothermal treatment of magnesium oxide (MgO) and aluminium trihydroxide (ATH) at 170 °C or by a two-step synthesis. By the latter method, first polytype $3R_1$ is hydrothermally formed with a Mg/Al ratio of 2.2 at 90 °C, which is subsequently converted at 170 °C into polytype $3R_2$ with a Mg/Al ratio of 1.1, by addition of ATH. The chemical composition and interlayer arrangement of this polytype were investigated. XRPD confirmed the formation of polytype $3R_2$ Mg-Al LDH by the strong $(10l)$ over $(01(l+1))$ $(l = 3n + 1, n = $ integer) reflections. A unique feature of polytype $3R_2$, which is the presence of tetrahedrally coordinated aluminium ions, was revealed by FT-IR and 27-Al MAS NMR measurements. These aluminium ions, present as aluminates, act as counter ions in the interlayer of polytype $3R_2$. From the STEM-EDX result it is concluded that the molar Mg/Al ratio in the octahedral layer is approximately 2.0. If all the charges in the octahedral layer are compensated by aluminate ions, the overall Mg/Al ratio would be 1.0. 27-Al NMR however, measured only about 40% tetrahedrally coordinated aluminium ions instead of 50%.

5.1. Introduction

Layered Double Hydroxides (LDH) refer to a group of anionic clays with a general formula $[M^{II}_{(1-x)}M^{III}_{(x)}(OH)_2][A^{n-1}]$ zH_2O. The basic structure of LDH is magnesium hydroxide (brucite) in which the magnesium ions occupy octahedral positions surrounded by hydroxide ions. The hydroxide ions are shared by neighbouring magnesium ions, thus forming an infinite sheet. A brucite lattice comprises a hexagonal stacking of such charge neutral octahedral layers. In LDH, a part of the Mg^{2+} ions is replaced by Al^{3+} ions, and the octahedral layers become positively charged. These charges must then be compensated by the incorporation of anions in the interlayer. Natural Mg-Al LDH contains carbonate anions and water molecules in the interlayer. Other LDHs also contain NO_3^-, SO_4^{2-}, or OH^- anions[1].

According to their stacking position, the hydroxides in the octahedral layer of Mg-Al LDH can occupy an A, B, or C position. The octahedrally coordinated metal cations can then occupy an a, b, or c position analogously. A single octahedral layer can thus be represented by e.g. AbC, or simplified by AC. This single layer can be stacked in various sequences, resulting in the formation of polytypes. Based on its stacking sequence, two possible interlayer arrangements can be formed: a trigonal prismatic (P-type) interlayer is formed when the layers are stacked e.g. as AC=CB, while an octahedral (O-type) interlayer is formed when the layers are stacked e.g. as AC-BA. Bookin and Drits [2] explored the variety of polytypes, and concluded that there are only two three-layer polytypes possible with a rhombohedral symmetry. These two polytypes are polytype $3R_1$ stacked as …=AC=CB=BA=AC=… having only P-type interlayer positions, and

polytype $3R_2$ stacked as …-AC-BA-CB-AC-… with only O-type interlayer positions. The anions, such as sulphate, can either alone or together with water molecules, be arranged in the P or O type interlayer positions without sharing their surrounding oxygens with the two adjacent octahedral layers. In some cases, the arrangement is a dumbbell structure [3]. Radha [3,4] also suggested that the intercalated sulphate ions could mediate the long-range ordering of the octahedral layers in such a way to generate either P or O-type interlayer positions (see chapter 1).

In nature, two polytypes of Mg-Al LDH are found that have either a hexagonal or rhombohedral symmetry. The polytype with a rhombohedral symmetry, hydrotalcite, belongs to the $3R_1$ polytype, while the one with a hexagonal symmetry, manasseite, belongs to polytype $2H_1$ with a …AC=CA=AC… stacking sequence. Both naturally occurring Mg-Al LDHs contain carbonate anions which perfectly fit in the trigonal prismatic interlayer arrangement. Synthetically, Mg-Al LDH is produced by various methods such as co-precipitation, urea method, sol-gel method, and hydrothermally [5] These methods mainly resulted in the formation of polytype $3R_1$, except for the hydrothermal method which was reported to produce polytype $3R_2$ upon synthesis at 170 °C [6]. Since no additional anions were added during the synthesis, Newman [6] suggested that the interlayer of polytype $3R_2$ contains hydroxide anions. In his preliminary study, the structure and the interlayer arrangement of the $3R_2$ polytype were not addressed.

In a previous study on the transformation of hydrothermally synthesized 3R polytypes of Mg-Al LDH [7], it was found that polytype $3R_2$ contains more aluminium than polytype $3R_1$. The aim of this study is to reveal the chemical

composition of polytype 3R$_2$ and to disclose the interlayer arrangement in the structure of polytype 3R$_2$. The chemical composition of polytype 3R$_2$ was determined by performing the hydrothermal synthesis at various initial magnesium-aluminium ratios and by analyzing the residual products. For determination of the interlayer arrangement, a two step hydrothermal synthesis method was used. Various analytical techniques such as FT-IR, ICP-MS, NMR, XRPD, and TEM-EDX were used to investigate the chemical composition and structure of polytype 3R$_2$. The shape of the crystals was determined by SEM.

5.2. Experimental

5.2.1. Direct hydrothermal synthesis at 170 °C at various initial Mg/Al ratios

Polytype 3R$_2$ of Mg-Al LDH was synthesized hydrothermally from magnesium oxide (MgO from Martin Marietta as Zolitho 40), aluminium trihydroxide (ATH as Alumill F505) and distilled water. Prior to the synthesis, the reactants were wet-ground together in a Fritsch planetary ball mill at 400 rpm for 30 minutes, until the particle size was reduced to 2-3 micron. The synthesis was then performed in an autoclave with a 10 wt % solid content of the slurry. The initial molar Mg/Al ratios of the reactants were varied from 1.0 to 1.8 and the synthesis temperature of 170 °C was maintained for 4 hours. Subsequently, the autoclave was cooled down to 80 °C and the slurry product was taken out.

5.2.2. Two step synthesis method

A two step method for the synthesis of polytype 3R$_2$ consisted of a synthesis step of polytype 3R$_1$, followed by a transformation step to

polytype $3R_2$. The synthesis of polytype $3R_1$ was carried out from a wet-ground 10% wt slurry of MgO and ATH in distilled water with a molar Mg/Al ratio of 2.2. The slurry was thermally treated in an autoclave at 90 ºC for 8 days. The transformation step to polytype $3R_2$ immediately followed the first step, by addition of an ATH slurry, either ground or not, to reach a molar ratio of Mg/Al in the slurry of 1.1. The slurry was then hydrothermally treated in the autoclave at 170 ºC for 1 day. Subsequently, the autoclave was cooled down to 80 °C and the slurry product was taken out.

5.2.3. Analytical techniques

Part of the slurry samples taken from the experiments were dried overnight in an oven at 50 ºC. The dried samples were analyzed by Fourier Transform-Infra Red (FT-IR) , Nuclear Magnetic Resonance Spectroscopy (NMR), Induced Couple Plasma – Atomic Emission Spectrometry (ICP-AES), X-Ray Powder Diffraction (XRPD), Thermogravimetry Analysis (TGA) and Differential Scanning Calorimetry (DSC), while the remaining slurry samples were used for Scanning Transmission Electron Microscopy – Energy Dispersive X-Ray Spectroscopy (STEM-EDX) and for Scanning Electron Microscopy (SEM).

The FT-IR measurements were carried out with a Nexus Thermo Nicolet 5700 spectrometer. Powder samples were pressed in small discs using a KBr matrix. The IR bands were recorded at a spectral range of 650-4000 cm^{-1}. For the ICP-AES measurements, powder samples were dissolved in nitric acid, diluted to the ppm scale and subsequently measured with a Spectro Arcos. The 27-Al MAS NMR measurements were done on a Bruker Avance-400 spectrometer at 104.2 MHz. The solid sample was measured at

a spinning speed of 11 kHz in a 4 mm Zr rotor using 0.08 s acquisition time with 1 s acquisition delay. Aluminium nitrate [1M] was used as an external chemical shift reference, and its chemical shift was set at 0 ppm. The XRPD measurements were done with a Bruker-AXS D5005 diffractometer with a Huber incident-beam Cu Kα monochromator and a Braun position sensitive detector (PSD). The 2θ-range was 5–70° with a step size of 0.0387° and a counting time per step of 1 s. In the TGA, the samples were heated under nitrogen atmosphere from room temperature to 825 °C at a rate of 10 °C/min. In the DSC, the samples were heated up to 525 °C at a rate of 10 °C/min.

The STEM measurements were done with a JEOL 2010F microscope with an accelerating voltage of 200 kV, equipped with ThermoNoran EDX. The powder sample was mixed with an Ultra Low Viscosity Kit (ULVK) and dried in an oven at 60 °C for 3 days. It was then cut by ultramicrotomy perpendicular to the settling direction. For STEM-EDX, the powder sample was mixed with nylon-6,6 and extruded. By this procedure the 3R$_2$ platelets were oriented by the extrusion forces, and cuts were made by ultramicrotomy perpendicular to the stretching direction. SEM pictures were taken with a Zeiss Gemini 1530 from the diluted slurry sample after vacuum filtration over a ceramic membrane filter Anodisc 25.

5.3. Results and Discussion

5.3.1. Direct hydrothermal synthesis at 170 °C at various initial Mg/Al ratios

Direct hydrothermal synthesis at 170 °C at various initial Mg/Al ratios resulted in the formation of polytype $3R_2$ and some by-products depending on the initial ratios. The by-products were mainly brucite (crystalline $Mg(OH)_2$) and boehmite (AlO(OH)). The formation of polytype $3R_2$ was confirmed by the presence of the non-basal (101), (104), and (107) reflections in the XRPD measurements. The basal spacings of the (003) and (006) reflections of the synthesized polytype $3R_2$ were smaller than those of polytype $3R_1$. According to Allmann [8], the c-value of polytype $3R_1$ is 2.281 nm; while the c-values of the $3R_2$ products found in this study varied from 2.155 – 2.192 nm, which correspond to a basal spacing between the subsequent layers of 0.718 – 0.731 nm (Table 1). This variation could be caused by the occurrence of stacking faults which is common in layered materials. The a-value given by the (110) reflection varied between 0.304 – 0.305 nm.

Table 1. Experimental results of the direct hydrothermal synthesis at various Mg/Al ratios

Mg/Al bulk measured by ICP-AES	a-value (nm)	c-value (nm)	brucite (weight basis)	Al-tetra (molar basis)
1.80 ± 0.05	0.304	2.179	5 ± 0.5 %	34 ± 4 %
1.47 ± 0.05	0.304	2.171	3 ± 0.2 %	37 ± 4 %
1.34 ± 0.05	0.304	2.155	1 ± 0.2%	39 ± 4 %
1.19 ± 0.05	0.305	2.192	0.5 ± 0.1 % *	40 ± 4 %
1.1 ± 0.05	0.304	2.188	0.5 ± 0.1 % *	37 ± 4 %
1.05 ± 0.05	0.305	2.192	< 0.5 ± 0.1 % *	30 ± 4 %

*minor amount of boehmite

The formation of brucite can be detected by an FT-IR band at ~3698 cm^{-1} (Figure 1) and a XRPD reflection at the 2θ value of 18.5. FT-IR, however, has a better sensitivity for brucite detection. For Mg/Al ratios above 1.1, these FT-IR measurements as well as XRPD data indicate the formation of brucite (Figure 1). The amount of brucite correlated with the initial Mg/Al ratio. The results show that the higher the initial Mg/Al ratio the higher amount of brucite was formed. At a Mg/Al ratio ≤ 1.2, only a trace amount of brucite was found. A synthesis using a Mg/Al ratio ≤ 1.2 resulted in the formation of boehmite as identified by an FT-IR band at ~1064 cm^{-1} (Figure 1) and a XRPD reflection at the 2θ value of 14.5. Some boehmite is apparently formed from the ATH at high temperature [9] before all ATH has the time to fully convert into 3R$_2$. These results indicate that formation of polytype 3R$_2$ with a minimum amount of by-product is achieved at an initial Mg/Al ratio of 1.1-1.2.
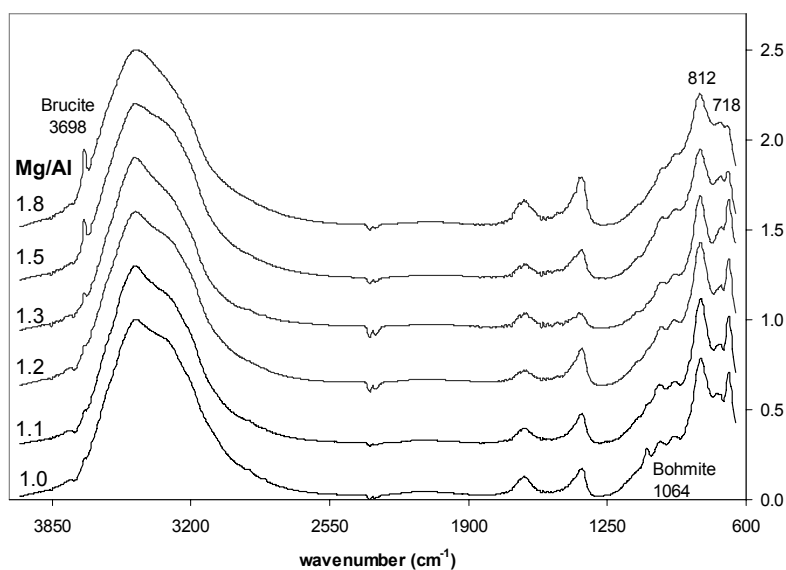
Figure 1. FT-IR spectra for direct hydrothermal synthesis at various initial Mg/Al ratios

5.3.2. Two step synthesis

In the two step synthesis method XRPD confirmed that polytype $3R_1$ with an a-value of 0.304 nm and a c-value of 0.2258 nm was formed (see Figure 2a) after 8 days synthesis at 90 ºC in an autoclave. The bulk Mg/Al ratio of the sample was confirmed to be 2.2 by ICP-AES. This result is in agreement with literature that the Mg/Al ratio in the octahedral layer of Mg-Al LDH can vary between 2-4 [1,10]. In the second step of the synthesis, a wet-ground slurry of ATH was added until a Mg/Al ratio of 1.1 was reached, and the slurry was hydrothermally treated at 170 ºC for 20 hours. The product of the second step was polytype $3R_2$, and most of its reflections could be indexed based on a unit cell with an a-value of 0.304 nm and a c-value of 0.2199 nm (see Figure 2b). This c-value is slightly smaller than the value of 0.2217 nm found by Newman [6]. As shown in Figure 2, the basal reflections of both $3R_1$ and $3R_2$ are very strong due to the preferred orientation of the plate-like LDH crystals. In polytype $3R_1$, the $(01(l+1))$ reflections are more pronounced than the $(10l)$ ($l = 3n + 1$, n = integer) reflections, and vice versa in polytype $3R_2$. Qualitatively, the same result has been found from simulated diffraction patterns where only the layer stacking was taken into account, and where the scattering of anions and water molecules in the interlayers were neglected [2,10]. The non indexed reflection at a 2θ value of 19.5 for $3R_2$ was suggested to be brucite as an impurity in the product [6].
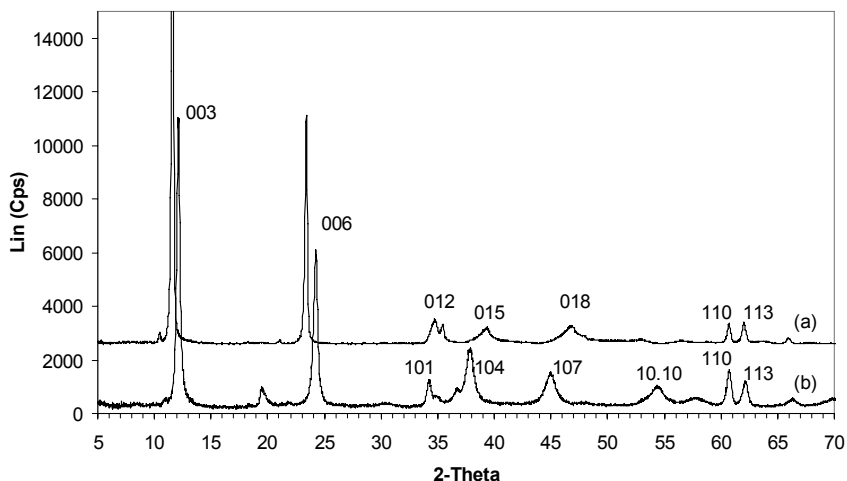
Figure 2. XRPD of the two-steps synthesis product. (a) polytype 3R$_1$ produced in step 1, (b) polytype 3R$_2$ produced in step 2.

A unique feature of polytype 3R$_2$ was revealed with 27-Al MAS NMR measurement as shown in Figure 3. In the spectra of the first step's product, only a single peak at 8.7 ppm is detected (a). This peak corresponds to aluminium ions with octahedral coordination [11]. The product spectra of the second step however show two peaks: a sharp peak at 8.7 ppm and a broad peak at 60-80 ppm. The broad peak corresponds to aluminium ions with tetrahedral coordination. The broadness of the tetrahedral aluminium peak indicates that there are various tetrahedral environment of the ion. The percentage of tetrahedrally coordinated aluminium ion, as calculated from the peak area of the tetrahedral and octahedral aluminium of the 27-Al NMR spectra, is about 40%. The percentages of aluminium ions with tetrahedral coordination of the direct hydrothermal synthesis method are listed in Table 1. As the synthesis took place at a pH of above 11, the ATH would dissociate into aluminate ions $(Al(OH)_4^-)$ [12]. This negative aluminate

ion is probably intercalated in the interlayer of the polytype $3R_2$ as a charge balancing anion.

Figure 3. ^{27}Al-NMR spectra of the two step synthesis product (a) polytype $3R_1$ produced in step 1, (b) polytype $3R_2$ produced in step 2.

In polytype $3R_1$, tetrahedrally coordinated Al ions are only observed in the dehydrated crystals after calcination. This change in the environment of a part of the Al ions was attributed to the dehydroxylation of the aluminium in the octahedral layer, and their octahedral coordination was restored upon the rehydration of the sample [13,14]. In polytype $3R_2$ however, the tetrahedrally coordinated Al ions are stable in the presence of water. In fact, the synthesis occurs in the presence of water.

High temperature XRPD measurement reveals that the reflections of polytype $3R_2$ remain the same up to a temperature of 200 °C. This observation is in contrast with polytype $3R_1$, which has been reported to show a decrease in basal spacing at 150 °C [15]. Apparently, polytype $3R_2$ has a better stability against an increase of temperature, which could be related

to the stabilization effect of the tetrahedrally coordinated Al ion in the interlayer.

Figure 4 shows the FT-IR spectra of the two step synthesis products, both giving typical bands for Mg-Al LDH. The band at approximately 3082-3471 cm^{-1} is the hydroxyl stretching mode of Mg–OH, Al–OH, H$_2$O and CO$_3$$^{2-}$– H$_2$O [16]. The bands at 1630 and 1641 cm^{-1} correspond to the bending mode of water (ν_2). The carbonate anti symmetric stretching mode band (ν_3) is observed at 1368 cm^{-1}. The band at 926 cm^{-1} could indicate a bending vibration of Al octahedral in a di-octahedral environment as identified by Kloprogge at 918 cm^{-1} [17,18], while the band at 682 cm^{-1} is the stretching mode of Al (octahedral) – O [19].
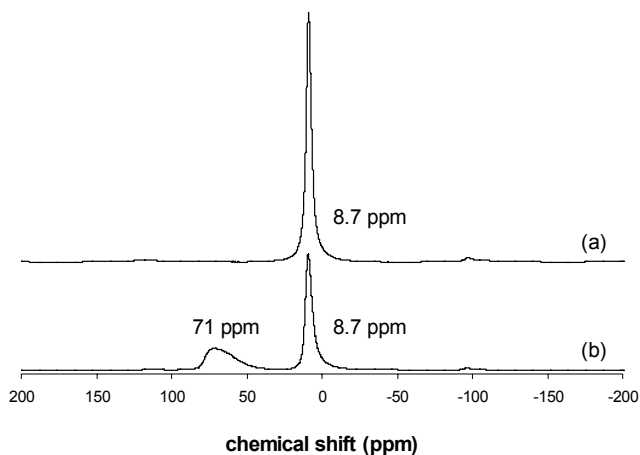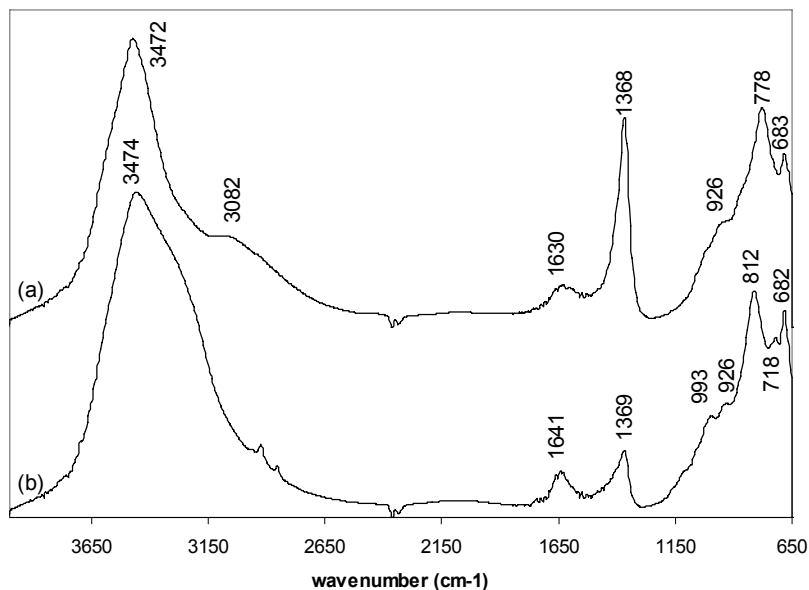

Figure 4. FT-IR spectra of the two-steps synthesis product (a) polytype 3R$_1$ produced in step 1, (b) polytype 3R$_2$ produced in step 2.

Despite the similarity of the IR spectra of both polytypes, several differences can be observed. The main difference is the amount of carbonate observed in the band around 1368 cm^{-1}. The AC=CB=CA layer stacking of polytype $3R_1$ results in the formation of a trigonal prismatic interlayer site in which carbonate ions lay horizontally connected via hydrogen bonds to the hydroxides of the octahedral layer. This explains the preference for carbonate as a counter ion in polytype $3R_1$. Most of the carbonate ions were not originally present in the synthesis mixture, but probably enter the lattice during drying of the product. For the AC-BA-CB layer stacking in polytype $3R_2$, an octahedral interlayer site is formed in which carbonate ions do not fit. The amount of carbonate indicated in the FT-IR spectrum of $3R_2$ reflects some residual $3R_1$ in the sample that is not converted during the second step of the synthesis.

Beside the carbonate content, there are also several other distinct bands for each polytype. In polytype $3R_1$ a band at 778 cm^{-1} was observed that was identified as the deformation mode of Al-OH [17], while in polytype $3R_2$, two different bands were observed at 812 cm^{-1} and 718 cm^{-1}. Both bands are ascribed to the vibration of tetrahedrally coordinated aluminium. The band at 812 cm^{-1} is the bending mode of Al(tetrahedral) – O(apical AlO$_4$) as was expected in region 750-850 cm^{-1} [17,19,20], while the band at 718 cm^{-1} is attributed to the stretching mode of (Al-O)$_{Td}$ [18,21]. The FT-IR measurements of the direct hydrothermal synthesis samples (Figure 1) also indicate the presence of the same tetrahedral aluminium band at 718 cm^{-1} and 820 cm^{-1}.

5.3.3. Chemical Composition and interlayer arrangement

Because 3R$_2$ is very insoluble in water, no single crystals could be prepared for single crystal XRD structure determination. For the establishment of the chemical composition and interlayer arrangement of polytype 3R$_2$, the products of the two step synthesis method were studied. The use of the two step synthesis facilitated comparison of polytype 3R$_1$ and 3R$_2$ which were subsequently synthesized in the same autoclave.

The 27-Al NMR measurement (Figure 3) shows that all aluminium ions in polytype 3R$_1$ are octahedrally coordinated. Since hardly any by-products were found, the Mg/Al ratio of the octahedral layer in the synthesized polytype 3R$_1$ was equal to its ratio of 2.2 as measured by ICP-AES. Both XRPD and FT-IR confirmed that the product of the second step contained polytype 3R$_2$ Mg-Al LDH without boehmite by product. However, there is about 1 wt% of brucite in the product. The bulk Mg/Al ratio of the solid product was measured to be 1.11 ± 0.01 by ICP-AES.

Sideris [22] showed that the ordering of the cations in the octahedral layer is such that an aluminium ion is surrounded by magnesium to prevent charge repulsion. This implies that the Mg/Al ratio in the octahedral layer should at least be 2.0. For a 3R$_2$ lattice with Mg/Al ratio of 2 in the octahedral layers and total charge compensation by aluminate ions in the interlayers, the percentage of tetrahedrally coordinated aluminium ions should be 50% and the total Mg/Al ratio of the sample should be 1.0. This value is not consistent with the measured bulk Mg/Al ratio (ICP-AES) of about 1.11 and with 40% aluminium in tetrahedral coordination (NMR). The discrepancy in the bulk Mg/Al ratio could be explained by the presence of a by-product with high magnesium content, while the discrepancy in the

percentage of tetrahedrally coordinated aluminium can either be caused by the fact that not all charge compensation in the $3R_2$ is provided by aluminate ions, or by the presence of by-products with a lower percentage of tetrahedrally coordinated aluminium ions, such as boehmite or polytype $3R_1$.

For this reason, the Mg/Al ratio of separate stacks of $3R_2$ crystals mixed in a matrix of nylon was measured by STEM-EDX. The images are parallel to the C-axis and the distance between the layers confirmed that the crystals are $3R_2$ crystals. Figure 5a shows that the crystal consists of straight platelets of approximately 50 layers with some stacking faults (red circles). The measured molar Mg/Al ratio of the crystals in Figure 5b is approximately 1.03 ± 0.05 with some areas having higher magnesium content (brighter yellow area). These areas with higher magnesium content indicate that the sample contains some brucite which could explain the discrepancy with the bulk Mg/Al ratio measured by ICP-AES.

(a)   (b)
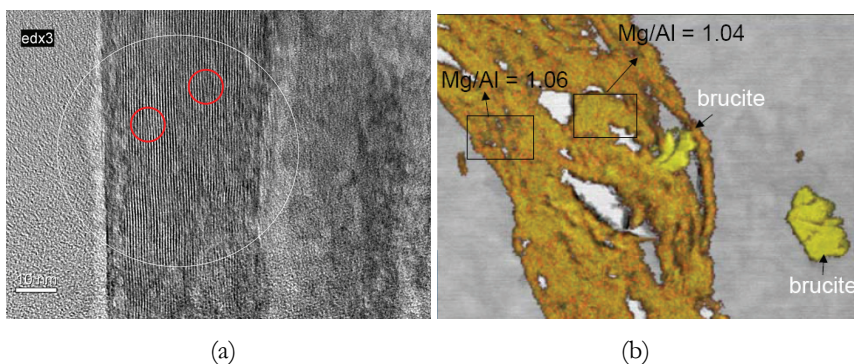
Figure 5. A higher magnification TEM image of polytype $3R_2$ from two-step synthesis method (a) and a STEM-EDX phase map of the stacks at a lower magnification (b)

More important however, is that the molar Mg/Al ratio measured by STEM-EDX mapping of 1.03 ± 0.05 confirms that the Mg/Al ratio in the octahedral layer is approximately 2.0 with most of the charge compensation in the interlayer occurring by aluminate ions. So the lower percentage of tetrahedrally coordinated Al (40%) measured by NMR has to be explained by the presence of by-products with only octahedrally coordinated Al. It is however, important to note that EDX measurements are relatively inaccurate compared to ICP.

It has recently been found, that in the presence of carbonate ions, only polytype 3R$_1$ can be formed and not 3R$_2$ even at 170 °C (chapter 7). Therefore, the carbonate content of the product was determined by wet chemical analysis, and turned out to be about 6 gram/kg.   Under the assumption that this carbonate corresponds with the amount of polytype 3R$_1$ in the sample, the weight fraction of 3R$_1$ with a Mg/Al ratio of 2.2 would be about 5 wt%. This unconverted polytype 3R$_1$ would increase the total Mg/Al ratio to approximately 1.03, which is in line with the STEM mapping. Such a small amount of polytype 3R$_1$ stacks manifested in a stacking fault in polytype 3R$_2$ can hardly be identified by XRPD. A slight shoulder on the left side of the (006) reflection of polytype 3R$_2$ (Figure 2b) could be consistent with a minor amount of polytype 3R$_1$, but this shoulder could also be caused by some stress in the 3R$_2$ polytype. Polytype 3R$_2$ with about 5 wt% of polytype 3R$_1$ would give 48% of aluminium having tetrahedral coordination. This still does not fully explain the lower content of tetrahedrally aluminium ions as found by NMR. An addition of 2-3 wt% brucite along with the 5 wt% polytype 3R$_1$ in the sample would explain the bulk Mg/Al ratio of 1.11 measured by ICP-AES. According to FT-IR, the sample contains about 1 wt% brucite, which still gives reasonable agreement

with the calculated value.   The discrepancy between the measured tetrahedral aluminium content by NMR and the ideal structure is subject of a more detailed study in chapter 6 on the structure of polytype $3R_2$.
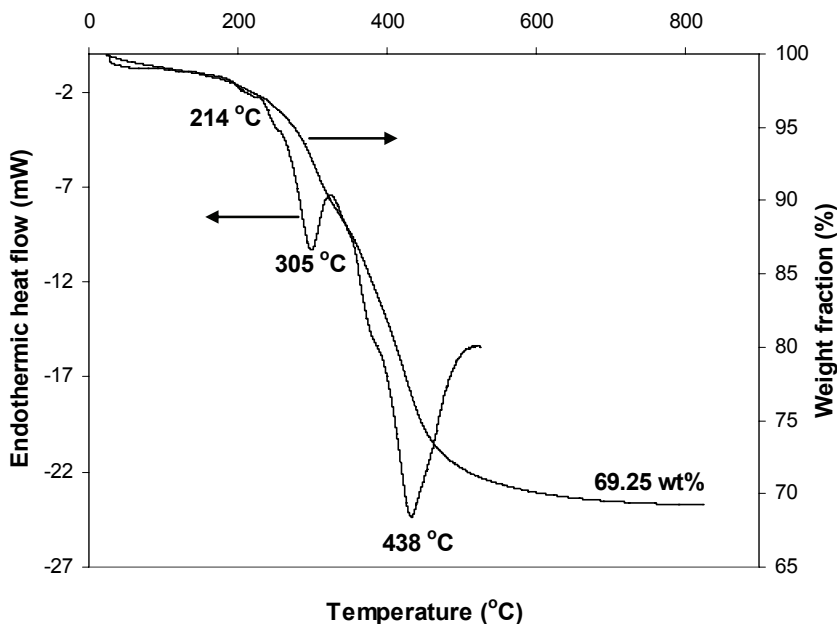
Figure 6. TGA and DSC measurements of polytype $3R_2$ from the two-step synthesis

The DSC plot shown in Figure 6 indicates three major heat flow events at 214, 305 and 438 °C which correspond to the dehydration, dehydroxylation of the interlayer and the hydroxylation of the octahedral metal layer respectively. The weight loss up to 214 °C of ± 2 wt% is related to that of the interlayer water content of the sample. This value is significantly smaller than the reported value for polytype $3R_1$ of ± 12 wt% [13,23]. Upon calcination up to 800 °C, the LDH degraded into MgO and Al_2O_3 [Rives 2003]. Calculation of the molecular formula from the measured value of 69.25 wt% resulted in $Mg_{0.66}Al_{0.33}[Al(OH)_3]_{0.33}(OH)_2 \cdot 0.09H_2O$ with a

calculated dry weight percentage of 70.1 %. In the above formula, the interlayer aluminate only contains three hydroxides, corresponding to a grafted option of the anion onto the octahedral metal layer as shown in Figure 7a. In nature, there are several groups of layered silicate minerals, with one or two tetrahedral sheets linked through oxygen atoms with one octahedral sheet[24].

(a)   (b)

⬤ =Mg or Al octahedral; ⬤ = Al tetrahedral; ⬤ = oxygen
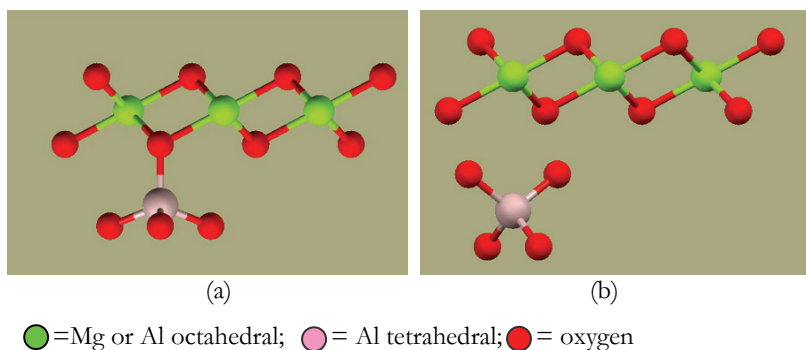
Figure 7. Possible arrangements of tetrahedral aluminium in the interlayer of polytype 3R$_2$. (a) the grafted option and (b) the non grafted option.

In an arrangement where the aluminates are not grafted onto the octahedral metal layer, the calculated dry percentage would be 65.8 wt%. For such an arrangement, the aluminates can be rotated in three dimensions. An example of such an aluminate arrangement is shown in Figure 7b. Since the difference between the TGA results and the calculated percentages for both options is small and within the error range of the measurements, both the grafted and non grafted options remain candidates for the structure.

5.4. Conclusions

The chemical composition and interlayer arrangement of polytype 3R$_2$ have been studied. Polytype 3R$_2$ Mg-Al LDH can be formed by direct conversion of MgO and ATH at 170 °C or by a two-step synthesis where polytype 3R$_1$

is first formed at 90 °C, and subsequently converted to polytype $3R_2$ at 170 °C after addition of ATH to a Mg/Al ratio of 1.1. A unique feature of polytype $3R_2$ is the presence of aluminium in a tetrahedral position as confirmed by 27-Al NMR and FT-IR. This tetrahedrally coordinated aluminium acts as counter ion for the charge compensation of the octahedral layer, and is thus located in the interlayer. These aluminates have a pillaring effect which also explains the increased stability of polytype $3R_2$ against elevated temperatures. From the TGA measurement it could not be firmly concluded whether the interlayer aluminate molecules were grafted to one side of the octahedral layer or be freely floating in the interlayer.

Experimental results showed that polytype $3R_2$ with a minimum amount of by-products (0.5 wt% of brucite and even less boehmite) could be formed by direct synthesis from an initial molar Mg/Al ratio between 1.05 and 1.2. The STEM-EDX mapping of polytype $3R_2$ produced from the two-step synthesis measured the total Mg/Al ratio of the crystal to be 1.03 ± 0.1. This confirms that the molar Mg/Al ratio in the octahedral layer is approximately 2.0 with most of the charge compensation in the interlayer provided by aluminate ions. 27-Al NMR however, measured only about 40% tetrahedrally coordinated aluminium ions instead of 50%. This discrepancy could not satisfactory be explained by the presence of minor amounts of $3R_1$ and boehmite as by-products with only octahedrally coordinated Al, and will be treated in more detail in chapter 6 on the structure of polytype $3R_2$.

Reference List

[1]   F.Cavani, F.Trifiro, A.Vaccari, Hydrotalcite-type anionic clays: Preparation, properties and applications, Catalysis Today 11 (1991) 173-301.

[2]   A.S.Bookin, V.A.Drits, Polytype diversity of the hydrotalcite-like minerals; I, Possible polytypes and their diffraction features, Clays and Clay Minerals 41 (1993) 551-557.

[3]   A.S.Bookin, V.I.Cherkashin, V.A.Drits, Polytype diversity of the hydrotalcite-like minerals; II, Determination of the polytypes of experimentally studied varieties, Clays and Clay Minerals 41 (1993) 558-564.

[4]   A.V.Radha, P.V.Kamath, C.Shivakumara, Conservation of order, disorder, and "crystallinity" during anion-exchange reactions among layered double hydroxides (LDHs) of Zn with Al, Journal of Physical Chemistry B 111 (2007) 3411-3418.

[5]   J.He et. al., Preparation of layered double hydroxides, Layered Double Hydroxides 119 (2006) 89-119.

[6]   S.P.Newman et. al., Synthesis of the 3R(2) polytype of a hydrotalcite-like mineral, Journal of Materials Chemistry 12 (2002) 153-155.

[7]   W.N.Budhysutanto et. al., Stability and transformation kinetics of 3R1 and 3R2 polytypes of Mg-Al layered double hydroxides, Applied Clay Science 48 (2010) 208-213.

[8]   R.Allmann, Double Layer Structures with Layer Ions (Me(Ii)(1-X)Me(Iii)(X)(Oh)2)(X+) of Brucite Type, Chimia 24 (1970) 99-&.

[9]   S.Music, D.Dragcevic, S.Popovic, Hydrothermal crystallization of boehmite from freshly precipitated aluminium hydroxide, Materials Letters 40 (1999) 269-274.

[10]   D.Evans and R.Slade, Structural Aspects of Layered Double Hydroxides, in: 2006, pp. 1-87.

[11]   J.Rocha, Solid-State NMR and EPR Studies of Layered Double Hydroxides, in: V.Rives (Ed.) , Layered Double Hydroxides: Present and Future, Nova Science Publisher, Inc, New York, 2001, pp. 193-214.

[12]   H.M.May, P.A.Helmke, M.L.Jackson, Gibbsite solubility and thermodynamic properties of hydroxy-aluminum ions in aqueous solution at 25°C, Geochimica et Cosmochimica Acta 43 (1979) 861-868.

[13]   M.Bellotto et. al., Hydrotalcite Decomposition Mechanism: A Clue to the Structure and Reactivity of Spinel-like Mixed Oxides, The Journal of Physical Chemistry 100 (1996) 8535-8542.

[14]   J.A.van Bokhoven et. al., Unique structural properties of the Mg-Al hydrotalcite solid base catalyst: An in situ study using Mg and Al K-edge XAFS during calcination and rehydration, Chemistry-A European Journal 7 (2001) 1258-1265.

[15]   J.Perez-Ramirez et. al., In situ investigation of the thermal decomposition of Co-Al hydrotalcite in different atmospheres, Journal of Materials Chemistry 11 (2001) 821-830.

[16]   J.T.Kloprogge, L.Hickey, R.L.Frost, The effect of varying synthesis conditions on zinc chromium hydrotalcite: a spectroscopic study, Materials Chemistry and Physics 89 (2005) 99-109.

[17]   J.T.Kloprogge, R.L.Frost, The effect of synthesis temperature on the FT-Raman and FT-IR spectra of saponites, Vibrational Spectroscopy 23 (2000) 119-127.

[18]   W.Xue et. al., FTIR investigation of CTAB-Al-montmorillonite complexes, Spectrochimica Acta Part A: Molecular and Biomolecular Spectroscopy 67 (2007) 1030-1036.

[19]   I.H.Joe et. al., FTIR as a Tool to Study High-Temperature Phase Formation in Sol-Gel Aluminium Titanate, Journal of Solid State Chemistry 131 (1997) 181-184.

[20]   T.I.Shishelova, M.S.Metsik, Changes in the IR Spectra of Micas on heating, Zhurnal Prikladnoi Spektroskopii 20 (1974) 1041-1044.

[21] I.Palinko, K.Lazar, I.Kiricsi, Cationic mixed pillared layer clays: infrared and M÷ssbauer characteristics of the pillaring agents and pillared structures in Fe,Al and Cr,Al pillared montmorillonites, Journal of Molecular Structure 410-411 (1997) 547-550.

[22] P.J.Sideris et. al., Mg/Al ordering in layered double hydroxides revealed by multinuclear NMR spectroscopy, Science 321 (2008) 113-117.

[23] Ts.Stanimirova et. al., Thermal evolution of Mg-Al-CO3 hydrotalcites, Clay Minerals 39 (2004) 177-191.

[24] M.F.Brigatti, E.Galan and B.K.G.Theng, Structures and Mineralogy of Clay Minerals, in: F.Bergaya, B.K.G.Theng, G.Lagaly (Eds.) , Handbook of Clay Science, Elsevier, Amsterdam, 2006, pp. 19-86.

Chapter 6

Structure of Polytype 3R$_2$ Mg-Al Layered Double Hydroxides

This chapter is submitted for publication in Applied Clay Science

ABSTRACT

A detailed analysis of the crystal structure of polytype 3R2 has been carried out based on XRPD diffractograms. Measurement of the transmission-XRPD pattern was also carried out in a spinning and tilting capillary using synchrotron radiation to eliminate the preferred orientation effect of the sample. In order to solve the structure of polytype 3R2, structural models, based on possible interlayer anion arrangement as revealed by FT-IR, 27-Al solid state NMR and XRPD, were constructed. The simulated diffractogram from the selected structural model was then subjected to a Rietveld refinement against the measured XRPD diffractogram. The study reveals that the interlayer is occupied by tetrahedral aluminate ions with their apical oxygen ions grafted onto the octahedral sheet. The refinement confirms that only 2/3 of the charge compensation is provided by aluminates.

6.1. Introduction

Polytypism in layered double hydroxides (LDH) has been studied by various researchers [1,2]. Polytypism arises from the different layer stacking of the octahedral metal layer in LDH. Based on the position of the atoms, a single octahedral metal layer can be identified as an AbC layer, with the capital letters and the lower case letter representing the oxygens and metal atom position respectively (see chapter 1). The stacking sequence of these layers with the bottom oxygen sub-layer in the same position as the following top oxygen sub-layer, such as in Ab**C = C**bA results in the formation of a trigonal prismatic interlayer denoted with the '=' sign. The other two possible stacking sequences are obtained when the top oxygen sub-layer of the adjacent octahedral metal layer occupies the same position as top oxygen sub-layer or as the cation of the previous octahedral metal layer, such as in **A**bC − **A**bC or AbC − **B**cA. These stacking sequences result in the formation of octahedral interlayer positions denoted with the '−' sign. Magnesium hydroxide (brucite) with the stacking sequence …− **A**bC − **A**bC −… can be considered as a one-layer polytype with a hexagonal symmetry (1H polytype).

Based on a theoretical study of the polytypes [1], there are two possible three-layer polytypes with rhombohedral symmetry, namely 3R$_1$ and 3R$_2$. In these two polytypes, all octahedral positions are occupied by either oxygen or metal atoms. However, polytype 3R$_1$ stacked as …= Ab**C = C**a**B = B**cA =… only has trigonal prismatic interlayers, while polytype 3R$_2$ (…− A**b**C − **B**cA − **C**aB −…) only has octahedral interlayers. Synthesis of LDH is conventionally carried out by co-precipitation of the metal salts at pH 10-12 [3,4]. The main polytype produced in this synthesis has 3R$_1$ symmetry.

Synthesis of Mg-Al LDH having $3R_2$ symmetry has only been reported by the hydrothermal method at temperatures above 110 °C [5,6]. The crystal structure however, is not yet fully solved and is a subject of this study.

In chapter 6, synthesis of polytype $3R_2$ Mg-Al LDH with a minor amount of by-products was reported to be experimentally feasible at a total Mg/Al ratio of 1.1-1.2. Local STEM-EDX measurement of the product however, gives a Mg/Al ratio of 1.03 ± 0.05. The interlayer of polytype $3R_2$ Mg-Al LDH synthesized by the hydrothermal method has been reported to contain mainly aluminates as counter ions. At the maximum isomorphic replacement of magnesium by aluminium in the octahedral metal layer (Mg/Al = 2.0) and assuming that the total charge compensation is fulfilled by aluminates, the total Mg/Al ratio would be 1.0. This would imply that the amount of tetrahedrally coordinated aluminium should be 50%. However, the amount of tetrahedrally coordinated aluminium, calculated from the 27-Al NMR is approximately 40%. These conflicting results cannot be justified by the presence of minor amount by-products in the sample. Another possibility is that another anion acts as counter ions in the interlayer as well. This counter ion could be hydroxide that is richly present in the solution at the synthesis pH of approximately 11.

Single crystals of polytype $3R_2$ could not be prepared because of the low solubility of the crystal at high temperature and its transformation to polytype $3R_1$ at low temperature [5]. So the only option to solve the structure of polytype $3R_2$ was from powder diffraction data. The structure of polytype $3R_1$ has been solved from naturally occurring single crystals [7] and will be used as the basis structure for this study. This structure has a high symmetry ($R\bar{3}m$), so only relatively few reflections are produced. Another

difficulty in the determination of the structure of 3R$_2$ is the preferred orientation of the platelets caused by the plate-like shape of the crystals. Layered materials are also prone to stacking faults which together with the crystallite size effect could result in hkl dependent broadening of the reflections.

6.2. Experimental

6.2.1. Synthesis of polytype 3R$_2$

Polytype 3R$_2$ was synthesized by a two-step hydrothermal method (chapter 6) from magnesium oxide (MgO from Martin Marietta as Zolitho 40), aluminium trihydroxide (ATH as Alumill F505) and distilled water. In the first step, 10% wt slurry of MgO and ATH in distilled water with a molar Mg/Al ratio of 2.2 was wet-ground and subsequently treated thermally in an autoclave at 90 °C for 8 days. The second step is the transformation to polytype 3R$_2$ that immediately followed the first step, by addition of ATH slurry to reach a molar ratio of Mg/Al in the slurry of 1.1. The slurry was then hydrothermally treated in the autoclave at 170 °C for 1 day. Subsequently, the autoclave was cooled down to 80 °C and the slurry was taken out. The slurry sample was dried at 50 °C in an oven and further powdered by mortar and pestle. The powder sample will be further referred to as two-step sample.

Polytype 3R$_2$ was also prepared by direct hydrothermal synthesis of a calcined MgO and ATH mixture. A mixture of MgO and ATH with molar ratio of 1.2 was calcined for 10 hours at 600 °C. The calcination step was followed by wet grinding and hydrothermal treatment in the autoclave at 170 °C for 1 day. The slurry product was taken out after the autoclave was

cooled down to 80 °C, dried at 50 °C in an oven and powdered by mortar and pestle. The sample will be further referred to as calcined sample.

6.2.2. Analysis with XRPD

The XRPD analysis was carried out with CuKα, CoKα and monochromatic synchrotron radiation. The normal theta-2theta measurements were made with CuKα radiation at TU Delft with a Bruker-AXS D5005 diffractometer with a Huber incident-beam CuKα monochromator and a Braun position sensitive detector (PSD). The wavelength was 1.5406 Å. The 2θ-range was 5–70° with a step size of 0.0387° and a counting time per step of 1 s. The specimens were made by dispersing the powder sample in ethanol and spreading it as a thin layer on a 2inch silicon [510] wafer.

The measurements with different tilting angles (ψ) were also done at TU Delft with a Bruker D8 Discover with Eulerian cradle; goniometer radius 300 mm was mounted in. Each measurement was carried out with CoKα radiation at wavelength 1.7903 Å of about 0.6 grams of sample in a backfill holder over a 2θ-range of 5–80° with a step size of 0.05° and a counting time per step of 4 s. The XRPD patterns were recorded at tilting angles (ψ) 0–75° with a step size of 5°.

The measurements with synchrotron radiation were carried out in the European Synchrotron Radiation Facility (ESRF) beam line BM01B for high-resolution powder diffraction in transmission mode. The measurement was performed in a robust 2-circle diffractometer equipped with 6 counting chains, capable of simultaneously collecting six complete patterns with an offset of ~1.1 degrees 2-theta. The wavelength was 0.50109 Å. The 2θ-

range was 1.5–40° with a step size of 0.003° and a counting time per step of 0.5 s. The specimens were contained in capillaries with 0.7 mm diameter and 0.01 mm wall thickness. During the measurement, the capillaries were spun.

Additional measurements were carried out in ESRF beam line BM01A with an image plate detector mar345. The wavelength of the measurement was 0.7000 Å. The detector was placed 200 mm from the specimen. During the measurement, the sample holder was rotated 1°/sec. The signal was integrated over the total exposure time of 120 sec.

6.2.3. Solving the crystal structure

In order to solve the structure of polytype 3R$_2$, structural models were built as Crystallographic Information Files (CIF). Visualisation of the structure and calculation of the powder diffraction pattern were then carried out with the Mercury 2.3 program. The measured diffractogram was refined with a Rietveld refinement program Rietica 1.7.7 [8] using the most probable model.

6.3. Result and Discussion

6.3.1. The measured XRPD patterns

All the XRPD patterns confirm that both samples (two-step and calcined) are of polytype 3R$_2$. Owing to the platelet shape of the crystal, the measurements with CuKα radiation from a thin layer specimen showed an enhancement of the intensities of the basal (00l) reflections due to preferred orientation (Figure 1). The intensity of the (003) reflection of the synchrotron measurement is approximately 36% of that in the CuKα radiation measurement.

The measurements with different tilting angles were used to determine the extent of the preferred orientation. The intensity (I) of the Bragg peaks can be modified to allow for preferred orientation due to the presence of plate like crystallites in the sample by using the March_Dollace equation [9]:

$$P_k = \left[P1^2 \cos^2 \alpha + P1^{-1} \sin^2 \alpha \right]^{-\frac{3}{2}} \tag{1}$$

$$I_{exp} = I_{random} \times P_k \tag{2}$$

where P1 is a refinable parameter and α is the acute angle between the scattering vector and the normal to the crystallites [8]. I_{random} is constant over all tilting angles, so for a proper value of P1, the relationship of Pk vs intensity should be linear. The P1 calculated from the samples resulted in a value of 0.65, which is similar to that of the synchrotron measurement. This indicates that the preferred orientation in the synchrotron measurement is significantly diminished.
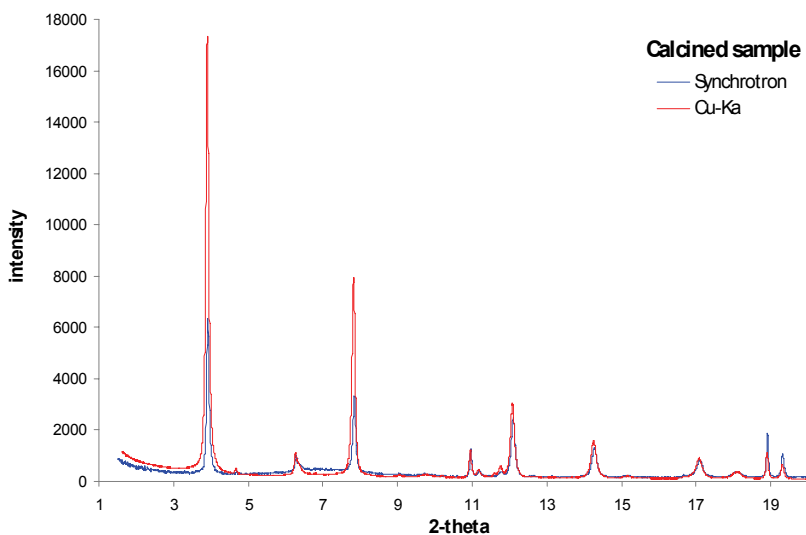
Figure 1. XRPD measurements of the calcined sample: by synchrotron radiation and CuKα radiation. For comparison, the diffraction patterns were both given for a wavelength of 0.50109 Å.

For crystallographic studies, the use of a spinning capillary essentially eliminates preferred orientation effects of the sample for all but the most anisotropic and grainy samples [10]. So the synchrotron radiation measurement carried out in a spinning capillary was expected to give better resolution, better angular accuracy and better relative intensities of the reflections. The synchrotron measurements were also expected to give narrower reflections which could reveal potentially overlapping reflections, especially for the polytype 3R$_1$ basal reflections. However, the synchrotron measurement (Figure 1) did not reveal additional reflections compared to the CuKα measurement. This implies that the broadening of the reflections are mainly caused by the sample and not by the instruments used. This also indicates that, should there be any 3R$_1$ present in the sample, it is most likely manifested as stacking faults.

Figure 2 shows the high-resolution synchrotron powder diffraction (HRPD) patterns of two differently prepared 3R$_2$ samples. In the HRPD setup, only measurements for a single azimuth angle could be done. Both samples exhibit similar diffraction patterns with the stronger (10l) over the (01(l+1)) (l = 3n + 1, n = integer) reflections. The unit cell parameters calculated from the diffraction pattern are a=b=0.305 nm ($\pm$ 0.001 nm) and c=2.196 nm ($\pm$ 0.01 nm). Additional measurements with an image plate detector mar345, however show that the use of the capillary still does not completely eliminate the preferred orientation.
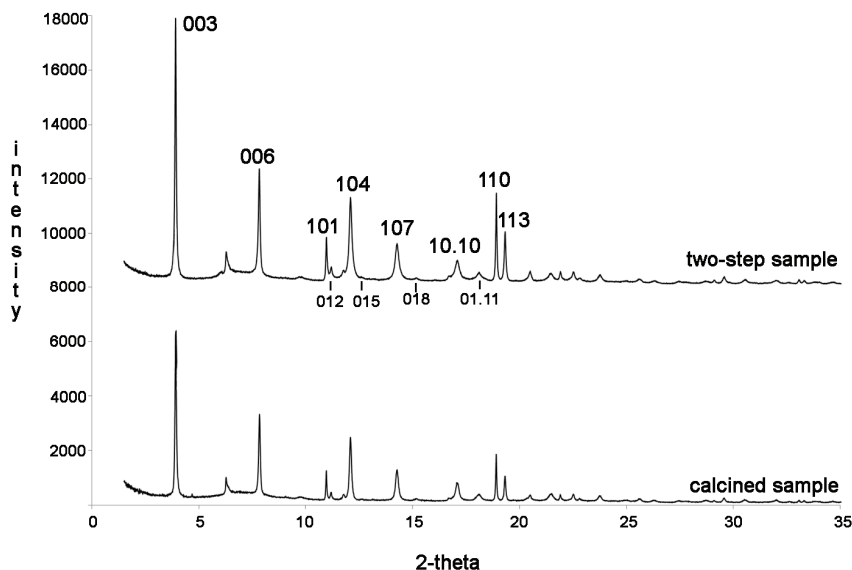
Figure 2. HRPD measurements of the $3R_2$ samples with synchrotron radiation

Shown in Figure 3 is the 2D diffraction image measured across various azimuth angles ($0 \leq \varphi \leq 360°$) for the calcined sample. Closer observation shows that preferred orientation can still be seen in the (003) and (006) reflections of this specimen although it is not major ($\pm 15\%$). However, the intensity ratios of the (003)/(006) reflections are constant throughout the various azimuth angles (see inserted picture in Figure 3), so the relative intensities measured at a single azimuth angle in the HRPD are still representative for the sample. A similar measurement carried out for the two-step sample however, showed more preferred orientation ($>40\%$) for both the basal and non-basal spacing (picture not shown). The calcined specimen with less preferred orientation was therefore selected for the Rietveld refinement below.
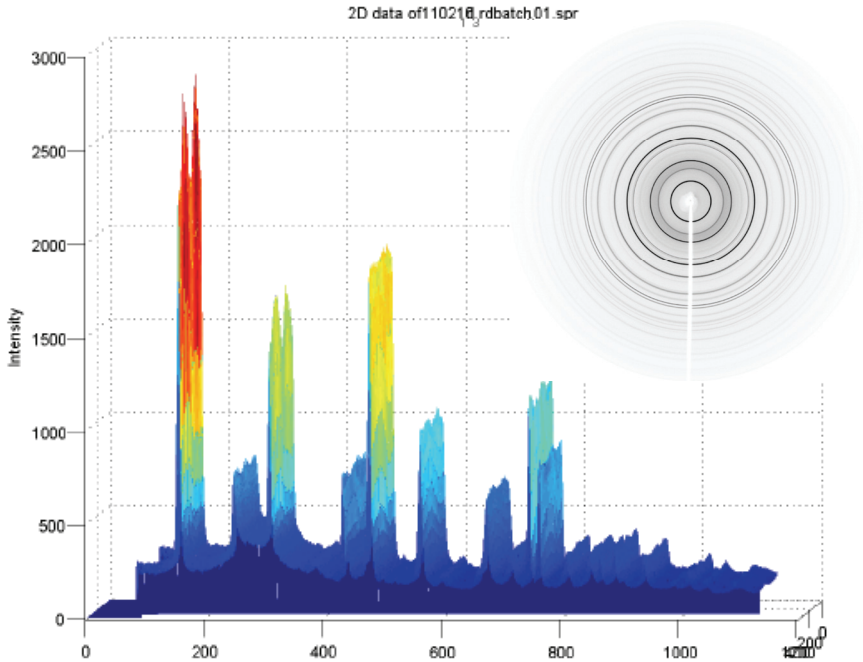
Figure 3. Diffractogram of the calcined 3R$_2$ sample at various azimuth angles measured with mar345 and the corresponding 2D diffraction image.

6.3.2. Interlayer Arrangement

Based on the (003) reflection of the 3R$_2$ sample from the two step synthesis, the c-value of the unit cell is calculated to be 2.196 nm (section 6.3.1). Since 3R$_2$ is a three-layer polytype, the thickness of one layer consisting of an octahedral layer and an interlayer, would thus be 0.732 nm. For polytype 3R$_1$ with Mg/Al = 2.0, the octahedral layer thickness is 0.19587 nm[11]. Using the same value for polytype 3R$_2$ would give an interlayer thickness of 0.5362 nm. The tetrahedral interlayer aluminates along with the charge repulsion distance must be accommodated in this space. The minimum charge repulsion distance, estimated as the sum of the Shannon ionic

radius[12] of an oxygen in the octahedral metal layer and an adjacent oxygen of a free floating aluminate ion in the interlayer is calculated to be 0.272 nm. The size of an $Al(OH)_4^-$ anion was estimated from the Shannon ionic radius[12] of a tetrahedrally coordinated Al ion, which is 0.039 nm and that of a hydroxide ion, which is 0.132 nm. So the Al-O distance is estimated to be 0.171 nm. For a perfect tetrahedron, the O-Al-O angle equals 109.47°. Several possible orientations of tetrahedrally coordinated aluminium ions in the interlayer could be considered as shown in Figure 4.
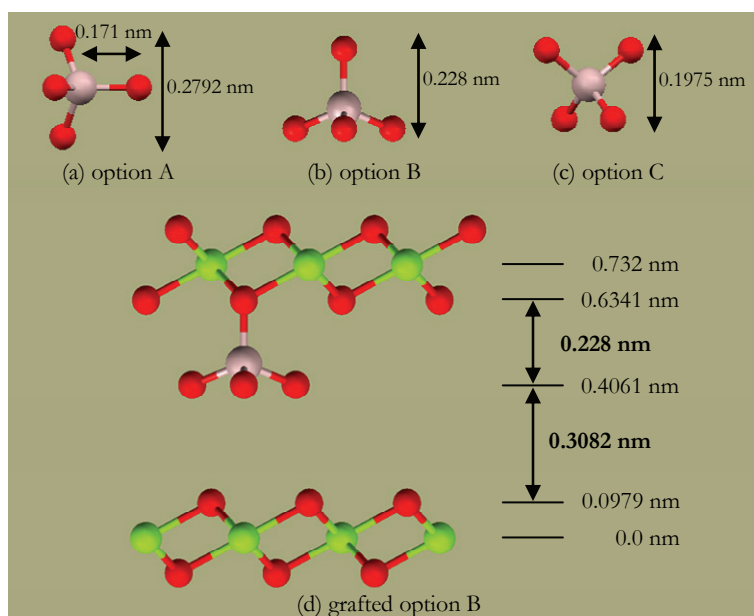
=Mg or Al octahedral; = Al tetrahedral; = oxygen

Figure 4. Possible arrangements of tetrahedral aluminate in the interlayer of polytype $3R_2$

In a structural model where the aluminates are floating freely in the interlayer gallery, two charge repulsion distances have to be accommodated, and none of the three options would fit. Also if only two-third of the counter ions is aluminate ions and the rest hydroxyl ions, there is not

enough space to accommodate the counter ions. For option B however, the apical oxygen could also be grafted onto the upper octahedral metal layer. In that case the distance between the oxygen of the octahedral metal layer below and the oxygen of the tetrahedral aluminates is approximately 0.3 nm, which could correspond with hydrogen bonding (Figure 4d). So the grafted option B is the only possible arrangement.

The thermal analysis of the two step sample (section 5.3.3) also favours the grafted option. This arrangement is found for many clay minerals. The structure of such clay minerals consists of one octahedral sheet and one or two tetrahedral sheets linked through oxygen atoms with the octahedral sheet. When a structure consists of 1 octahedral and 1 tetrahedral sheet, it is denoted as an 1:1 clay, such as kaolin, serpentine and feldspar groups. In all three groups, the main cation occupying the tetrahedral sheet is silica, but in feldspar, the tetrahedral position is also occupied by aluminate. Examples of 2:1 clays are the illite and smectite groups.

6.3.3. Building of a structural model

In this section structural models of all four options of polytype 3R₂ will be built for comparison of their simulated and the experimental powder diffraction pattern to see if based on these comparisons the free-floating options could also be excluded.

For all LDH structures with positively charged octahedral metal layers and compensating anions in the interlayer the space group is $R\bar{3}m$ with trigonal axes settings of $\alpha = \beta = 90°$ and $\gamma = 120°$. The unit cell parameters for polytype 3R₂ calculated from the HRPD pattern of the calcined sample are

a = b = 0.305 nm and c = 2.1962 nm. If both polytypes $3R_1$ and $3R_2$ are of the same space group, then the following translational symmetry holds:

$$(0,0,0) \qquad +(\tfrac{2}{3},\tfrac{1}{3},\tfrac{1}{3}) \qquad +(\tfrac{1}{3},\tfrac{2}{3},\tfrac{2}{3}) \qquad\qquad (3)$$

The construction of the structural model is based on the solved single crystal structure of polytype $3R_1$ [7,11] as shown in Table 1. The structural model of polytype $3R_2$ has been built with a Mg/Al ratio in the octahedral layer of 2, and with all charge compensation in the interlayer fulfilled by aluminates.

Table 1. Atomic position for polytype $3R_1$ Mg-Al LDH [11]

sample	Mg/Al = 2.0
space group	R3m
lattice parameters	a = 3.0460(1) Å
	c = 22.772(2) Å
preferred orientation	m = 1.000(2)
statistical indices	R_{wp} = 0.0893
	χ^2 = 4.2

Atomic Positions Mg/Al = 2.0

atom	x	y	z	100U	site	occupancy
Mg	0.0	0.0	0.0	2.27(5)	3a	2/3
Al	0.0	0.0	0.0	2.27(5)	3a	1/3
O(1)	0.0	0.0	0.37634(9)	3.85(8)	6c	1
H(1)	0.0	0.0	0.418(1)	8.4(7)	6c	1
O(2)	0.1058(7)	−0.1058(7)	0.5	2.9(2)	18h	1/6
C	1/3	2/3	0.5	8.4(7)	6c	1/12
H(2)	1/3	2/3	0.5	8.4(7)	6c	1/2

The positioning of the free floating aluminates in the four options has been done in a way to create the largest possible space between adjacent oxygen ions in the tetrahedral and octahedral layers for charge repulsion. In option A, the vertical oxygens of the tetrahedral aluminate are in a similar position as the top oxygen sub-layer of the octahedral metal layer. In option B, the tetrahedral aluminium ion is in a similar position as the top oxygen sub-layer

of the octahedral metal layer. In option C, the tetrahedral aluminium ion is positioned at the same x, y coordinates as the octahedrally coordinated magnesium or aluminium ions. In the grafted option B, the tetrahedral aluminate position is dictated by the bottom oxygen sub-layer of the octahedral metal layer

The structural models in the form of CIF were then visualised by the Mercury 2.3 program. The program also enables simulation of the XRPD patterns of the various models. The simulations were carried out at a wavelength of 0.50109 Å for the 2-theta range of 1.5 – 20° in order to cover all reflections up to the (113) reflection. The simulated XRPD patterns are shown in Figure 5.
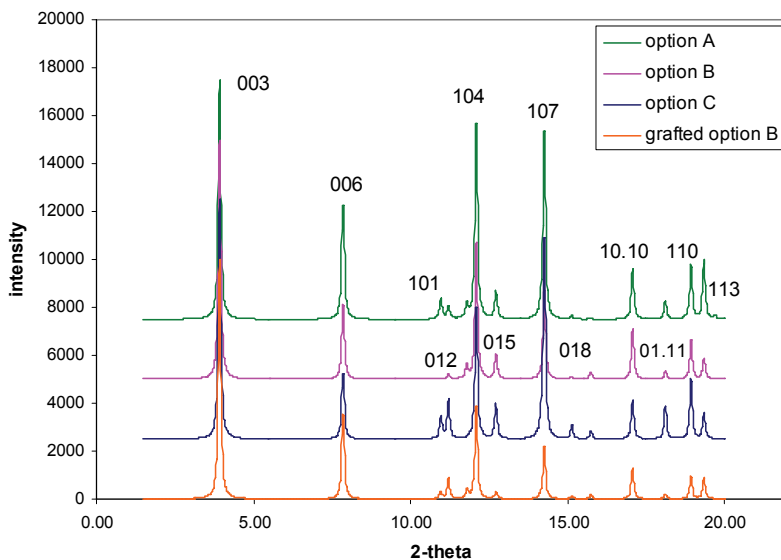
Figure 5. Simulated XRPD patterns of structural models of polytype 3R$_2$

In order to select the best fitting option the relative intensities of the (006)/(003) reflections, the non-basal reflections, and the (113)/(110)

reflections were compared . In the measured pattern (Figure 2), the intensity of the (006) is about half that of the (003) reflection and the intensity of the (113) is about 2/3 of the (110) reflection. According to Bookin and Drits [1], in the non-basal reflections region, the intensities of the (10l) reflections must be stronger compared to the (01(l+1)) (l = 3n + 1, n = integer) reflections (see chapter 1).

For option A, the intensity of the (006) reflection is stronger than for the others. This is understandable since for option A, two oxygens of the aluminates are at the same height as the aluminium ion, thus contributing to the atom density of the (006) plane. For all options, the rules of non-basal reflections are fulfilled except of the (012) vs. (101) reflections. Only option A follows the expected non-basal reflection intensities (012)> (101), so based on the simulated diffraction pattern it would be the most likely arrangement of aluminates in the interlayer. Replacement of some aluminate with hydroxyl ions would only proportionally lower the intensities of all reflections with respect to the (003) reflection, but would not influence the ratios.

There are however, other discrepancies between all four calculated and the measured pattern. The intensities of the (104) and (107) reflections are stronger than the (006) in the simulated patterns, except for the (107) reflection of grafted option B. The most striking discrepancy is however, the absence of the low-angle reflection at a 2θ value of 6.3 in the measured pattern (* in Figure 6 for grafted option B). This reflection is unique for the 3R$_2$ polytype and has been attributed up to now to brucite impurities [6] but can also follow from ordering of anions in the direction of the A or B axis. Since the FT-IR measurement does not indicate the presence of brucite in

this sample, the reflection might be due to a lower symmetry of the lattice combined with anion ordering. In order to simulate anion ordering, a larger unit cell of a' = a√3 = 0.5279 nm and c' = c has to be introduced. This larger cell has three possible tetrahedral positions of the aluminates with each position having 1/3 occupancy. In the structural models, however, the anion ordering is simplified by positioning the aluminium in only one of the three possible tetrahedral positions at full occupancy. This reduces the cell symmetry to P1, but still simulates the average structure of the crystal, and. results in many extra reflections; one of them corresponds to one at the 2θ value of 6.3 in the measured pattern (Figure 6). These extra reflections arise from the violation of the R$\overline{3}$m symmetry; their intensities are still too strong, as will be commented in section 6.3.4.
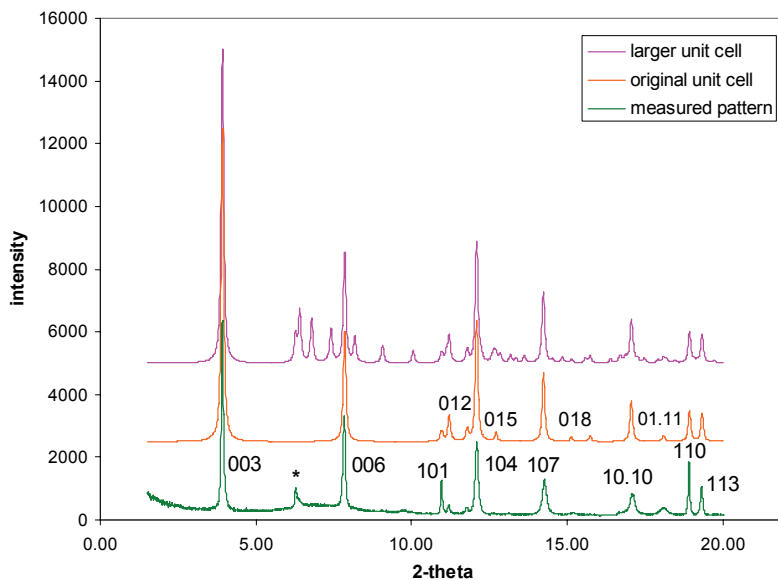
Figure 6. Comparison of the simulated grafted option B with the measured pattern

In summary, the grafted option B with a bulk Mg/Al ratio of polytype $3R_2$ ≤ 1.2 as measured by ICP-AES, with 40% of the aluminium ions to be tetrahedrally coordinated as shown by 27-Al solid NMR measurements and with the residual charge compensation coming from the hydroxyl ions is the most likely structure. The molecular formula would then be $Mg_{0.66}Al_{0.33}[Al(OH)_3]_{0.22}(OH)_{0.11}(OH)_2 \cdot 0.09H_2O$, with the water content calculated from TGA result. The dry weight percentage of such a molecule is 68.7 wt% compared to 65.5 wt% for the free-floating aluminate in the interlayer. The value for the grafted option comes closest to that of the dry weight of 69.25 wt% measured by TGA (chapter 5).

6.3.4. Rietveld refinement

Of the four CIF models described in the previous section, the model of the grafted option B has been selected for Rietveld refinement with the Rietica program. A larger unit cell of $a' = a\sqrt{3} = 0.5279$ nm is used in the refinement. The Mg/Al ratio in the octahedral layer is 2 with 2/3 charge compensation provided by grafted option B arrangement and the rest by hydroxyl anions.

In the refinement, the simulated XRPD pattern is compared to the measured one. In this exercise, the octahedral metal layer is assumed to be fixed, so only the position of the interlayer anions and their occupancies will be fitted. But the first fitting would be the removal of the background, followed by the fitting of the a and c parameters of the model. The refinement from the first two fitting procedures for the grafted option B model is shown in Figure 7.
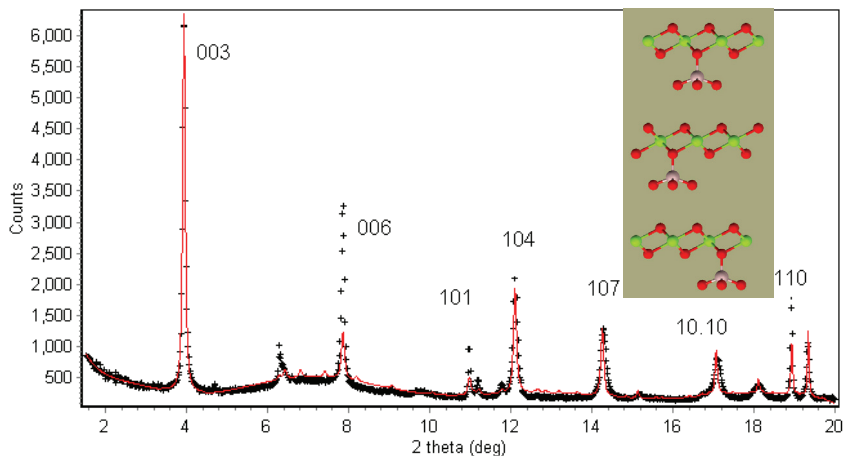
Figure 7. Rietveld refinement result of the grafted option B model. The black line represents the measured sample and the red one represents the refined pattern. The corresponding model is depicted in the inset.

Reduction of the aluminate occupancy in the interlayer by 1/3 indeed lowers the intensity of the extra reflections that were the consequence of the choice of P1 symmetry. The position of the hydroxyl anions does not have significant influence on the intensity ratios of the reflections. The main remaining discrepancies between the simulated and the measured model are the intensities of the (006), (101) and (110) reflections. The intensity of the (006) reflection is very much influenced by the anisotropy of the crystals and their tendency towards preferred orientation. A similar intensity discrepancy can also be observed for polytype 3R₁, as in the solved single crystal structure of 3R₁ the $I006/I003 = 0.15$ [7], while in a XRPD pattern of synthetic 3R₁ the ratio could be up to 0.5.

Table 2. Atomic position for polytype 3R$_2$ Mg-Al LDH from the Rietveld refinement

sample	Mg/Al = 1.0
space group	P1
lattice parameters	a = b = 0.52785 nm
	c = 2.19846 nm
	α = β = 90º
	γ = 120º
overall Thermal	U = 2.00
statistical indices	Rp = 18.26
	Rwp = 14.01
	χ^2 = 27.87

Name	Atom	x	y	z	site	occupancy
MG1A	Mg	0.0000	0.0000	0.0000	1a	0.6667
MG1B	Mg	0.3333	0.6667	0.0000	1a	0.6667
MG1C	Mg	0.6667	0.3333	0.0000	1a	0.6667
MG2A	Mg	0.6667	0.0000	0.3333	1a	0.6667
MG2B	Mg	0.0000	0.6667	0.3333	1a	0.6667
MG2C	Mg	0.3333	0.3333	0.3333	1a	0.6667
MG3A	Mg	0.3333	0.0000	0.6667	1a	0.6667
MG3B	Mg	0.0000	0.3333	0.6667	1a	0.6667
MG3C	Mg	0.6667	0.6667	0.6667	1a	0.6667
AL1A	Al	0.0000	0.0000	0.0000	1a	0.3333
AL1B	Al	0.3333	0.6667	0.0000	1a	0.3333
AL1C	Al	0.6667	0.3333	0.0000	1a	0.3333
AL2A	Al	0.6667	0.0000	0.3333	1a	0.3333
AL2B	Al	0.0000	0.6667	0.3333	1a	0.3333
AL2C	Al	0.3333	0.3333	0.3333	1a	0.3333
AL3A	Al	0.3333	0.0000	0.6667	1a	0.3333
AL3B	Al	0.0000	0.3333	0.6667	1a	0.3333
AL3C	Al	0.6667	0.6667	0.6667	1a	0.3333
ALT1	Al	0.3333	0.6667	0.2125	1a	0.6667
ALT2	Al	0.0000	0.6667	0.5458	1a	0.6667
ALT3	Al	0.0000	0.3333	0.8791	1a	0.6667
OT1B	O	0.5096	0.4904	0.1865	1a	0.6667
OT1C	O	0.5096	0.0193	0.1865	1a	0.6667
OT1D	O	-0.0192	0.4904	0.1865	1a	0.6667
OT2B	O	0.1763	0.4904	0.5199	1a	0.6667
OT2C	O	0.1763	0.0193	0.5199	1a	0.6667

Name	Atom	x	y	z	site	occupancy
OT2D	O	-0.3526	0.4904	0.5199	1a	0.6667
OT3B	O	0.1763	0.1571	0.8532	1a	0.6667
OT3C	O	0.1763	-0.3141	0.8532	1a	0.6667
OT3D	O	-0.3526	0.1571	0.8532	1a	0.6667
O1A	O	0.3333	0.0000	-0.0430	1a	1.0000
O1B	O	0.0000	0.3333	-0.0430	1a	1.0000
O1C	O	0.6667	0.6667	-0.0430	1a	1.0000
O1D	O	0.6667	0.0000	0.0430	1a	1.0000
O1E	O	0.0000	0.6667	0.0430	1a	1.0000
O1F	O	0.3333	0.3333	0.0430	1a	1.0000
O2A	O	0.0000	0.0000	0.2903	1a	1.0000
O2B	O	0.3333	0.6667	0.2903	1a	1.0000
O2C	O	0.6667	0.3333	0.2903	1a	1.0000
O2D	O	0.3333	0.0000	0.3763	1a	1.0000
O2E	O	0.0000	0.3333	0.3763	1a	1.0000
O2F	O	0.6667	0.6667	0.3763	1a	1.0000
O3A	O	0.6667	0.0000	0.6237	1a	1.0000
O3B	O	0.0000	0.6667	0.6237	1a	1.0000
O3C	O	0.3333	0.3333	0.6237	1a	1.0000
O3D	O	0.0000	0.0000	0.7097	1a	1.0000
O3E	O	0.3333	0.6667	0.7097	1a	1.0000
O3F	O	0.6667	0.3333	0.7097	1a	1.0000
OH1	O	0.1281	0.1009	0.2125	1a	0.3333
OH2	O	0.7381	0.0294	0.5458	1a	0.3333
OH3	O	0.4384	0.1791	0.8791	1a	0.3333
H1A	H	0.3333	0.0000	-0.0818	1a	1.0000
H1B	H	0.0000	0.3333	-0.0818	1a	1.0000
H1C	H	0.6667	0.6667	-0.0818	1a	1.0000
H1D	H	0.6667	0.0000	0.0818	1a	1.0000
H1E	H	0.0000	0.6667	0.0818	1a	1.0000
H1F	H	0.3333	0.3333	0.0818	1a	1.0000
H2A	H	0.0000	0.0000	0.2516	1a	1.0000
H2B	H	0.3333	0.6667	0.2516	1a	1.0000
H2C	H	0.6667	0.3333	0.2516	1a	1.0000
H2D	H	0.3333	0.0000	0.4151	1a	1.0000
H2E	H	0.0000	0.3333	0.4151	1a	1.0000
H2F	H	0.6667	0.6667	0.4151	1a	1.0000

Name	Atom	x	y	z	site	occupancy
H3A	H	0.6667	0.0000	0.5849	1a	1.0000
H3B	H	0.0000	0.6667	0.5849	1a	1.0000
H3C	H	0.3333	0.3333	0.5849	1a	1.0000
H3D	H	0.0000	0.0000	0.7484	1a	1.0000
H3E	H	0.3333	0.6667	0.7484	1a	1.0000
H3F	H	0.6667	0.3333	0.7484	1a	1.0000

The resulted fitting parameters and atomic positions are given in Table 2. Due to the uncertainties in aluminate positions as well as to the potential presence of stacking faults in the sample, the fit is not optimal. However, the refinement shows that in accordance with the 27-Al NMR results, only 2/3 charge compensation in the interlayer is provided by aluminates and the rest by hydroxyls. Based on the TGA measurement and the interlayer distance, option B with one of its apical oxygen grafted onto the octahedral sheet is the most plausible arrangement of aluminates in the interlayer of polytype $3R_2$.

6.4. Conclusion

In order to solve the structure of polytype $3R_2$ from powder diffraction data, it is essential to have sharp and distinct reflections with diminished the preferred orientation and sample broadening effects. The XRPD measurements were carried out on a thin layer and bulk (backfill method) for CuKα and CoKα radiation and in a capillary for synchrotron radiation. Because of the high symmetry of the crystal, not many reflections are visible, adding to the difficulty of the refinement of the structure. The measurements with different instruments show that the broadening of the reflections is mainly due to the sample effect. A signifcant elimination of the preferred orientation was however achieved in the synchrotron radiation measurement in spun capillaries. For this reason, the synchrotron

measurement of the calcined sample was taken as the input for the Rietveld refinement.

Structural CIF models were built for four potential aluminates arrangements in the interlayer. The octahedral metal layer of the structure was assumed to be the same as in the solved structure of 3R$_1$ while the Mg/Al ratio was taken to be 2 at the maximum isomorphic replacement of magnesium by aluminium ions. Based on the XRPD measurements, the interlayer distance could only fit a grafted arrangement of aluminates ion. This result also matches best with the molecular formula deducted from the TGA analysis. In this arrangement, the apical oxygen of the aluminates is grafted onto the oxygen of the octahedral metal layer. A larger unit cell of a' = a√3 = 0.5279 nm and c' = c = 2.1985 nm was used to simulate the anion ordering needed to get an observed reflection with a 2θ value of 6.3. The calculated pattern from the model was used as the input for Rietveld refinement of the measured XRPD pattern. The potential presence of stacking faults as well as the anisotropy of the crystals limited the accuracy of the refinement., The Rietveld refinement however, confirms the 27-Al NMR result that only 2/3 of the layer charge compensation is fulfilled by aluminates.

Reference List

[1]   A.S.Bookin, V.A.Drits, Polytype diversity of the hydrotalcite-like minerals; I, Possible polytypes and their diffraction features, Clays Clay Miner. 41 (1993) 551-557.

[2]   G.S.Thomas, M.Rajamathi, P.V.Kamath, DIFFaX Simulations of Polytypism and Disorder in Hydrotalcite, Clays and Clay Minerals 52 (2004) 693-699.

[3]   F.Cavani, F.Trifiro, A.Vaccari, Hydrotalcite-type anionic clays: Preparation, properties and applications, Catalysis Today 11 (1991) 173-301.

[4]   D.Evans and R.Slade, Structural Aspects of Layered Double Hydroxides, in: 2006, pp. 1-87.

[5]   W.N.Budhysutanto et. al., Stability and transformation kinetics of 3R1 and 3R2 polytypes of Mg-Al layered double hydroxides, Applied Clay Science 48 (2010) 208-213.

[6]   S.P.Newman et. al., Synthesis of the 3R(2) polytype of a hydrotalcite-like mineral, J. Mater. Chem. 12 (2002) 153-155.

[7]   R.Allmann, Double Layer Structures with Layer Ions (Me(Ii)(1-X)Me(Iii)(X)(Oh)2)(X+) of Brucite Type, Chimia 24 (1970) 99-&.

[8]   B.A.Hunter, C.J.Howard, in: LHPM A computer program for Rietveld analysis of X-Ray and Neutron Powder Diffraction Patterns, (Lucas Heights Research Laboratories, Menai, 1998).

[9]   W.A.Dollase, Correction of intensities for preferred orientation in powder diffractometry: application of the March model, Journal of Applied Crystallography 19 (1986) 267-272.

[10]   Fitch, A.N., The Highe Resolution Powder Diffraction Beam Line at ESRF, Journal of Research of the National Institute of Standars and Technology 109 (2004) 133-142.

[11]   M.Bellotto et. al., A Reexamination of Hydrotalcite Crystal Chemistry, The Journal of Physical Chemistry 100 (1996) 8527-8534.

[12]   R.D.Shannon, Revised Effective Ionic Radii and Systematic Studies of Interatomic Distances in Halides and Chalcogenides, Acta Crystallographica A 32 (1976) 751-767.

Chapter 7

Stability of Polytypes 3R$_2$ Mg-Al Layered Double Hydroxides towards Various Anions

ABSTRACT

Polytype $3R_2$ Mg-Al layered double hydroxides contains tetrahedral aluminates ion in its interlayer. In this research, the possibility of other tetrahedral coordinated ions to mediate the $3R_2$ layer stacking was investigated in the two-step hydrothermal synthesis at 170 °C. None of the investigated tetrahedrally coordinated ions, such as sulphate, borate or gallate could mediate the formation of the $3R_2$ stacking in the two step synthesis. Ion exchange of aluminate ions in the interlayer of polytype $3R_2$ is feasible in the following order of preference: $CO_3^{2-}>SO_4^{2-}>$stearate$>C_2O_4^{2-}>Br^-$. The $3R_2$ stacking is however not conserved, as the ion exchanged products have $3R_1$ stacking sequence.

7.1. Introduction

The structure of Layered Double Hydroxides (LDH) is based on the mineral brucite ((MgOH)$_2$) structure. Isomorphic replacement of some of the magnesium by aluminium ions causes the metal hydroxides layers to become positively charged.   Anions are therefore contained in the interlayers for charge compensation. Each metal hydroxides layer consists of two AC stacked sub-layers of oxygen ions with Mg and Al cations in the octahedral interstitial positions between the sub-layers. The total layer, that will be referred to as an octahedral metal hydroxides layer is then denoted as AbC. Based on the kind of stacking of the subsequent layers, two types of interlayer arrangement can be formed. When the top sub-layer of oxygen ions of the next octahedral layer is identically positioned as the bottom sub-layer of the previous stack, as in AbC = CbA, a trigonal prismatic interlayer is formed. When however, the top sub-layer of oxygen ions is positioned just as the top sub-layer of the previous stack or as the cation positions as in AbC–AbC or AbC–BcA respectively, an octahedral interlayer is formed. This has consequences for the coordination of the anions and the water molecules that are contained in the interlayers. Variations in stacking sequence of the octahedral layers are primarily responsible for the different crystal structures of LDHs. These various structures with their respective unit cells are known as polytypes.

In their theoretical study on potential polytypes, Bookin and Drits[1] concluded that there are one 1-layer polytype, three 2-layer polytypes, nine 3-layer polytype, and even more 6-layer polytypes. The naturally occurring Mg-Al LDHs are manasseite, a 2-layer polytype with hexagonal symmetry (2H$_1$) stacked as ...AbC=CbA=AbC... and hydrotalcite, a 3-layer polytype

with rhombohedral symmetry ($3R_1$) stacked as ...AbC=CaB=BcA=AbC...
Both polytypes have trigonal prismatic interlayers. Of the nine potential 3-
layer polytypes, only two have rhombohedral symmetry: polytype $3R_1$ and
polytype $3R_2$ stacked as ...AbC–BcA–CaB–AbC.... The main difference
between these polytypes is the interlayer arrangement with $3R_1$ having only
trigonal prismatic interlayers and $3R_2$ having only octahedral ones.

Polytype $3R_1$ Mg-Al LDH can be made synthetically by co-precipitation of
metal salt solutions at fixed and variable pH[2], by precipitation with urea as
a base retardant[3], by a sol-gel technique from metal alkoxide[4,5] and by
hydrothermal treatment of the metal oxides[6,7]. The molar Mg/Al ratio in
the octahedral metal layer hydroxides of this polytype can vary between 1.5
and 4[8]. Depending on the method of synthesis various anions present in
the synthesis mixture can be accommodated as counter ions in the interlayer,
which also contains water molecules. In hydrothermal synthesis of $3R_1$ from
MgO and $Al(OH)_3$, hydroxide ions serve as counter ions since no other
anions are present in the reaction mixture.

Up to now the $3R_2$ polytype of Mg-Al LDH could only be made by
hydrothermal synthesis from the oxides[7]. In a recent paper[9], it was shown
that the total molar Mg/Al ratio of $3R_2$ was approximately 1.0-1.2, and that
it could be hydrothermally synthesized either directly from the oxides at 170
°C or in a two step synthesis route. The transition temperature of polytype
$3R_1$ into $3R_2$ is approximately 110 °C[10]. So in the two-step synthesis first
$3R_1$ with a molar Mg/Al ratio of 2.3 was prepared at 90 °C, that was
subsequently converted into $3R_2$ at 170 °C after addition of $Al(OH)_3$ up to a
Mg/Al ratio of 1.2. In $3R_2$ not only hydroxides act as counter ions[9], but
also aluminate ions ($Al(OH)_4^-$). These aluminate ions share their apical

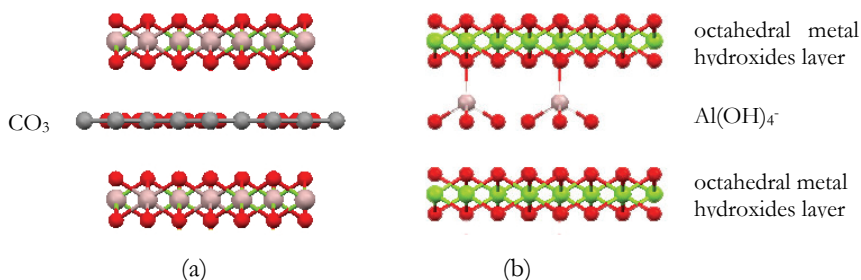oxygens with one side of the octahedral layers, and are therefore grafted to these layers Figure 1(b).

Figure 1. Interlayer arrangement of Mg-Al LDH polytype 3R$_1$ with carbonate anions (a) and polytype 3R$_2$ with grafted aluminate anions (b)

For an octahedral layer with a minimal Mg/Al ratio of 2:1 and a total charge compensation caused by aluminates, the Mg/Al ratio of the crystal should be 1:1. The ratio deduced from the 27-Al NMR measurements however, amounted to 1.2:1. Charge compensation by grafted aluminates also explains why the interlayer distance of polytype 3R$_2$ (d=7.28 Å) is smaller than in 3R$_1$-CO$_3$ or in 3R$_1$-OH   (d=7.60 Å) where the anion is freely floating in the interlayer.

Polytype 3R$_1$ Mg-Al LDH has been widely used as an anionic exchanger; its interlayer is known to expand depending on the anions accommodated within[11]. Carbonate anion with its planar arrangement is preferentially accommodated in a trigonal prismatic interlayer such as present in the polytype 3R$_1$[12] interlayer. The oxygens from the CO$_3^{2-}$ are hydrogen bonded with the OH groups of the metal layers. Thermodynamically, anion exchange is favoured for in-going anions with a high charge density[13]. Miyata[14] gave a list of ion selectivity for monovalent anions: OH$^-$>F$^-$>Cl$^-$

>Br$^-$>NO$_3^-$>I$^-$ and for divalent anions: CO$_3^{2-}$> Naphthol Yellow S> SO$_4^{2-}$. As shown above, the interlayer of polytype 3R$_2$ Mg-Al LDH is occupied by aluminate ions (Al(OH)$_4^-$) grafted onto one side of the octahedral layer[9]. This different bonding is expected to affect its use as an anionic exchanger. The aim of this investigation is to find out whether other anions than aluminates with a tetrahedrally coordinated metal ion could mediate the formation of polytype 3R$_2$ in a two-step synthesis, and to study the ion-exchangeability of polytype 3R$_2$.

7.2. Experimental

7.2.1. Two step synthesis of Polytype 3R$_2$

Polytype 3R$_2$ Mg-Al LDH was synthesized hydrothermally in a two step synthesis. In the first step, a mixture of magnesium oxide (MgO from Martin Marietta as Zolitho 40) and aluminium trihydroxide (ATH as Alumill F505) having a molar ratio of 2.3 were wet-ground in water using a Fritsch planetary ball mill at 400 rpm for 30 minutes. The final particle size of the reactant was approximately 2-3 micron. The slurry of reactants were diluted to 10 wt% and subsequently heated to 90 ºC in an autoclave for 24 hours in order to make polytype 3R$_1$. In the second step of the synthesis, wet ground ATH slurry was added until the Mg/Al molar ratio of the reactants reached 1.2. The slurry was then hydrothermally treated at 170 ºC for 1 day in order to make 3R$_2$-aluminate. Attempts to make 3R$_2$-sulphate, 3R$_2$-borate, or 3R$_2$-gallate were carried out by addition of ammonium sulphate solution, boric acid solution or gallium oxide in the second step of the synthesis. The autoclave was cooled down to 80 °C after the synthesis and the slurry product was taken out.

7.2.2. Ion Exchange

The ion exchange experiments were carried out with 3R$_2$-aluminate which was made with the two step synthesis. Several groups of anions were investigated: oxides, inorganic salts, and organic salts. The oxides investigated were SiO$_2$ quartz and ZnO. The inorganic salts investigated were NH$_4$SO$_4$, (NH$_4$)$_2$CO$_3$, Na$_2$SiO$_3$, KBr and KH$_2$PO$_4$. The organic salts investigated were sodium oxalate and sodium oleate. Ion exchange with stearic acid was also investigated. The ion exchange experiments were carried out by dissolving the salts in distilled water, or by making slurry of the oxides in water and by adding the solution or slurry to the 3R$_2$-aluminate slurry. The experiments were carried out at 170 ºC for 24 hours in an autoclave, unless stated otherwise. After cooling down to 80 °C, the slurry product was taken out. Part of the slurry was filtered and washed to eliminate the excess salts.

7.2.3. Analytical techniques

Part of the slurry samples taken from the experiments were dried overnight in an oven at 50 ºC. The dried samples were analyzed by FT-IR, NMR, Induced Couple Plasma – Atomic Emission Spectrometry (ICP-AES), and XRPD. The FT-IR measurements were done with a Nexus Thermo Nicolet 5700 spectrometer. Powder samples were pressed in small discs using a KBr matrix. The IR bands were recorded at a spectral range of 650-4000 cm^{-1}. For the ICP-AES measurements, powder samples were dissolved in nitric acid, diluted to the ppm scale and subsequently measured with a Spectro Arcos. The 27-Al MAS NMR measurements were done on a Bruker Avance-400 spectrometer at 104.2 MHz. The solid sample was measured at a spinning speed of 11 kHz in a 4 mm Zr rotor using 0.08 s acquisition time

with 1 s acquisition delay. Aluminium nitrate [1M] was used as an external chemical shift reference, and its chemical shift was set at 0 ppm. The XRPD measurements were done with a Bruker-AXS D5005 diffractometer with a Huber incident-beam Cu Kα monochromator and a Braun position sensitive detector (PSD). The 2θ-range was 5–70° with a step size of 0.0387° and a counting time per step of 1 s.

7.3. Result and Discussion

7.3.1. Formation of Polytype 3R$_2$

FT-IR and XRPD confirmed that the product of the first step of the synthesis is polytype 3R$_1$ Mg-Al LDH. In the second step synthesis, polytype 3R$_2$-aluminate was produced after addition of ATH slurry and hydrothermal synthesis at 170 °C for 24 hours. The basal d-spacing of 3R$_2$-aluminate is smaller than that of 3R$_1$ (Table 1). The presence of aluminium in the 3R$_2$ interlayer as aluminate ions with tetrahedral coordination is confirmed by 27-Al NMR and FT-IR. Sulphate anions were also expected to mediate the formation of polytype 3R$_2$[15] because of their tetrahedral coordination. Addition of ammonium sulphate solution to the 3R$_1$ slurry, and the subsequent hydrothermal treatment at 170 °C did not however, result in polytype 3R$_2$. Instead, polytype 3R$_1$-sulphate with a basal spacing of 10.53 Å was produced. The intercalation of sulphate anions in the interlayer of polytype 3R$_1$ can incorporate an additional water molecule resulting in a larger interlayer distance compared to the non hydrated variant. The basal spacing of our 3R$_1$-sulphate corresponds with the reported values in literature [12,14,16] for the hydrated type.

Both boron and gallium are group IIIB elements in the periodic table and were chosen as candidates for substitution for aluminium on the grounds of their ionic size, valency and electronegativity. The addition of boric acid, which is also known to have tetrahedral coordination, did not result in the formation or polytype 3R$_2$. Upon addition of boric acid and hydrothermal treatment at 170 °C for 24 hours, the polytype 3R$_1$ remains with partial ion exchange of the OH anion by borate. In the case of gallium, XRPD showed reflections of gallium oxide and polytype 3R$_1$ crystals after addition of gallium oxide in the second step synthesis.

Table 1. Experimental Ion Exchange Results

Process	Product	Cell parameter (XRD)		NMR
		a (Å)	c$_0$ (Å)	% Al-tetrahedral
first step	3R$_1$-OH	3.04 - 3.05	7.48-7.59	0%
second step				
Al(OH)$_3$	3R$_2$-aluminate	3.05	7.28	36 - 41%
(NH$_4$)$_2$SO$_4$	3R$_1$-SO$_4$	3.04	10.53	n/a
H$_3$BO$_3$	3R$_1$-OH	3.05	7.66	n/a
Ga$_2$O$_3$	3R$_1$-OH		7.54	n/a
ion exchange				
SiO$_2$ (quartz)	3R$_2$-aluminate	3.05	7.26	42%
ZnO	3R$_2$-aluminate	3.05	7.48	
(NH$_4$)$_2$SO$_4$	3R$_1$-SO$_4$	3.04	10.62	0%
(NH$_4$)$_2$CO$_3$	3R$_1$-CO$_3$	3.04	7.6	0%
Na$_2$SiO$_3$	3R$_2$-aluminate	3.05	7.22	44%
KBr	3R$_2$-aluminate	3.04	7.34	33%
	LDH-Br		7.83	
KH$_2$PO$_4$	3R$_2$-aluminate	3.05	7.12	40%

7.3.2. Ion exchange with oxides

The aluminium ions located in the interlayer of polytype $3R_2$ have tetrahedral coordination, so it is worthwhile to study whether other oxides that can coordinate tetrahedrally can replace these interlayer aluminate ions. In various clay minerals, silica is known to occupy a tetrahedral position[17], so silica is a potential candidate for ion exchange. Zinc was investigated because $[Zn(OH)_4]^{2-}$ with tetrahedral coordination is facoured under conditions of high pH. However, no ion exchange had occurred in both cases after 24 hours. XRPD of the products still indicated the reflections of the initial polytype $3R_2$ with additional reflections from the added oxides.

7.3.3. Ion exchange with inorganic salts

Ion exchange of polytype $3R_2$–aluminate with sulphate anions from an $(NH_4)_2SO_4$ solution resulted in the formation of polytype $3R_1$-sulphate crystals. No trace of polytype $3R_2$-aluminate was found afterwards by either XRPD or FT-IR. XRPD indicated that the solid product contains hydrated $3R_1$-sulphate crystals having a basal d-spacing of 10.62 Å. The intercalation of the sulphate anion is also confirmed by a band at 1115 cm^{-1} in the FT-IR spectrum (Figure 2b). Along with the formation of $3R_1$-sulphate, boehmite $(AlO(OH))$ was formed from the aluminate ions released from the interlayer of $3R_2$-aluminate. The reflections of boehmite are denoted by * in the XRPD pattern (Figure 3). In the FT-IR pattern the formation of boehmite is reflected by a band at 1066 cm^{-1}.
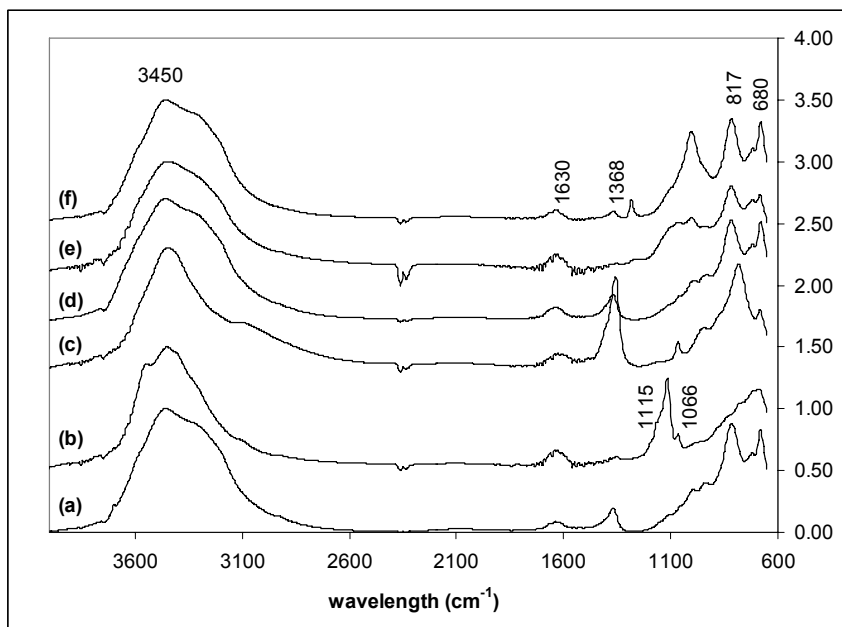
Figure 2. FT-IR spectra of polytype 3R$_2$-Al(OH)$_4$ (a) and its ion exchange product with (NH$_4$)$_2$SO$_4$ (b), NH$_2$COONH$_4$ (c), KBr (d), KH$_2$PO$_4$ (e) and Na$_2$SiO$_3$ (f).

3R$_2$-aluminate was also ion exposed to an ammonium carbamate (NH$_2$COONH$_4$) solution at 170 °C. The carbamate ion hydrolises to ammonium carbonate, which resulted in the formation of 3R$_1$-CO$_3$ with some boehmite by-product, as shown by XRPD (Figure 3c). No trace of 3R$_2$-aluminate can be found in the XRPD pattern. FT-IR indicated a strong carbonate band at 1368 cm^{-1}, and the disappearance of the tetrahedral aluminium band at 812 cm^{-1} (Figure 2c). 27-Al solid NMR of the product after ion exchange only detected the presence of aluminium ions with octahedral coordination confirming the disappearance of 3R$_2$-aluminate. The aluminate ions released from the interlayer of polytype 3R$_2$, precipitated as boehmite, are detected by both FT-IR and XRPD.
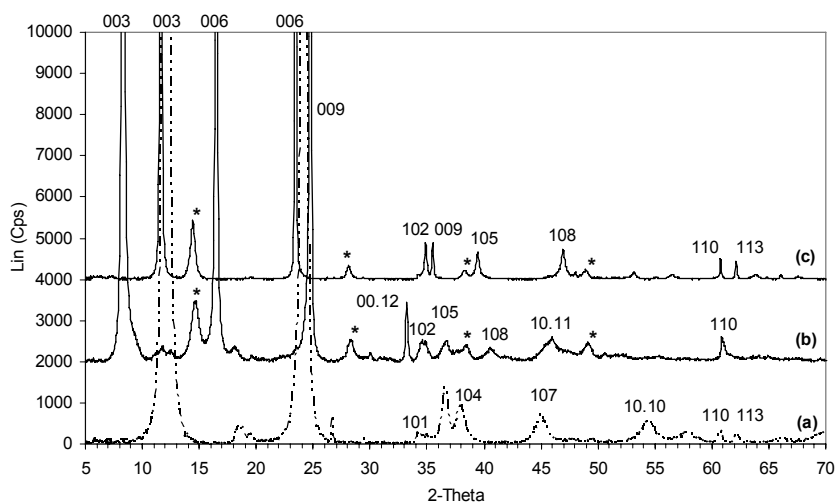
Figure 3. XRPD spectra of polytype $3R_2$-Al(OH)$_4$ from the two step synthesis (a) and its anion exchange product with NH$_4$SO$_4$ (b) and NH$_2$COONH$_4$ (c). The reflections denoted by * belong to boehmite.

When potassium bromide was used in the ion exchange experiment, part of the aluminate ions were apparently replaced by bromide ions after 24 hours, since XRPD showed reflections of layered material with a basal d-spacing that fits the bromide anion size. Unfortunately the stronger reflections of the residual $3R_2$-Al(OH)$_4$ and KBr prevented identification of the LDH-bromide polytype. Formation of some boehmite in the end product was also visible in the XRPD pattern. The intercalation of bromide anions in the interlayer was also supported by the decrease of the tetrahedral aluminium content from 40% to 34% as revealed by 27-Al NMR.

Ion exchange of sodium silicate with polytype $3R_2$-aluminate did not occur. XRPD showed additional reflections that belong to Na$_2$SiO$_3$, but the reflections of $3R_2$-aluminate remained. 27-Al NMR however, indicated an increase in tetrahedral aluminium content from 36% to 44% for an

unexplained reason. For potassium dihydrogen phosphate no change in the 3R$_2$-aluminate pattern was observed by either XRPD, Al-NMR, or FT-IR.

7.3.4. Ion exchange with organic material

Various references have reported the successful intercalation of oxalate[18], oleate[19] and stearate[20] anions in 3R$_1$ Mg-Al LDH with an increase in thermal stability compared to 3R$_1$-carbonate. For that reason, the potential ion exchange of 3R$_2$-aluminate with those anions was investigated. Ion exchange with sodium oxalate resulted in a partial intercalation of the oxalate ions in the interlayer, as shown by the increase in basal d$_{003}$-spacing to 7.8 Å (see Figure 4a). Polytype 3R$_2$-aluminate is still present in the end product, along with some boehmite, which precipitated from the aluminate ions previously present in the interlayer of 3R$_2$-aluminate. The non basal reflections of the product show the (102) and (105) reflections which indicates that the LDH-oxalate formed has the 3R$_1$ layer stacking.
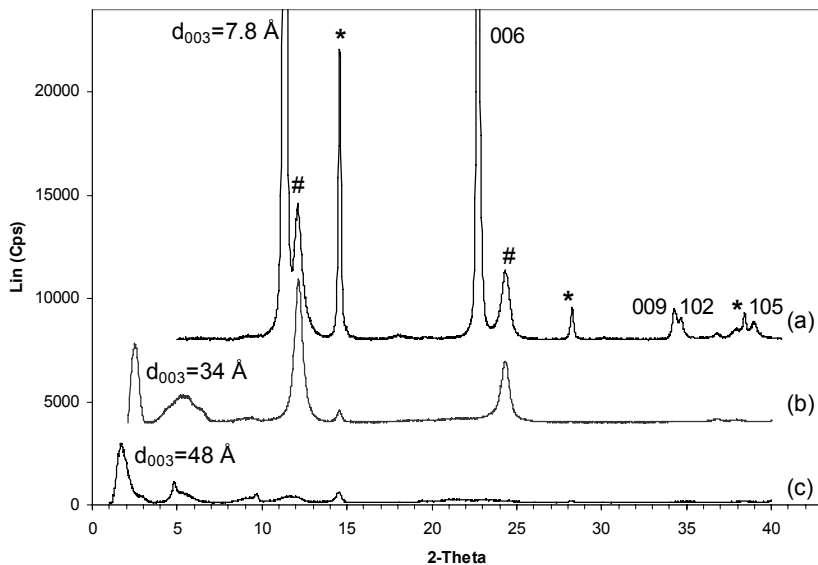
Figure 4. XRPD pattern of the product from $3R_2$ ion exchange with Na-oxalate (a), Na-oleate (b) and stearic acid (c). The reflections denoted by # and * belong to $3R_2$-aluminate and boehmite respectively.

The intercalation of oleate and stearate ions in the Mg-Al LDH was confirmed by XRPD through the increase in d_{003}-spacing and the formation of boehmite. The LDH-oleate formed during the ion exchange experiment has a d_{003}-spacing of 34 Å (Figure 4b), similar to the value reported in literature[19,21]. Furthermore, the XRPD pattern also indicates the existence of unconverted $3R_2$-aluminate, as well as of formed boehmite. Since the experiment with Na-oleate was performed at 120 °C, a lot of $3R_2$-aluminate remains in the sample since the exchange is not yet finished. As shown in Figure 4c, the resulting LDH-stearate has a d-spacing of 47 Å, consistent with a formerly reported bilayer intercalation of stearate in LDH[22]. Due to the stretching of the interlayer distance the non basal reflections are no longer visible, so the layer stacking of both the oleate and stearate LDH could not be determined.

7.3.5. Discussion

From the various anions being investigated, only polytype 3R$_2$-aluminate can be synthesized. This can only be done hydrothermally in the absence of other counter ions than hydroxides. In the two-step synthesis, addition of sulphate, borate or gallium oxide to polytype 3R$_1$, followed by hydrothermal treatment at 170 °C for 24 hours did not result in the 3R$_2$ stacking.

Despite the grafting of aluminates ions onto the octahedral metal layer in polytype 3R$_2$, ion exchange of those aluminates with various anions is still feasible, although the 3R$_2$-aluminate lattice then converts into the apparently more stable 3R$_1$-anion lattice Ion exchange took place with carbonate, sulphate, bromide, oxalate, oleate, and stearate anions. The order of anion preference in the interlayer of polytype 3R$_1$ LDHs is reported to be related to the anionic charge, the charge density of the metal octahedral layer and the hydrogen bonding potential[23]. Carbonate, sulphate and oxalate have a higher charge compared to aluminate. Its lower charge also explains the slower exchange rate for bromide.

In case of carbonate, it is well known that it only fits in trigonal prismatic interlayers, such as those in the 3R$_1$ stacking sequence[24]. Conversion into 3R$_1$-carbonate even occurs at 170 °C, where the 3R$_2$-aluminate is the stable polytype[10] compared to 3R$_1$-OH in pure water. This indicates that the 3R$_1$ stacking is stabilized by the hydrogen bonding of carbonate with the octahedral metal layers. Pausch[25] also observed that in the presence of CO$_2$, only hydrotalcite (3R$_1$-CO$_3$) was formed at higher temperature and at a higher Al content of the starting material.

Even though the symmetry of the sulphate ion should fit in both a trigonal prismatic and an octahedral interlayer arrangement[15], the $3R_1$ stacking sequence is preferentially formed during hydrothermal synthesis or by ion exchange at 170 ºC. Bish[26] reported the occurrence of polytype $3R_2$-SO_4 Ni-Al LDH in nature, but some of the non basal reflections do not fit the structure. As to our knowledge, no other occurrence of Mg-Al LDH $3R_2$-SO_4 has been reported.

According to the presence of $3R_2$-aluminate and boehmite in the product after ion exchange, the preference for ion exchange could be listed in the following order: CO_3^{2-}> SO_4^{2-}> oleate> $C_2O_4^{2-}$> Br^-.

Both oleate and stearate are only single negatively charged, but both have a rather long a-polar tail. These tails can be densely packed as in a compressed Langmuir layer perpendicular to the stacking of the Mg-Al LDH layers. This dense packing together with the H-bridges of the heads of the oriented molecules with these LDH layers could explain the low lattice energy of such structures compared to that of $3R_2$-aluminate.

 The attempts to ion exchange $3R_2$-aluminate with other salts and oxides did not succeed. This inability of aluminate anions in polytype $3R_2$ to be ion exchanged could be due to the fact that it is grafted upon the octahedral layer. For a grafted structure, a metal-oxide bond has to be broken for the interlayer anion (aluminate) to become labile, and hence exchange. This might explain its apparent reluctance and the low yields of the exchanged products with $3R_2$. Furthermore, to form a stable $3R_2$ structure with a substituted anion, a similar bond probably has to form to accommodate the

anion geometry. This may be the reason why substitution occurs much more readily in the 3R$_1$ structure, where no such bonding is involved.

7.4. Conclusion

Polytype 3R$_2$ Mg-Al LDH can be synthesized by hydrothermal treatment of MgO and ATH at 170 ºC in a two step synthesis. The aluminate ion seems to mediate the formation of 3R$_2$. Of all the octahedrally coordinated anions only aluminate ions mediate the 3R$_2$ stacking sequence. This 3R$_2$ stacking sequence cannot be sustained during ion exchange with carbonate, sulphate or oxalate anions as it converts into the 3R$_1$ stacking sequence. The anion selectivity for the exchange is in the following order: CO_3^{2-}>SO_4^{2-}>stearate>$C_2O_4^{2-}$>Br^-. Oleate and stearate also induce ion exchange, but the stacking sequence of the layers could no longer be identified.

Reference List

[1]   A.S.Bookin, V.A.Drits, Polytype diversity of the hydrotalcite-like minerals; I, Possible polytypes and their diffraction features, Clays and Clay Minerals 41 (1993) 551-557.

[2]   J.He et. al., Preparation of layered double hydroxides, Layered Double Hydroxides 119 (2006) 89-119.

[3]   M.Adachi-Pagano, C.Forano, J.P.Besse, Synthesis of Al-rich hydrotalcite-like compounds by using the urea hydrolysis reaction-control of size and morphology, J. Mater. Chem. 13 (2003)1988-1993.

[4]   S.Paredes et. al., Sol-gel synthesis of hydrotalcite like compounds, Journal of Materials Science 41 (2006) 3377-3382.

[5]   J.S.Valente et. al., Preparation and Characterization of Sol-Gel MgAl Hydrotalcites with Nanocapsular Morphology, The Journal of Physical Chemistry C 111 (2006) 642-651.

[6]   G.Mascolo, Synthesis of anionic clays by hydrothermal crystallization of amorphous precursors, Applied Clay Science 10 (1995) 21-30.

[7]   S.P.Newman et. al., Synthesis of the 3R(2) polytype of a hydrotalcite-like mineral, J. Mater. Chem. 12 (2002) 153-155.

[8]   F.Cavani, F.Trifiro, A.Vaccari, Hydrotalcite-type anionic clays: Preparation, properties and applications, Catalysis Today 11 (1991) 173-301.

[9]   W.N.Budhysutanto et. al., Chemical Composition and Interlayer Arrangement of Polytype $3R_2$ Mg-Al Hydroxide, to be published (2010).

[10]   W.N.Budhysutanto et. al., Stability and transformation kinetics of 3R1 and 3R2 polytypes of Mg-Al layered double hydroxides, Applied Clay Science 48 (2010) 208-213.

[11]   D.Evans and R.Slade, Structural Aspects of Layered Double Hydroxides, in: 2006, pp. 1-87.

[12]   A.S.Bookin, V.I.Cherkashin, V.A.Drits, Polytype diversity of the hydrotalcite-like minerals; II, Determination of the polytypes of experimentally studied varieties, Clays and Clay Minerals 41 (1993) 558-564.

[13]   Y.Israëli et. al., Thermodynamics of anion exchange on a chloride-intercalated zinc–aluminum layered double hydroxide: a microcalorimetric study, Journal of Chemical Society. Dalton Transactions (2000) 791-796.

[14]   K.Miyata, Anion-Exchange Properties of Hydrotalcite-Like Compounds, Clays and Clay Minerals 31 (1983) 305-311.

[15]   S.Radha, P.V.Kamath, Polytype Selection and Structural Disorder Mediated by Intercalated Sulfate Ions Among the Layered Double Hydroxides of Zn with Al and Cr, Crystal Growth & Design 9 (2009) 3197-3203.

[16]   V.R.L.Constantino, T.J.Pinnavaia, Basic Properties of Mg1-X(2+)Alx(3+) Layered Double Hydroxides Intercalated by Carbonate, Hydroxide Chloride and Sulfate Anions, Inorganic Chemistry 34 (1995) 883-892.

[17]   M.F.Brigatti, E.Galan and B.K.G.Theng, Structures and Mineralogy of Clay Minerals, in: F.Bergaya, B.K.G.Theng, G.Lagaly (Eds.) , Handbook of Clay Science, Elsevier, Amsterdam, 2006, pp. 19-86.

[18]   J.C.A.A.Roelofs et. al., The thermal decomposition of Mg-Al hydrotalcites: Effects of interlayer anions and characteristics of the final structure, Chemistry - A European Journal 8 (2002) 5571-5579.

[19]   M.Ogawa, K.Inomata, Preparation of Mg/Al Layered Double Hydroxide: Oleate Intercalation Compound by a Reconstruction Method under Hydrothermal Condition, Chemistry Letters 34 (2005) 810-811.

[20]   J.Liu, G.Chen, J.Yang, Preparation and characterization of poly(vinyl chloride)/layered double hydroxide nanocomposites with enhanced thermal stability, Polymer 49 (2008) 3923-3927.

[21]   Y.Kameshima et. al., Preparation of sodium oleate/layered double hydroxide composites with acid-resistant properties, Journal of Colloid and Interface Science 298 (2006) 624-628.

[22]   B.Magagula, N.Nhlapo, W.W.Focke, Mn2Al-LDH- and Co2Al-LDH-stearate as photodegradants for LDPE film, Polymer Degradation and Stability 94 (2009) 947-954.

[23]   X.Z.Ping, P.Braterman and F.Yarberry, Layered Double Hydroxides (Ldhs), in: Handbook of Layered Materials, CRC Press, 2009.

[24]   A.S.Bookin, V.A.Drits, Polytype diversity of the hydrotalcite-like minerals; I, Possible polytypes and their diffraction features, Clays and Clay Minerals 41 (1993) 551-557.

[25]   I.Pausch et. al., Syntheses of disordered and Al-rich hydrotalcite-like compounds, Clays and Clay Minerals 34 (1986) 507-510.

[26]   D.L.Bish, Anion-Exchange in Takovite - Applications to Other Hydroxide Minerals, Bulletin de Mineralogie 103 (1980) 170-175.

Summary

Layered Double Hydroxides (LDH) is a unique group of clays that have an anionic exchange capability. The structure of LDH consists of divalent and trivalent metal cations octahedrally coordinated with oxygen atom. Due to isomorphic replacement of some divalent cations by the trivalent ones, the so-called octahedral metal layers are positively charged. These charges are compensated by the incorporation of anions in the space between the layers, herewith referred to as interlayer. An example of a naturally occurring LDH is hydrotalcite, an Mg-Al LDH with carbonate anion in the interlayer. Synthetically, LDH is mainly produced by co-precipitation of metal salts solution at alkaline condition, followed by washing step to remove the salts and aging step to increase the crystallinity of the product. An alternative method to produce Mg-Al LDH is by hydrothermal treatment of the magnesium oxide (MgO) and aluminium trihydroxide (ATH). This hydrothermal method is simple and in principle does not produce any waste since all the added reactants are incorporated in the product. Furthermore, this synthesis method is capable of synthesizing two different Mg-Al LDH polytypes, namely $3R_1$ and $3R_2$. The term polytype referred to variation of the stacking sequence of the octahedral metal layer. These sequences also determine the number of layers per unit cell. As hydrothermal synthesis is the only reported method for the formation of polytype $3R_2$ and

considering the fore-mentioned advantages of the method, this thesis aimed to examine the synthesis and characterization of the produced 3R polytypes.

In the first part of the investigation, optimization of the hydrothermal synthesis was carried out. As the synthesis proceeds through dissolution of the solid reactant and the subsequent precipitation of the LDH product, particle size of the reactant is an essential variable. The effect of various pre-treatment technique such as blending, ultrasound treatment and wet grinding of reactant slurries with regards to the conversion rate, product yield and polytype selectivity were investigated in chapter 2. The synthesis was carried out at 90 °C and 170 °C in an autoclave for polytype $3R_1$ and $3R_2$ respectively. All the pre-treatment technique decreased the particle size of the reactant whereby wet grinding induces the strongest effect and fastest conversion rate at both temperatures accordingly. In the pre-treatment technique, the longer exposure of MgO to water causes the formation of crystalline $Mg(OH)_2$ or brucite, an un-reactive compound which could blind the surface of the MgO and hampers the conversion. The formation of brucite is less in the mixed pre-treatment of the reactants as the dissociated magnesium ion could partially precipitate as LDH.

In chapter 3, the use of a microwave system as an alternative energy source is studied. Compared to the conventional heating, synthesis with microwave can lead to a four times faster conversion towards comparable product crystallinity. The microwave heating was then studied further for variation of initial Mg/Al ratio of 1, 2 and 3, and variation of microwave power of 400, 800 and 1600 watts. The rapid heating provided by the microwave resulted in a novel crystal shape of hexagonal platelet with a hole in the middle, referred to the donut-shaped Mg-Al LDH. This morphology

provides enlargement of the specific surface area of the {hk0} faces, needed for adsorption application. These donut-shaped crystals are more pronouncedly formed at lower Mg/Al ratios of one to two and at higher microwave power. The growth mechanism of such donut-like crystals is studied by AFM as well as by STEM-EDX. The nucleation of Mg-Al LDH is postulated to start on the amorphous surface of spherical MgO particles, which have a much lower solubility compared to the ATH at the synthesis pH (~11). The outgrowing nucleus provides re-entrant corners on both sides. These are preferential sites for the addition of new growth units, allowing lateral growth of the LDH crystal encircling the MgO particles. The dissolving MgO provides the supersaturation needed for growth and once depleted, a donut-like structure remains.

The interrelation of polytype $3R_1$ and $3R_2$ is addressed in chapter 4 of this thesis. The investigation was directed toward the feasibility of the transformation from one polytype into the other, the stabile temperature regimes, transformation kinetics and relative solubility of the two polytypes. The results showed that the transformations of one polytype into the other are feasible by addition of seeds. The transition temperature is approximately at 110 °C with $3R_1$ being stabile at lower temperatures and $3R_2$ at higher temperatures. The transformation of polytype $3R_1$ into $3R_2$ however, is prevented by the presence of carbonates. This study also shows that the transformation of polytype $3R_1$ to $3R_2$ is accompanied by the formation of brucite. This result indicates that $3R_2$ has a higher aluminium content than polytype $3R_1$ thus a different composition, which will be investigated further in chapter 5.

The next chapters are focused more on the polytype $3R_2$ Mg-Al LDH. In chapter 5, the composition and interlayer arrangement of polytype $3R_2$ is revealed. Polytype $3R_2$ was synthesized by direct hydrothermal synthesis method and two-step hydrothermal synthesis method. In the latter method, polytype $3R_1$ with Mg/Al ratio of 2.3 is hydrothermally formed at 90 °C and subsequently converted to polytype $3R_2$ at 170 °C after addition of ATH. The composition of polytype $3R_2$ was investigated by direct hydrothermal synthesis method with initial Mg/Al ratio of 1.0 to 2.0. Experimentally, polytype $3R_2$ with the least amount of magnesium or aluminium by-products can be synthesized at Mg/Al ratio of 1.2. The interlayer arrangement of polytype $3R_2$ was revealed and illustrated from the product of the two-step synthesis method by XRPD, FT-IR, and 27-Al solid NMR. XRPD indicates that polytype $3R_2$ has a lower interlayer distance compared to the $3R_1$. The main feature of polytype $3R_2$ however, is the presence of aluminium in tetrahedral coordination as shown by both 27-Al solid NMR and FT-IR. These tetrahedral $Al(OH)_4^-$ (aluminate) ions are located in the interlayer as the charge compensation.

In chapter 6, a detailed analysis is of the crystal structure of polytype $3R_2$ was carried out based on the XRPD diffractogram. The measurement of the XRPD diffractogram was carried out in spinning capillary to diminish the preferred orientation effect of the sample. In order to solve the structure of polytype 3R2, structural models, based on possible interlayer arrangements as revealed by FT-IR and 27-Al solid NMR was build. The simulated diffractogram from the model was then subjected to a Rietveld refinement against the measured XRPD diffractogram. The study confirmed that the interlayer is indeed occupied by aluminate compensating for 2/3 of the charge as found from Al NMR measurements. The apical oxygen of the

aluminate is grafted onto the octahedral metal layer. Due to the interlayer arrangement, a larger unit cell parameter is required to explain the observed extra reflection.

Chapter 7 investigated the possibility of tetrahedral coordinated ion such as aluminate, sulphate, borate and gallate to mediate the formation of polytype $3R_2$ in the two-step hydrothermal synthesis method. The result showed that of the anions investigated, the $3R_2$ layer stacking can only be formed with aluminates anion in the interlayer. Furthermore, the stability of polytype $3R_2$ towards various anions was also examined. Polytype $3R_2$ was synthesized by the two-step hydrothermal synthesis method and subsequently subjected to anion salt solutions at 170 °C. The anion salts studied includes, carbonate, sulphate, bromide, dihydrogen phosphate, oxalate, oleate and stearate. All of the studied anion, except for dihydrogen phosphate is reactive towards polytype $3R_2$. The $3R_2$ layer stacking cannot however be sustained upon exposure to carbonate, sulphate or oxalate, as polytypes $3R_1$ with the corresponding anion were formed. Ion exchange of bromide, oleate and stearate anions towards $3R_2$-aluminate were also feasible, even though the determination of the layer stacking of the product were not possible.

Samenvatting

Gelaagde metaal hydroxiden (GMH) vormen een unieke groep van kleisoorten met anionuitwisselende capaciteiten. De structuur van GMH bestaat uit tweewaardige en driewaardige metaal kationen die octaëdrisch omringd zijn door zuurstofatomen. Als gevolg van de isomorfe vervanging van een aantal tweewaardige kationen door driewaardige kationen, zijn deze zogenoemde octaëdrische metaallagen positief geladen. Deze lading wordt gecompenseerd door anionen in de ruimte tussen de lagen te accommoderen. Een voorbeeld van een natuurlijk GMH is hydrotalciet, een Mg-Al GMH met carbonaat anionen in de tussenlaag. Synthetisch worden GMH voornamelijk geproduceerd door co-precipitatie vanuit een mengsel van metaalzout- oplossingen onder alkalische condities, gevolgd door een wasstap om de gevormde oplosbare zouten te verwijderen en een rijpingsstap om de kristalliniteit van het product te verbeteren. Een alternatieve methode voor de productie van Mg-Al GMH is door hydrothermale behandeling van een mengsel van magnesiumoxide (MgO) en aluminiumtrihydroxide (ATH). Deze hydrothermale methode is eenvoudig en produceert in principe geen opgelost zout als afval aangezien alle toegevoegde reactanten onderdeel vormen van het eindproduct. Bovendien kunnen, afhankelijk van de synthese condities, twee verschillende Mg-Al GMH polytypen, namelijk $3R_1$ en $3R_2$ worden

gevormd. De term polytype duidt hier op een andere volgorde in de stapeling van de zogenaamde octaëdrische metaallagen. Deze volgorde bepaalt ook het aantal lagen per eenheidscel. Omdat hydrothermale synthese de enige in de literatuur vermelde methode is voor de vorming van polytype $3R_2$ en rekening houdend met de hierboven genoemde voordelen van de methode, richt dit proefschrift zich op de synthese en karakterisering van de twee geproduceerde 3R polytypen.

Het eerste deel van het onderzoek betreft de optimalisering van de hydrothermale synthese. De deeltjesgrootte van de reactant is een essentiële variabele omdat de synthese is gebaseerd op het oplossen van de vaste reactanten gevolgd door precipitatie van het GMH product. De invloed van verschillende voorbehandelingstechnieken van de reactanten zoals voormenging in een blender, ultrasound behandeling en natte maling op de reactiesnelheid, de mate van conversie en de selectiviteit van het polytype komen aan de orde in hoofdstuk 2. De synthese werd uitgevoerd bij 90 ° C en 170 ° C in een autoclaaf om respectievelijk polytype $3R_1$ en $3R_2$ te maken. Alle voorbehandelingstechnieken reduceren de deeltjesgrootte van de reactanten, waarbij nat malen het sterkste effect heeft en ook bij beide temperaturen het meeste de omzettingssnelheid verhoogt. Een langere contacttijd van MgO met water tijdens de voorbehandeling leidt tot vorming van kristallijn $Mg(OH)_2$ of bruciet, een niet-reactief mineraal dat het oppervlak van het MgO kan blinderen en de conversie tot GMH belemmert. De vorming van bruciet treedt minder op in de gemengde voorbehandeling van de reactanten aangezien het magnesium ion al gedeeltelijk kan worden omgezet in GMH.

In hoofdstuk 3 wordt het gebruik van een magnetron systeem als alternatieve energiebron bestudeerd. Vergeleken met een conventionele warmtebron, is voor het verkrijgen van een vergelijkbare product kristalliniteit de synthese met behulp van de magnetron vier keer sneller. De synthese in de magnetron is vervolgens verder bepaald als functie van de initiële molaire Mg/Al verhouding van 1, 2 en 3, en als functie van een variatie in magnetron vermogen van 400, 800 en 1600 watt. De snelle verhitting in de magnetron resulteerde in een nieuwe kristalvorm bestaande uit zeshoekige plaatjes met een gat in het midden, die verder zullen worden aangeduid als Mg-Al GMH donuts. Deze morfologie leidt tot een vergroting van het specifieke oppervlak van de {hk0} vlakken, die nodig zijn voor toepassing als adsorbens. Bij een lagere Mg/Al verhoudingen van een tot twee en bij hogere magnetron vermogens worden meer van deze donuts gevormd. Het groei mechanisme van deze donuts werd onderzocht met AFM en STEM-EDX. Nucleatie van Mg-Al GMH wordt verondersteld te beginnen op het amorfe oppervlak van de bolvormige MgO deeltjes, die veel minder oplosbaar zijn dan het ATH bij de gegeven synthese pH (~ 11). Een uitgroeiende kiem creëert inverse hoeken aan beide zijden. Deze hoeken zijn preferentiële plaatsen voor aanhechting van nieuwe groei-eenheden, waardoor het GMH kristal lateraal aangroeit rondom het MgO deeltje. Het oplossen van het resterende MgO biedt de benodigde oververzadiging voor groei en als alle MgO is opgelost, blijft een donutachtige structuur over.

De relatie tussen polytype $3R_1$ en $3R_2$ wordt behandeld in hoofdstuk 4. Het onderzoek was gericht op de transformatie van het ene polytype in het andere, de stabiele temperatuur regimes, de transformatie kinetiek en de relatieve oplosbaarheid van de twee polytypes. De resultaten toonden aan

dat omzetting van het ene polytype in het andere mogelijk is door te enten. De overgangstemperatuur is ongeveer 110 ℃ waarbij $3R_1$ stabiel is bij lagere en $3R_2$ bij hogere temperaturen. De omzetting van polytype $3R_1$ in $3R_2$ wordt echter verhinderd in aanwezigheid van carbonaten. Deze studie toont ook aan dat tijdens de omzetting van polytype $3R_1$ in $3R_2$ bruciet wordt gevormd. Dit resultaat toont aan dat $3R_2$ meer aluminium bevat dan $3R_1$, hetgeen verder wordt onderzocht in hoofdstuk 5.

De volgende hoofdstukken zijn meer gericht op polytype $3R_2$ Mg-Al GMH. In hoofdstuk 5 wordt de samenstelling en de structuur van de tussenlaag in polytype $3R_2$ onthuld. Polytype $3R_2$ werd geproduceerd in een directe hydrothermale en in een twee-staps hydrothermale synthese. Bij de laatste methode, wordt eerst hydrothermaal polytype $3R_1$ gevormd met een Mg/Al-verhouding van 2,3 bij 90 ° C, wat vervolgens wordt omgezet in polytype $3R_2$ bij 170 ° C door toevoeging van ATH. De samenstelling van polytype $3R_2$ werd onderzocht door middel van de directe hydrothermale synthese methode met initiële Mg/Al verhoudingen variërend van 1,0 tot 2,0. Experimenteel kan polytype $3R_2$ met de minste hoeveelheid magnesium of aluminium bijproducten worden gesynthetiseerd bij een Mg/Al verhouding van 1,1 tot 1,2. De structuur van de tussenlaag van polytype $3R_2$ geproduceerd in een twee-staps synthese werd onthuld door middel van poeder X-ray diffractie (XRPD), infrarood (FT-IR) en 27-Al vastestof NMR. XRPD toont aan dat bij polytype $3R_2$ de afstand tussen de lagen korter is dan bij $3R_1$. Het belangrijkste kenmerk van polytype $3R_2$ is echter de aanwezigheid van aluminium ionen in tetraedrische coördinatie zoals blijkt uit zowel 27-Al vastestof NMR als FT-IR. Deze tetraëdrische $Al(OH)_4^-$ (aluminaat)-ionen bevinden zich in de tussenlagen ter compensatie van de lading van de octaëdrische lagen.

In hoofdstuk 6 wordt een gedetailleerde analyse gemaakt van de kristalstructuur van polytype $3R_2$ op basis van XRPD patronen gemeten met CuKα, CoKα en synchrotron straling. Voor de XRPD patronen die gemaakt werden met synchrotron-straling, werden de monsters geroteerd in een capillair om de voorkeursoriëntatie van de hexagonale plaatjes zoveel mogelijk te beperken. Om de structuur van polytype $3R_2$ op te helderen werden structuurmodellen gebouwd gebaseerd op mogelijke tussenlaag structuren die correspondeerden met de FT-IR en 27-Al vastestof NMR metingen. Het gesimuleerde diffractogram van het meest waarschijnlijke model werd vervolgens verfijnd volgens de Rietveld methode ten opzichte van het gemeten PXRD patroon. Deze verfijning toonde aan dat de tussenlaag inderdaad bezet is door aluminaat ionen die 2/3 van de lading compenseren conform de Al NMR metingen. Het apicale zuurstof atoom van het aluminaat wordt geleverd door een zuurstof atoom van de octaëdrische metaallaag, zodat het tetraëdrische aluminaat ion aan één kant verankerd is aan een octaëdrische metaallaag. Als gevolg van deze structuur van de tussenlaag is een grotere a of c cel parameter nodig is om de waargenomen extra reflectie te verklaren.

In hoofdstuk 7 wordt de mogelijkheid onderzocht om tetraëdisch gecoördineerde ionen, zoals aluminaat, sulfaat, boraat en gallaat te gebruiken om polytype $3R_2$ te vormen in een twee-staps hydrothermale synthese. Het resultaat toonde aan dat van de geteste anionen de $3R_2$ gelaagde structuur alleen kan worden gevormd met aluminaat in de tussenlaag. Bovendien werd de stabiliteit van polytype $3R_2$ tegen uitwisseling met verschillende anionen onderzocht. Polytype $3R_2$ werd gesynthetiseerd via de twee-staps hydrothermale synthese en vervolgens werd een anion zoutoplossing geïntroduceerd en werd de suspensie verder behandeld op

170 ° C. De bestudeerde anionen zijn carbonaat, sulfaat, bromide, diwaterstoffosfaat, oxalaat, oleaat en stearaat. Van alle bestudeerde anionen, is alleen diwaterstoffosfaat niet reactief met polytype $3R_2$. De $3R_2$ lagenstapeling is echter niet bestand tegen toevoeging van carbonaat, sulfaat of oxalaat, aangezien polytype $3R_1$ met het bijbehorende anion in de tussenlaag werd gevormd. Ionenuitwisseling van bromide, oleaat en stearaat anionen met $3R_2$-aluminaat was ook haalbaar, hoewel de bepaling van de lagenstapeling in het verkregen product niet mogelijk was.

Intisari

Layered Double Hydroxides (LDH) adalah golongan lempung yang memiliki kemampuan pertukaran anion. Struktur LDH terdiri dari ion logam bermuatan dua dan tiga yang terkoordinasi secara oktahedral dengan enam atom oksigen. Pergantian sebagian dari ion bermuatan dua dengan yang bermuatan tiga membuat lapisan logam oktahedral tersebut memiliki muatan positif. Muatan tersebut dikompensasi oleh anion yang terletak di bidang antar lapisan. Salah satu contoh LDH alami adalah hydrotalcite, yang mengandung campuran logam magnesium and aluminium serta anion karbonat di bidang antar lapisannya. LDH sintetik biasanya dibuat dengan mengendapkan larutan campuran logam pada kondisi basa, mencuci endapan dan meningkatkan kristalinitas produk. Cara alternatif untuk membuat LDH Mg-Al adalah dengan kristalisasi hidrothermal dari magnesium oksida (MgO) dan aluminium hidroksida (ATH). Metode ini sederhana dan tidak menghasilkan limbah karena semua reaktan terakomodasi dalam produk. Selain itu metode ini dapat menghasilkan dua macam politipe LDH Mg-Al, yaitu $3R_1$ dan $3R_2$. Politipe terbentuk dari variasi urutan tumpukan lapisan logam oktahedral pada kristal, yang menentukan juga jumlah lapisan pada tiap unit sel kristal. Disertasi ini mengambil topik sintesa dan karakterisasi politipe 3R LDH Mg-Al secara

hidrothermal karena metode ini adalah satu-satunya metode yang dapat membuat politipe $3R_2$ dan juga karena keunggulan-keunggulan lainnya.

Bagian pertama disertasi ini merupakan optimisasi metode hidrothermal tersebut. Dalam metode ini, sintesa produk berlangsung melalui pelarutan reaktan-reaktan padat yang kemudian mengendap bersama menjadi produk LDH. Oleh sebab itu, ukuran partikel adalah variabel penting. Bab 2 membahas pengaruh pre-treatment reaktan seperti blender, ultrasound dan penggerusan basah terhadap konversi, hasil dan selektivitas politipe. Sintesanya dilakukan di dalam autoklaf pada suhu 90 °C untuk membuat politipe $3R_1$ dan 170 °C untuk membuat politipe $3R_2$. Dari semua pre-treatment yang dilakukan, pengecilan ukuran reaktan paling efektif terjadi pada penggerusan basah sehingga menghasilkan konversi tercepat untuk sintesa di kedua suhu. Saat pre-treatment, kontak MgO dengan air dapat memicu pembentukan $Mg(OH)_2$ kristal atau brucite. Komponen ini tidak reaktif dan dapat menutup permukaan MgO sehingga tidak dapat bereaksi lebih jauh. Jika pre-treatment dilakukan pada campuran kedua reaktan, jumlah brucite yang terbentuk lebih terbatas karena ion magnesium yang terlarut dapat mengendap sebagai LDH.

Bab 3 mempelajari tentang penggunaan microwave sebagai energi alternatif dalam metode hidrothermal. Dibandingkan dengan sintesa menggunakan jaket pemanas, sintesa dengan microwave membutuhkan waktu empat kali lebih singkat untuk menghasilkan kualitas produk yang sebanding. Studi ini mempelajari variasi perbandingan Mg/Al reaktan 1, 2 dan 3, serta variasi energi microwave 400, 800 dan 1600W. Efek pemanasan microwave yang simultan dan seragam menghasilkan bentuk kristal unik berupa lempengan hexagonal berlubang, yang selanjutnya disebut sebagai LDH Mg-Al serupa

donat. Morfologi ini menghasilkan peningkatan luas permukaan efektif untuk adsorpsi pada bidang {hk0}. Kristal serupa donat ini terbentuk pada perbandingan Mg/Al antara satu dan dua serta pada daya 1600W. Mekanisme pertumbuhan kristal serupa donat ini juga dipelajari dengan AFM dan STEM-EDX. Nukleasi LDH diperkirakan terjadi pada permukaan amorphous partikel MgO yang kelarutannya jauh lebih rendah dari ATH pada kondisi sintesa (pH~11). Kedua bidang antara lempengan nukleus dan MgO merupakan lokasi pilihan untuk pertumbuhan kristal LDH, sehingga kristal tersebut akan tumbuh secara lateral mengelilingi partikel MgO. Partikel MgO yang larut tersebut memberikan supersaturasi yang dibutuhkan untuk pertumbuhan kristal LDH. Pada saat semua MgO terlarut, yang tersisa adalah kristal LDH serupa donat.

Hubungan antara politipe $3R_1$ dan $3R_2$ dipelajari di bab 4. Studi ini di difokuskan pada transformasi dari satu politipe ke politipe lain, suhu stabil politipe, kinetik transformasi dan kelarutan relatif kedua politipe tersebut. Hasil penelitian menunjukkan bahwa transformasi antar politipe dapat dicapai dengan penambahan bijih. Suhu transisi antar politipe adalah sekitar 110 ºC, politipe $3R_1$ stabil di bawah suhu tersebut dan politipe $3R_2$ di atas suhu tersebut. Transformasi politipe $3R_1$ menjadi $3R_2$ tidak dapat berlangsung jika ada kandungan karbonat. Selain itu, studi ini juga menunjukkan bahwa transformasi politipe $3R_1$ menjadi $3R_2$ disertai dengan pembentukan brucite. Ini berarti polytype $3R_2$ memiliki kandungan aluminium lebih besar daripada $3R_1$ dan komposisi kedua politipe tersebut berbeda satu sama lain.

Selanjutnya, bab-bab dari disertasi ini difokuskan pada LDH Mg-Al politipe $3R_2$. Bab 5 menguraikan komposisi dan dan susunan bidang antar lapisan

pada politipe $3R_2$. Politipe $3R_2$ disintesa dengan metode hidrotermal satu langkah dan dua langkah. Pada sintesa dua langkah: pertama, politipe $3R_1$ dengan perbandingan Mg/Al=2,3 dibuat pada suhu 90 °C dan selanjutnya direaksikan jadi politipe $3R_2$ pada suhu 170 °C setelah ditambah ATH. Komposisi politipe $3R_2$ dipelajari dengan sintesa hidrotermal satu langkah pada variasi perbandingan Mg/Al 1,0 sampai 2,0. Secara eksperimen, politipe $3R_2$ dengan jumlah produk samping magnesium dan aluminium minimum dapat dicapai pada Mg/Al=1,2. Susunan bidang antar lapisan pada politipe $3R_2$ dipelajari dari produk sintesa dua langkah dengan XRPD, FT-IR, dan 27-Al NMR padatan. XRPD menunjukkan jarak antar lapisan politipe $3R_2$ lebih kecil daripada $3R_1$. Ciri khas politipe $3R_2$ adalah kandungan aluminium tetrahedral seperti terungkap dengan NMR dan FT-IR. Aluminium tetrahedral $Al(OH)_4^-$ ini memberikan muatan negatif di bidang antar lapisan.

Bab 6 memuat analisa detail struktur kristal politipe $3R_2$ berdasarkan data XRPD. Pengukuran XRPD dilakukan di kapiler berputar untuk menghilangkan efek orientasi pilihan sampel. Simulasi model struktural dibuat berdasarkan kemungkinan susunan bidang antar lapisan seperti yang terungkap dengan NMR dan FT-IR. Simulasi pola XRPD dari model tersebut kemudian dibandingkan dengan pola XRPD yang telah diukur. Studi ini memastikan bahwa bidang antar lapisan pada politipe $3R_2$ diisi oleh aluminium tetrahedral yang mengkompensasi 2/3 muatan lapisan, sebagaimana yang diukur oleh Al NMR. Oksigen puncak dari aluminium tetrahedral tersebut terikat dengan lapisan logam oktahedral. Sebagai konsekuensi dari susunan molekul di bidang antar lapisan, dibutuhkan unit sel kristal yang lebih besar untuk mensimulasikan refleksi tambahan yang terlihat di pola XRPD terukur.

Bab 7 menyelidiki kemungkinan berbagaimacam molekul yang memiliki tetrahedral koordinasi seperti aluminat, sulfat, borat and gallat untuk membentuk politipe $3R_2$ dengan metode hidrotermal dua langkah. Hasil penelitian ini menunjukkan bahwa susunan $3R_2$ hanya dapat terbentuk dengan aluminat di bidang antar lapisan. Selain itu, stabilitas politipe $3R_2$ terhadap berbagaimacam anion juga dipelajari. Untuk studi ini, politipe $3R_2$ disintesa dengan metode hidrotermal dua langkah, dan selanjutnya ditambahkan larutan garam dan treatment tersebut dilanjutkan pada suhu 170 °C. Garam-garam anion yang diselidiki adalah karbonat, sulfat, bromida, dihidrogen fosfat, oksalat, oleat, dan stearat. Dari semua anion yang diselidiki, hanya dihidrogen fosfat yang tidak reaktif terhadap politipe $3R_2$. Tetapi susunan politipe $3R_2$ tidak dapat dipertahankan setelah treatment dengan karbonat, sulfat dan oksalat. Susunan kristal setelah treatment berubah menjadi politipe $3R_1$. Pertukaran anion dengan bromida, oleat dan aluminat dengan politipe $3R_2$ juga dapat dilakukan, tetapi urutan tumpukan produknya tidak dapat ditentukan.

Acknowledgements

All in all, it has been a very long and memorable journey, in which I have been fortunate enough to share experiences with many wonderful people. I would like to thank my promoter Andrzej Stankiewicz; it's an honour to be the first PhD student you promoted. I would like to thank Peter Jansens, for giving me the opportunity to do this PhD and supporting my decisions along the way. To Herman Kramer, my supervisor, thank you for all the opportunities you gave me, for all your support, your guidance, and for putting up with me all this time. I will not bug you with making appointments anymore ☺. My utmost gratitude goes to Gerda van Rosmalen, the best sparing partner a PhD student can have. I enjoyed our discussions very much and sure have learned a lot from you. In the last year, I have also worked with Peter Cains who always give me a different point of view. Thank you Peter, your ideas intrigue me to think further.

I would also like to thank some people from Akzo: Dimitri van Agterveld, Elwin Schomaker, Auke Talma, Brenda Rossenaar, and Hettie Verlaan. Dimitri, thank you for all your ideas and support until I reach the light at the end of the tunnel. Elwin, thank you for your interest, contributions and constant challenge to always be better. Auke, thank you for giving me the opportunity to work on the project. And to Pablo Domínguez de María, thank you for encouraging me to do a PhD.

Working in the laboratory could be very tiring and time consuming, especially when you didn't know where things are and how things work. I would like to thank Michel van den Brink, who always has answer for the questions in our laboratory. Ruud Hendrikx, I learned a lot about XRPD from you. Thank you. Kristina Djanashvili, thanks for all the NMR measurements. Ben Norder, thank you for the TGA measurements. Wouter van Beek helped us a lot when doing measurements in ESRF, thank you.

To my co-worker in Nijmegen: Fieke van den Bruele, Willem van Enckevort, Elias Vlieg, thank you for your hospitality, ideas and contributions.

To my officemates in chronological order Jelan, Christian, Ali Imran, Stijn, Somnath, Norbert, Dennis, and Sander: thank you for all the various discussions and the wonderful times we spend together. A special thank to Jelan for setting up the example of speaking Dutch with me. It's been a pleasure to always be the only girl in the room ☺. Please don't let the plant in our office dies out…

Thanks to all my P&E friends and colleagues. Xiaohua, my dear friend, thanks for all your friendship, attention and caring words. Shanfeng, we experienced a lot together. Ali, my long time friend, thank you for walking the same path and sharing experiences with me. Magda, Tomek, Aylin, Marta, Richard, Elif, Albert, Ana, Cristi, pak Kamarza, bu Elsa, Stevia, and many more, thank you for making my time in P&E so colourful and definitely enjoyable. The research work will not be running as smoothly without the help of our wonderful management assistants: Leslie, Helma and Ilona. Thank you.

Living in a different country is never easy, but I am so thankful to have my dear housemates to get me through. Julito, Yenni and Anin: thank you for your friendship and supports, and for all the cooking, baking, travelling, chatting and shopping time we spent together. Also to my other Indonesian friends: Ferry, Ika, Jeffry, Danang, Joe, Agung, Irene, Monica, Tony, Surya, Sylvia and the two little boys… My time in Holland would not have been as much fun without you.

Oom Hwie Kian, tante Kim Lian, and Siok Swan, thank you for making me a part of your family. It really means a lot to me. To my dear little boy, Widita Budhysutanto: thank you Boya for all your support and encouragements. You're the best little brother ever, not to mention the best computer manager. To my dear koko, Cipta Budhysutanto and his wife, Imelda Wurangian, though distance separates us, but you always support me from a far away distance. Thank you. And to my dear Emak and Engkong, terima kasih banyak atas doa dan dukungan Emak Engkong selama ini.

A very special thanks to my parents Budhy Sutanto and Lie Ay Hwa. Mami, Papi, terima kasih banyak untuk semua kasih sayang Mami Papi selama ini dan terima kasih sudah memberikan Wewe kesempatan untuk bisa ke Belanda. Wewe bisa menyelesaikan PhD ini berkat dukungan, semangat dan doa restu dari Mami Papi.

And last but not least, to my Lieverd, Arief: thank you Lieverd, for putting up with me and supporting me throughout the good and bad time. But most of all, thank you for giving me the reason to do what I do.

Widya Nugraha Budhysutanto
Delft, November 2010

Curriculum Vitae

Widya Nugraha Budhysutanto was born in Semarang, Indonesia on January 2nd, 1980. She attended high school at SMUK Frateran in Surabaya and graduated in 1998. In the same year she started her study at the Psychology Department of Universitas Airlangga Surabaya. In 1999, she started her study in Chemical Engineering Department of Universitas Katolik Widya Mandala Surabaya, which she graduated in 2003 as a Bachelor of Chemical Engineering. She graduated her Bachelor of Psychology in 2004 and moved to the Netherlands to pursue her Master study of Chemical Engineering in Delft University of Technology on the same year. During the course of her study, she joined AkzoNobel as a stagiair from August 2005 until April 2006. She graduated as Master of Science in August 2006. Starting from September 2006, she joined the Process and Energy Laboratory in Delft University of Technology as a PhD Researcher. During the course of her research, she has developed knowledge and skill in crystallization process, crystal polytypism, and correlation between product characterization and application properties. This research has led to the present PhD thesis.

Publications

Journal publications

W.N. Budhysutanto, H.J.M. Kramer, D. van Agterveld, A.G. Talma, P.J. Jansens, Pre-treatment of raw materials for the hydrothermal synthesis of hydrotalcite-like compounds, Chemical Engineering Research and Design 88 (2010) 1445-1449.

W.N. Budhysutanto, D. van Agterveld, E. Schomaker, A.G. Talma, H.J.M. Kramer, Stability and Transformation Kinetics of Polytype $3R_1$ and $3R_2$ Mg-Al Layered Double Hydroxides, Applied Clay Science 48 (2010) 208-213.

W.N. Budhysutanto, F.J. van den Bruele, B.D. Rossenaar, D. Van Agterveld, W.J.P. van Enckevort, H.J.M. Kramer, A Unique growth mechanism of Donut Shaped Mg-Al Layered Double Hydroxide revealed by AFM and STEM-EDX, Journal of Crystal Growth (doi: 10.1016/j.jcrysgro.2010.10.083).

W.N. Budhysutanto, D van Agterveld, E Schomaker, B.D. Rossenaar, G.M. van Rosmalen, H.J.M. Kramer, Chemical Composition and Interlayer Arrangement of Polytype $3R_2$ Mg-Al Layered Double Hydroxides, (submitted for publication in Applied Clay Science).

W.N. Budhysutanto, R.W.A. Hendrikx, H.J.M. Kramer, Structure of Polytype $3R_2$ Mg-Al Layered Double Hydroxides, (submitted for publication Applied Clay Science).

W.N. Budhysutanto, D. van Agterveld, H.J.M. Kramer, Stability of Polytypes $3R_2$ Mg-Al LDH towards Various Anions, (will be submitted for publication in a journal).

Patent Application

A.G. Talma, E. Schomaker, S. Bruijn, **W.N. Budhysutanto**, Layered Double Hydroxide with a Specific Morphology, Its preparation and Use, European Patent Application, June 3, 2009, Serial No. 09161849.6

Other Publications

W.N. Budhysutanto, et al. (2009), Microwave – Alternative Energy Source for Hydrothermal Synthesis of Mg-Al Layered Double Hydroxide. In: M. Louhi-Kultanen, H. Hatakka, (Editors). Proceeding of 16th International Workshop on Industrial Crystallization, Lappeenranta, Finland. Digipaino, Lappeenranta, Finland, pp. 69-76.

W.N. Budhysutanto, S. Jiang, J.H. ter Horst (2009), Neat Grinding of o-Aminobenzoic Acid Polymorph, NPS 9, Veldhoven, the Netherlands.

WN Budhysutanto, et al. (2009), Stability and transformation kinetics of $3R_1$ and $3R_2$ polytypes of Mg-Al LDH. In: S.Fiore, C. Belviso, M.L. Giannossi (Editors). Micro et Nano: Scientiæ Mare Magnum, vol. I. 14th Int. Clay Confr., Castellaneta M., Italy. Digilabs s.a.s Pub., Bari, Italy, p. 258.

W.N. Budhysutanto, et al. (2008), Enhancing hydrothermal synthesis rate of hydrotalcite-like compounds by raw materials pre-treatment. In: G.H. Banis, Proceedings of NPS 8, Veldhoven, the Netherlands, p. 75.

W.N. Budhysutanto, et al. (2008), Pre-treatment of raw materials for the hydrothermal synthesis of hydrotalcite-like compounds. In: P.J.Jansens, J.Ultrich (Editors). Proceedings ISIC 17, vol. III, Maastricht, the Netherlands, pp. 1719-1724.

W.N. Budhysutanto, et al. (2007), Milling as an activation technique in hydrothermal synthesis of hydrotalcite-like material, NPS 7, Veldhoven, the Netherlands.

W.N. Budhysutanto, et al. (2007), Synthesis and Characterization of Hydrotalcite-like Compounds Produced via Hydrothermal Treatment. In: R.Gani, K.Dam-Johansen, ECCE-6 Book of Abstracts, Copenhagen, Denmark. Norhaven Book, Denmark, pp. 533-534.

Oral Presentations

16th International Conference on Crystal Growth, Beijing, China, August 2010 (two oral presentations).

16th International Workshop on Industrial Crystallization, Lappeenranta, Finland, September 2009.

14th International Clay Conference, Castellaneta Marina, Italy, June 2009.

Netherlands Process Technology Symposium 8, Veldhoven, The Netherlands, October 2008.